On the Simulation of Boson Stars in General Relativity

Author: Robin Croft

Supervisor: Dr. Ulrich Sperhake

uni_logo.png

Contents

Chapter 1

Introduction

1.1 Introduction

general gr shit? mention einstein derivation (hilbert derivation a potentially earlier but vacuum), karl schwarzschild (ironicaly meaning black shield), then low mass limit, photon deflection and mercury perihelion around sun. mention cosmology, gravitational waves, more black holes, minkowski. more compact objects.

1.2 Introduction to Compact Objects and Boson Stars

The first non-trivial solution to Einstein's equation found was that of the spherically symmetric, static and asymptotically flat vacuum spacetime by Karl Schwarzschild in 1915. The solution was designed to be used outside a spherically symmetric, non-spinning, body of mass; however it turned out to provide use in describing black holes. This metric was then modified by Tolman, Oppenheimer and Volkov in 1939 to describe the non-vacuum case of a constant density neutron star. This turned out to give an unphysical estimate of $0.7 M_\odot$ for the upper limit of neutron star mass due to the equation of state.

The study of compact exotic objects can be traced back to John Wheeler who investigated Geons in 1955 for their potential similarity to elementary particles. Geons are gravito-electromagnetic objects with the name arising from "gravitational electromagnetic entity". In 1968 David Kaup published [] describing what he called "Klein-Gordon Geons", nowadays referred to as boson stars. Importantly, boson stars are a localised complex Klein-Gordon configuration, with the real counterparts being unstable. Many variants such as (Spin 1) proca stars [], electromagnetically charged boson stars and many others have been studied.

Interest in boson stars remains for many reasons. Given the recent discovery of the higgs boson, we know that scalar fields exist in nature and any gravitational wave signals created by compact objects could theoretically be detected with modern gravitational wave interferometers. Secondly, boson stars are a good candidate for dark matter haloes. Boson stars are also useful as a proxy to other compact objects in general relativity; there is a lot of freedom in the construction of different types of boson star and they can be fine tuned to model dense neutron stars for one example. The advantage this would have over simulating a real fluid is that the Klein Gordon equation is linear in the principal part meaning smooth data must always remain smooth; thus avoiding shocks and conserving particle numbers relatively well with less sophisticated numerical schemes.

On a slightly different topic, collisions of boson stars could be a natural method to produce scalar hair around black holes which will be discussed later in more detail.

1.2.1 Conventions

Throughout this thesis physical quantities will be expressed as a dimensionless ratio of the Planck length, time and mass L_{pl}, T_{pl} and M_{pl} respectively; consequently the constants c, G and $\hbar$ evaluate numerically to 1. As an example, Newtons equation of gravity would be recast like

$$F = \frac{GMm}{r^2} \rightarrow \left(\frac{F}{F_{pl}}\right) = \frac{\left(\frac{M}{M_{pl}}\right)\left(\frac{m}{M_{pl}}\right)}{\left(\frac{r}{L_{pl}}\right)^2} \tag{1.2.1}$$

where $F_{pl} = M_{pl}L_{pl}T_{pl}^{-2}$ is the Planck force. $c = G = \hbar = 1$, unless stated otherwise. The metric signature will always be $(-,+,+,+)$.

Tensor fields will be denoted using bold font for index free notation and normal font for the components. The dot product between two vector fields will be written interchangeably as $\boldsymbol{A} \cdot \boldsymbol{B} \leftrightarrow A_\mu B^\mu$ for readability. Additionally, ∇_μ denotes the covariant derivative and ∂_μ is the partial derivative, both with respect to coordinate x^μ.

When considering the ADM decomposition, as in [REF SECT], objects can be associated with both the 3+1 dimensional manifold $\mathcal{M}$ or the 3 dimensional hypersurface Σ. To differentiate here, standard Roman letters such as R represent the object belonging to $\mathcal{M}$ and calligraphic letters such as $\mathcal{R}$ correspond to the projected object belonging to Σ. [MAYBE JUST REMOVE THIS BIT AND MAKE IT OBVIOUS IN THE ACTUAL 3+1 SECTION].

Finally, unless stated otherwise, Greek indices such as $\{\alpha, \beta, ..., \mu, \nu, ...\}$ label four dimensional tensor components whereas late Latin indices such as $\{i, j, k, ...\}$ label three dimensional tensor components and early Latin indices such as $\{a, b, ...\}$ label two dimensional ones. When the index range is unspecified and unimportant Greek letters will also be used.

make explicit th inner product, dot product, outer product (otimes) and wedge product (for forms, antisymm)

1.3 Differential Geometry

1.3.1 Introduction to Geometry / Manifolds (maybe change this)

From a young age, everyone has known Pythagoras' theorem $s^2 = x^2 + y^2$ for a right angled triangle with height y, width x and hypotinuse length s. This can be shown very simply by looking at Fig. 1.1. The area of the partially rotated square is obviously s^2, but we can also calculate it from the the area of the larger square A_{sq} and subtracting four times the area of one of the triangles A_{tr}. Clearly $A_{sq} = (x+y)^2$ and $A_{tr} = \frac{1}{2}xy$, therefore

$$s^2 = (x+y)^2 - 2xy = x^2 + y^2 \tag{1.3.1}$$

and we have proved Pythagoras' theorem. Using an infinitessimally small triangle, we can write $\mathrm{d}s^2 = \mathrm{d}x^2 + \mathrm{d}y^2$ and this can be trivially extended to arbitrary dimensions like

$$\mathrm{d}s^2 = \mathrm{d}x^2 + \mathrm{d}y^2 + \mathrm{d}z^2 + ... \ . \tag{1.3.2}$$
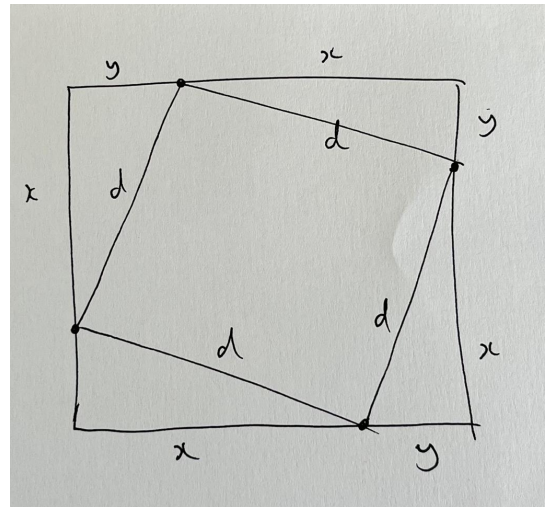

Figure 1.1: Diagram for proof of Pythagoras' theorem.

The infinitessimal form of Pythagoras' theorem is very powerful as it lets us calculate the length of a generic curve by approximating the curve as a collection of infinitessimally small straight lines with length ds. So far we have assumed that space is flat meaning Eq. (1.3.2) is true for all points in space, this is an assumpion we will have to drop if we want to study gravity in the strong regime. In the next sections we will explore the generalisation of Pythagoras' equation to curved spaces and use it to measure curve lengths answsell as volumes and areas.

Differential Geometry (DG) is the extension of calculus, linear algebra and multilinear algebra to general geometries. Einstein's Theory of Relativity is written using the language of DG as it is the natural way to deal with curves, tensor calculus and differential tensor equations in curved spaces. For a basic introduction to DG, we should start with a manifold $\mathcal{M}$ which is an N dimensional space that locally looks like $\mathbb{R}^N$, N dimensional Euclidean space. This is important as at a point $p \in \mathcal{M}$ we can find infinitesimally close neighbouring points $p + \delta p \in \mathcal{M}$. In the following sections we will explore how curves, functions, tensors and calculus are defined within DG.

1.3.2 Functions, Curves and Tensors on Manifolds

A real scalar function f over $\mathcal{M}$ maps any point $p \in \mathcal{M}$ to a real number, this is denoted as $f : p \to \mathbb{R}$. An important example of a set of scalar functions is the coordinate system ϕ, $\phi : p \to \mathbb{R}^N$, this is normally written x^μ where $\mu \in \{0, 1, ..., N - 1\}$ is an index labelling the coordinate. The map ϕ is called a chart, and unlike Euclidean space one chart may not be enough to cover the entire manifold; in this case a set of compatible charts should be smoothly joined, collectively known as an atlas.

Now that functions have been discussed, the next simplest object we can discuss is a curve, or path, through $\mathcal{M}$. A curve Γ is a set of smoothly connected points $p(\lambda) \in \mathcal{M}$ that smoothly depend on an input parameter $\lambda \in [\lambda_0, \lambda_1]$. This can be expressed in terms of coordinates as $x^\mu(\lambda)$ where $\phi : p(\lambda) \to x^\mu(\lambda)$. Differentiating a function f along Γ with respect to λ gives

$$\frac{\mathrm{d}}{\mathrm{d}\lambda} f(x^\mu(\lambda)) = \frac{\mathrm{d}x^\nu}{\mathrm{d}\lambda} \frac{\partial f(x^\mu)}{\partial x^\nu} = \frac{\mathrm{d}x^\nu}{\mathrm{d}\lambda} \partial_\nu f, \tag{1.3.3}$$

where $\partial_\nu = \partial/\partial x^\nu$ and the Einstein summation convention was invoked, summing over all values of ν. Equation (1.3.3) was derived independantly of the choice of f, therefore we can generally write

$$\frac{\mathrm{d}}{\mathrm{d}\lambda} = \frac{\mathrm{d}x^\nu}{\mathrm{d}\lambda} \partial_\nu. \tag{1.3.4}$$

The operator d/dλ can act on any function f and return a new function $\tilde{f}$ over $\mathcal{M}$, formally this is written as d/d$\lambda(f) = \tilde{f}$ where $\tilde{f} : p \in \mathcal{M} \to \mathbb{R}$. We can also think of d/dλ as a vector $\boldsymbol{X}$ with components $X^\mu = \mathrm{d}x^\mu/\mathrm{d}\lambda$ and basis vectors $\boldsymbol{e}_\mu := \partial_\mu$ taken from Eq. (1.3.4). The vector $\boldsymbol{X}$ can be written as $\boldsymbol{X} = X^\mu \boldsymbol{e}_\mu$ and can act on a general function f over $\mathcal{M}$ as $\boldsymbol{X}(f) = X^\mu \boldsymbol{e}_\mu(f) = X^\mu \partial_\mu f$.

Considering the set of all possible curves through a points $p \in \mathcal{M}$, the tangent vector components dx^μ/dλ span an N dimensional space with basis $\boldsymbol{e}_\mu = \partial_\mu$; this space is called the tangent space and is denoted as $\mathcal{T}_p(\mathcal{M})$. For the tangent space to be a vector space we need to define an inner product between two general vectors $\boldsymbol{X}, \boldsymbol{Y} \in \mathcal{T}_p(\mathcal{M})$, linear in it's arguments, like

$$(a\boldsymbol{X}) \cdot (b\boldsymbol{Y}) = ab X^\mu Y^\nu \boldsymbol{e}_\mu \cdot \boldsymbol{e}_\nu \tag{1.3.5}$$

for any coefficients a and b. In General Relativity it is helpful to define the dot product with the metric components $g_{\mu\nu}$ like $\boldsymbol{e}_\mu \cdot \boldsymbol{e}_\nu = g_{\mu\nu}$; alternatively

$$\boldsymbol{X} \cdot \boldsymbol{Y} = X^\mu Y^\nu g_{\mu\nu}. \tag{1.3.6}$$

The next object to discuss is the co-vector which is defined as a map from vectors to real numbers; this is not the same as the dot product, and doesnt need one to exist [MAKE THIS BETTER]. Similarly to

vectors, a co-vector $\boldsymbol{\omega}$ can be expressed as a sum of components ω_μ and basis co-vectors $\boldsymbol{\theta}^\mu$ like $\boldsymbol{\omega} = \omega_\mu \boldsymbol{\theta}^\mu$. Contrary to vectors, co-vector components have downstairs indeces and the basis has upstairs indeces; this choice improves the readability of tensor equations when working with components. The power of co-vectors is that they map a vector to a real number like $\boldsymbol{\omega} : \boldsymbol{X} \to \mathbb{R}$ or $\boldsymbol{\omega}(\boldsymbol{X}) \to \mathbb{R}$. Vectors are equally able to map co-vectors to real numbers like $\boldsymbol{X} : \boldsymbol{\omega} \to \mathbb{R}$. Co-vectors are defined such that $\boldsymbol{\theta}^\mu : \boldsymbol{e}_\nu = \delta^\mu_\nu$ where δ^μ_ν are the components of the Kroneka delta equating to zero unless $\mu = \nu$ in which case they equal unity. The general operation of a co-vector $\boldsymbol{\omega}$ on a vector $\boldsymbol{X}$ is

$$\boldsymbol{\omega} : \boldsymbol{X} = \omega_\mu X^\nu \boldsymbol{\theta}^\mu : \boldsymbol{e}_\nu = \omega_\mu X^\nu \delta^\mu_\nu = \omega_\mu X^\mu \in \mathbb{R}. \tag{1.3.7}$$

This map is linear and identical under reversing the order of operation; $\boldsymbol{\omega} : \boldsymbol{X} = \boldsymbol{X} : \boldsymbol{\omega}$. Similarly to vectors, the set of all possible co-vectors at a point $p \in \mathcal{M}$ span an N-dimensional space called the co-tangent space, written as $\mathcal{T}_p^*(\mathcal{M})$.

Now that linear maps have been covered, we can generalise to multilinear maps and tensor fields. Consider a tensor field $\boldsymbol{T}$, this can be expressed in component form like

$$\boldsymbol{T} = T^{\alpha\beta,\cdots}_{\mu\nu,\cdots} \boldsymbol{e}_\alpha \otimes \boldsymbol{e}_\beta \otimes ... \otimes \boldsymbol{\theta}^\mu \otimes \boldsymbol{\theta}^\nu \otimes ... \tag{1.3.8}$$

for an arbitrary number of [MAKE THIS MAKE SNENSE]. A tensor field with m co-vector bases and n vector bases is called an (m,n) tensor field, therefore vectors, co-vectors and scalars are $(1,0)$, $(0,1)$ and $(0,0)$ vectors respectively. Tensors can act as multilinear maps between tensor fields to other tensor fields. We have already seen how a vector and co-vector can map each other to a scalar, extending this we can use an $(0,2)$ tensor field $\boldsymbol{T} = T_{\mu\nu}\boldsymbol{\theta}^\mu \otimes \boldsymbol{\theta}^\nu$ to map two vector fields $\boldsymbol{X}$ and $\boldsymbol{Y}$ to a scalar like

$$\boldsymbol{T}(\boldsymbol{X}, \boldsymbol{Y}) = T_{\mu\nu}X^\alpha Y^\beta (\boldsymbol{\theta}^\mu : \boldsymbol{e}_\alpha)(\boldsymbol{\theta}^\nu : \boldsymbol{e}_\beta) = T_{\mu\nu}X^\mu Y^\nu. \tag{1.3.9}$$

This equation is identical to Eq. (1.3.6) and we can see that the space-time metric is an $(0,2)$ tensor on our spacetime. As mentioned already, the multilinear map can output generic tensors, for example consider

$$\boldsymbol{T}(\boldsymbol{X}, \star) = T_{\mu\nu}X^\alpha (\boldsymbol{\theta}^\mu : \boldsymbol{e}_\alpha)\boldsymbol{\theta}^\nu = T_{\mu\nu}X^\mu \boldsymbol{\theta}^\nu, \tag{1.3.10}$$

which uses the $(0,2)$ tensor $\boldsymbol{T}$ to map the vector $\boldsymbol{X}$ to a co-vector $\boldsymbol{W}$ with components $W_\mu = T_{\mu\nu}X^\mu$. [DOES THE STAR MAKE SENSE?] One final example of a mapping is from a single tensor to a lower rank tensor, this is called contraction. To illustrate this, let's take a $(1,3)$ tensor $\boldsymbol{Z} = Z^\alpha_{\mu\nu\rho}\boldsymbol{e}_\alpha \otimes \boldsymbol{\theta}^\mu \otimes \boldsymbol{\theta}^\nu \otimes \boldsymbol{\theta}^\rho$. We can choose to use the basis vector $\boldsymbol{e}_\alpha$ to act on any of the three co-vector bases, choosing $\boldsymbol{\theta}^\mu$ this is

$$Z^\alpha_{\mu\nu\rho}(\boldsymbol{e}_\alpha : \boldsymbol{\theta}^\mu)\boldsymbol{\theta}^\nu \otimes \boldsymbol{\theta}^\rho = Z^\mu_{\mu\nu\rho}\boldsymbol{\theta}^\nu \otimes \boldsymbol{\theta}^\rho = \tilde{Z}_{\nu\rho}\boldsymbol{\theta}^\nu \otimes \boldsymbol{\theta}^\rho \tag{1.3.11}$$

where $\tilde{Z}_{\nu\rho} = Z^\mu_{\mu\nu\rho}$.

check faking field vs obect at a point p

1.3.3 General Covariance / Coordinate transformations

The power of tensor algebra and tensor calculus is that if a tensor equation can be written in one coordiante system then must hold (in abstact from) in any [NON-PATHOLOGICAL?] coordinate system. This is a consequence of the tensor transformation law and hence the saying "the definition of a tensor is an object that transforms like a tensor" [FIND QUOTE OR PUT THIS IN A BETTER PLACE?]. Looking back, we can write a generic vector field $\boldsymbol{X}$ as $X^\mu \boldsymbol{e}_\mu = X^\mu \partial_\mu$ and if we choose a coordinate transformation $x^\mu \to \tilde{x}^\mu$ then we see that in the transformed coordinate system the vector $\boldsymbol{X}$, written

$\tilde{\boldsymbol{X}}$, becomes

$$\tilde{\boldsymbol{X}} = \tilde{X}^\mu \frac{\partial}{\partial \tilde{x}^\mu}, \tag{1.3.12}$$

$$= \tilde{X}^\mu \frac{\partial x^\nu}{\partial \tilde{x}^\mu} \frac{\partial}{\partial x^\nu}, \tag{1.3.13}$$

$$= X^\nu \frac{\partial}{\partial x^\nu}, \tag{1.3.14}$$

$$= \boldsymbol{X}, \tag{1.3.15}$$

where $X^\nu = \tilde{X}^\mu \frac{\partial x^\nu}{\partial \tilde{x}^\mu}$ is required to make $\boldsymbol{X} = \tilde{\boldsymbol{X}}$. This says that the underlying geometric object (a vector in this case) is independant of the coordinates used to describe them; the tradeoff for this useful property is that the vectors components X^μ have to transform under the tensor transformation law, $\tilde{X}^\mu = \frac{\partial \tilde{x}^\mu}{\partial x^\nu} X^\nu$ [THIS IS TEH OTHER WAY ROUDN TO BEFORE]. Working from a co-vector ω we can write it as $\omega_\mu \boldsymbol{\theta}^\mu = \omega_\mu \mathrm{d}x^\mu$ in component-basis form [REF THIS?] and the same coordinate transform gives

$$\tilde{\boldsymbol{\omega}} = \tilde{\omega}_\mu \mathrm{d}\tilde{x}^\mu, \tag{1.3.16}$$

$$= \tilde{\omega}_\mu \frac{\partial \tilde{x}^\mu}{\partial x^\nu} \mathrm{d}x^\nu, \tag{1.3.17}$$

$$= \omega_\nu \mathrm{d}x^\nu, \tag{1.3.18}$$

where the co-vector components transform like $\omega_\nu = \tilde{\omega}_\mu \frac{\partial \tilde{x}^\mu}{\partial x^\nu}$, the opposite way to the vector components. These transformation laws ensure that a scalar field created from the product of a vector field and a co-vector field, like $\boldsymbol{\omega} : \boldsymbol{X}$, is a Lorentz scalar not transforming under coordinate transformations. This can be seen from

$$\tilde{\boldsymbol{\omega}} : \tilde{\boldsymbol{X}} = \tilde{X}^\mu \tilde{\omega}_\mu, \tag{1.3.19}$$

$$= X^\nu \frac{\partial \tilde{x}^\mu}{\partial x^\nu} \frac{\partial x^\rho}{\partial \tilde{x}^\mu} \omega_\rho, \tag{1.3.20}$$

$$= X^\nu \frac{\partial x^\rho}{\partial x^\nu} \omega_\rho, \tag{1.3.21}$$

$$= X^\nu \delta_\nu{}^\rho \omega_\rho, \tag{1.3.22}$$

$$= X^\nu \omega_\nu, \tag{1.3.23}$$

$$= \boldsymbol{\omega} : \boldsymbol{X}. \tag{1.3.24}$$

The general tensor transformation law comes from chaining multiple of the previous examples together [REWITE BETTER], for example

$$\tilde{T}^{\mu\nu\dots}{}_{\rho\sigma\dots} = T^{\alpha\beta\dots}{}_{\gamma\delta\dots} \left(\frac{\partial \tilde{x}^\mu}{\partial x^\alpha} \frac{\partial \tilde{x}^\nu}{\partial x^\beta}, \dots \times \frac{\partial x^\gamma}{\partial \tilde{x}^\rho} \frac{\partial x^\delta}{\partial \tilde{x}^\sigma}, \dots \right). \tag{1.3.25}$$

discuss coords, paths, vectoirs, forms, tensors, derivatives (lie, cov, partial ...), pullbacks (needed later), Riemann and stuff. see intro and appendix of smith kight. talk about forms? 0-form scalar, 1-form vector, 2-form antisymmetric 0,2 tensor ... exterior derivds and lie derivs?

use words lorentz invariant and covariant

1.3.4 Differential Forms

A differential p-form is an antisymmetric $(0, p)$ tensor; the tensor components (e.g. $A_{\alpha\beta\dots\varsigma}$) vanish if there is a repeating index, equal 1 for an even permutation of indeces (like 1,2,3,...,N) and -1 for an odd

permutation (such as 2,1,3,4,...,N). Note that a 0-form is a function, a 1-form is a co-vector and for an N-dimensional manifold the N-form is unique and the p-forms with $p > N$ vanish.

When considering differential forms, the conventional covector basis is often changed from $\boldsymbol{\theta}^\mu$ to $\mathrm{d}x^\mu$ which will lend itself nicely to integrating p-forms on manifolds later. This convention means we can write the metric as $\boldsymbol{g} = g_{\mu\nu}\mathrm{d}x^\mu \otimes \mathrm{d}x^\nu$; the same can be done for any tensor. Note that the metric cannot be a 2-form as it is not a symmetric tensor, infact the metric is a symmetric tensor.

1.3.5 Differentiation on Manifolds

There are three types of derivative, all related to each other, that we care about on a manifold. [CHECK WHOLE PARAGRAPH] The simplest is the exterior derivative of a p-form, returning a $p+1$-form. For a p-form $\boldsymbol{A} = A_\mu \mathrm{d}x^\mu$, the exterior derivative is given by

$$(\mathrm{d}A)_{\mu_1...\mu_{p+1}} = (p+1)\partial_{[\mu_1} A_{\mu_2...\mu_{p+1}]}, \tag{1.3.26}$$

where the square brackets mean the antisymmetric [check as i might need epsilons here]. This derivative guarentees to return a tensor without the need for a connection or metric on the manifold, unlike the partial derivative that we will see next. One common example of an exterior derivative is of a 1-form, say $\boldsymbol{A}$ giving

$$(\mathrm{d}A)_{\mu\nu} = \partial_\mu A_\nu - \partial_\nu A_\mu, \tag{1.3.27}$$

and we will see soon, as with all exterior derivatives of forms, returns a tensor object.

The most common type of derivative is the coraviant derivative (∇), which reduces to the partial derivative (∂) in flat space with cartesian coordinates. The purpose of the covariant derivative is to take a (p,q) tensor $\boldsymbol{T}$ and return a $(p, q+1)$ tensor $\boldsymbol{\nabla T}$ which obeys the tensor transformatino law [REF]. For a scalar field φ the partial derivative does obey the tensor transformation law for a co-vector, demonstraed here

$$\frac{\partial}{\partial \tilde{x}^\mu} \tilde{\varphi} = \frac{\partial}{\partial \tilde{x}^\mu} \varphi, \tag{1.3.28}$$

$$= \frac{\partial x^\nu}{\partial \tilde{x}^\mu} \frac{\partial}{\partial x^\nu} \varphi \tag{1.3.29}$$

and therefore the components $\partial_\mu \varphi$ transform like a co-vector. Note the fact $\varphi = \tilde{\varphi}$ as a scalar remains unchanged in a coordinate transformation. Unfortunately, when taking the partial derivative of any other tensor we do not receive a new tensor; let's demonstrate this with a vector X.

$$\frac{\partial}{\partial \tilde{x}^\mu} \tilde{X}^\alpha = \frac{\partial}{\partial \tilde{x}^\mu}\left(\frac{\partial \tilde{x}^\alpha}{\partial x^\beta} X^\beta\right), \tag{1.3.30}$$

$$= \frac{\partial x^\nu}{\partial \tilde{x}^\mu} \frac{\partial}{\partial \tilde{x}^\nu}\left(\frac{\partial \tilde{x}^\alpha}{\partial x^\beta} X^\beta\right), \tag{1.3.31}$$

$$= \underbrace{\frac{\partial \tilde{x}^\alpha}{\partial x^\beta} \frac{\partial x^\nu}{\partial \tilde{x}^\mu}}_{\text{Tensor transformation law}} \frac{\partial}{\partial \tilde{x}^\nu} X^\beta + X^\beta \frac{\partial x^\nu}{\partial \tilde{x}^\mu} \frac{\partial}{\partial \tilde{x}^\nu}\left(\frac{\partial \tilde{x}^\alpha}{\partial x^\beta}\right), \tag{1.3.32}$$

$$\tag{1.3.33}$$

and only the term on the right obeys the tensor transformation law. Interestingly, if we take the exterior

derivative from [REF dA] we see it transforms like

$$\frac{\partial}{\partial \tilde{x}^\mu} \tilde{A}_\nu - \frac{\partial}{\partial \tilde{x}^\nu} \tilde{A}_\mu = \frac{\partial x^\rho}{\partial \tilde{x}^\mu} \frac{\partial}{\partial x^\rho} \left(\frac{\partial x^\sigma}{\partial \tilde{x}^\nu} A_\sigma \right) - \frac{\partial x^\sigma}{\partial \tilde{x}^\nu} \frac{\partial}{\partial x^\sigma} \left(\frac{\partial x^\rho}{\partial \tilde{x}^\mu} A_\rho \right), \tag{1.3.34}$$

$$= \frac{\partial x^\rho}{\partial \tilde{x}^\mu} \frac{\partial x^\sigma}{\partial \tilde{x}^\nu} \left(\frac{\partial}{\partial x^\rho} A_\sigma - \frac{\partial}{\partial x^\sigma} A_\rho \right) + \frac{\partial x^\rho}{\partial \tilde{x}^\mu} \frac{\partial}{\partial x^\rho} \left(\frac{\partial x^\sigma}{\partial \tilde{x}^\nu} \right) A_\sigma - \frac{\partial x^\sigma}{\partial \tilde{x}^\nu} \frac{\partial}{\partial x^\sigma} \left(\frac{\partial x^\rho}{\partial \tilde{x}^\mu} \right) A_\rho, \tag{1.3.35}$$

$$= \frac{\partial x^\rho}{\partial \tilde{x}^\mu} \frac{\partial x^\sigma}{\partial \tilde{x}^\nu} \left(\frac{\partial}{\partial x^\rho} A_\sigma - \frac{\partial}{\partial x^\sigma} A_\rho \right) + \left(\frac{\partial^2 x^\rho}{\partial x^\mu \partial \tilde{x}^\nu} - \frac{\partial^2 x^\rho}{\partial \tilde{x}^\nu \partial \tilde{x}^\mu} \right) A_\rho, \tag{1.3.36}$$

$$= \frac{\partial x^\rho}{\partial \tilde{x}^\mu} \frac{\partial x^\sigma}{\partial \tilde{x}^\nu} \left(\frac{\partial}{\partial x^\rho} A_\sigma - \frac{\partial}{\partial x^\sigma} A_\rho \right), \tag{1.3.37}$$

and the tensor tranformation law is obeyed.

The final type of derivative we need is the Lie deivative, denoted $\mathcal{L}$. This maps a (p,q) tensor to a (p,q) tensor, acting as more of a directional derivative with respect to some vector X. It represents to rate of change of an object with respect to the inverse mapping of an infinitessimal diffeomorphism locally along vector X^μ [WRITE THIS BETTER]. Copy Lie reriv def here. A common Lie derivative is the derivative of a vector [DO] and the metric [DO] which leads to killings equaiton.

talk about linearity and liebnitz rule [check correct definitino] derive covariant deriv and torsion free, metric compatibility.

1.3.6 Integrating Forms on Manifolds

1.3.7 Length and Geodesics on Manifolds

The natural entry point for studying calculus on manifolds it to revisit Pythagoras' theorem. For this we need a manifold $\mathcal{M}$ equipped with a metric g, written as $(\mathcal{M}, g)$ for short. [MAYBE NATURAL POINT IS LIE/OUTER DERIVS] The distance $\mathrm{d}s$ between two infinitessimaly close points $p \in \mathcal{M}$ and $p + \delta p \in \mathcal{M}$, with coordinates x^μ and $x^\mu + \mathrm{d}x^\mu$, is given by

$$\mathrm{d}s^2 = g_{\mu\nu} \mathrm{d}x^\mu \mathrm{d}x^\nu, \tag{1.3.38}$$

where $g_{\mu\nu}$ are the components of the metric tensor. This is the generalisation of Eq. (1.3.2) to curved space; noteably the line element can now have smoothly varying coefficients from $g_{\mu\nu}$ and cross terms such as $\mathrm{d}x\mathrm{d}y$. The special choice of $g_{\mu\nu} = \delta_{\mu\nu}$ gives us flat space, also called Euclidean space, where $\delta_{\mu\nu} = 1$ if $\mu = \nu$ and vanishes otherwise. With the line elemend defines, we can immediately apply it to calculating the length of a general curve in curved space. Consider the curve Γ consisting of a set of smoothly connected points $p(\lambda) \in \mathcal{M}$ smoothly parameterised by λ. We can calculate the length Δs of the curve between $\lambda_1 \geq \lambda \geq \lambda_0$ by

$$\mathrm{d}s^2 = \frac{\partial x^\mu}{\partial \lambda} \frac{\partial x^\nu}{\partial \lambda} g_{\mu\nu} \mathrm{d}\lambda^2, \tag{1.3.39}$$

$$\Delta s = \int_{\lambda_0}^{\lambda_1} \sqrt{\left(\frac{\partial x^\mu}{\partial \lambda} \frac{\partial x^\nu}{\partial \lambda} g_{\mu\nu} \right)} \mathrm{d}\lambda. \tag{1.3.40}$$

In the simplified case where λ is one of the coordinates, say ξ, the length Δs becomes,

$$\Delta s = \int_{\xi_0}^{\xi_1} \sqrt{g_{\xi\xi}} \mathrm{d}\xi. \tag{1.3.41}$$

Now that lengths on manifolds have been discussed, we can approach volumes on manifolds. Take an N dimensional manifold with metric $(\mathcal{M}, g)$ with coordinates $\{x_1, x_2, ..., x_N\}$.

line elements, integrals and derivatives? Generalise this to algebraic metric rather than constant kroneka delta metric. Give exmaple in spherical polars. Maybe use this to calculate areas/lengths. Maybe insert picture of sphere. Insert proof that root det g is needed for volume elment from transforming a generic metric from one coord system to another? maybe need to invoke diff forms?

For a manifold equipped with metric $(\mathcal{M}, g)$ the curve with shortest distance between two points $p, q \in \mathcal{M}$ is called a geodesic. To find the geodesic joining p and q we need to use calculus of variation on the total length Δs from Eq. (1.3.40) of a general curve between two points. Given that the integrand $\mathcal{L}$ of Eq. (1.3.40) is a function like $\mathcal{L}(x^\mu, \dot{x}^\mu)$, where the dot means differentiation by λ, we can use the Eular-Lagrange equation,

$$\frac{\partial \mathcal{L}}{\partial x^\mu} - \frac{\mathrm{d}}{\mathrm{d}\lambda} \frac{\partial \mathcal{L}}{\partial \dot{x}^\mu} = 0 \tag{1.3.42}$$

to give a differential equation with solution being a geodesic. Applyin the EL equation to the integrand of Eq. (1.3.40) is algebraically messy, it is easier to square the integrand and start from $\mathcal{L}^2$ giving the same solution [EXPLAIN THIS BETTER]

$$\frac{\partial \mathcal{L}^2}{\partial x^\alpha} - \frac{\mathrm{d}}{\mathrm{d}\lambda} \frac{\partial \mathcal{L}^2}{\partial \dot{x}^\alpha} = 0, \tag{1.3.43}$$

$$\frac{\partial}{\partial x^\alpha} \left(g_{\mu\nu} \dot{x}^\mu \dot{x}^\nu \right) - \frac{\mathrm{d}}{\mathrm{d}\lambda} \frac{\partial}{\partial \dot{x}^\alpha} \left(g_{\mu\nu} \dot{x}^\mu \dot{x}^\nu \right) = 0, \tag{1.3.44}$$

$$(\partial_\alpha g_{\mu\nu}) \dot{x}^\mu \dot{x}^\nu - 2 \frac{\mathrm{d}}{\mathrm{d}\lambda} \left(g_{\alpha\nu} \dot{x}^\nu \right) = 0, \tag{1.3.45}$$

$$(\partial_\alpha g_{\mu\nu}) \dot{x}^\mu \dot{x}^\nu - 2 \left(\dot{x}^\rho \partial_\rho \left(g_{\alpha\nu} \right) \dot{x}^\nu \right) - 2 \ddot{x}^\nu g_{\alpha\nu} = 0. \tag{1.3.46}$$

Rearranging and multiplying by $g^{\alpha\beta}$ gives

$$\ddot{x}^\beta + \frac{1}{2} g^{\alpha\beta} \left(\partial_\mu g_{\alpha\nu} + \partial_\nu g_{\alpha\mu} - \partial_\alpha g_{\mu\nu} \right) \dot{x}^\mu \dot{x}^\nu = 0, \tag{1.3.47}$$

$$\ddot{x}^\beta + \Gamma^\beta{}_{\mu\nu} \dot{x}^\mu \dot{x}^\nu = 0, \tag{1.3.48}$$

where $\Gamma^\beta{}_{\mu\nu}$ is the components of the connection-symbol from Eq. (**??**). A trivial solution to Eq. (1.3.48) is in flat space using cartesian coordinates where $\Gamma^\beta{}_{\mu\nu} = 0$ and therefore $\ddot{x}^\beta = 0$ so $\dot{x}^\beta$ is a constant; this tells us the shortest distance between two points in flat space is a straight line. In other words, geodesics are straight lines in flat space.

1.3.8 Maps Between Manifolds

In this work we will be interested in the mapping of objects between two manifolds M and N of similar dimension [VERIFY]. This has many uses such as finding the metric (or any tensor) on an embedded surface and very importantly allowed us to perform the 3+1 decomposition [REF] on a spacetime.

Let's start by defining a smooth map $\Phi : M \to N$ between manifolds on some coordinate patch; we will always deal with maps that have a smooth inverse $\Phi^{-1} : N \to M$ which are diffeomorphisms. Two common examples of diffeomorphisms are coordinate changes and translations [CHECK]. Labelling coordinates $x^\mu \in M$ and $y^\mu \in N$ the map $\Phi : x^\mu \to y^\mu$ is equivalent to $y^\mu(x^\nu)$. Scalar functions must also map trivially $f_N(y^\mu(x^\nu)) = f_M(x^\mu)$ where $f_N \in N$ and $f_M \in M$, thus we will no longer identify which manifold a function is on. Looking back to [REF] we define a vector field $\boldsymbol{X} = X^\mu \partial_\mu$ on M, the abstract object $\boldsymbol{X}$ should be pushed from M to N in a way such that it's action on a function f is the same in either manifold. Given that

$$\boldsymbol{X}(f) = X^\mu \frac{\partial f}{\partial x^\mu} = \left(X^\mu \frac{\partial y^\nu}{\partial x^\mu} \right) \frac{\partial f}{\partial y^\nu} = (\Phi_* X^\mu) \frac{\partial f}{\partial y^\nu} = \Phi_* \boldsymbol{X}(\Phi : f), \tag{1.3.49}$$

where $\Phi_* \boldsymbol{X} \in N$ denotes the push-foreward of $\boldsymbol{X}$, we can calculate the push-foreward of vector field components like

$$(\Phi_* X)^\mu = \frac{\partial y^\mu}{\partial x^\nu} X^\nu. \tag{1.3.50}$$

Given a co-vector field $\boldsymbol{\omega} \in N$ we can pull the field back from $N \to M$, denoted $\Phi^* \boldsymbol{\omega}$, by demanding that $\Phi^* \boldsymbol{\omega}(\boldsymbol{X}) \in M = \boldsymbol{\omega}(\Phi_* \boldsymbol{X}) \in N$. Evaluating this gives

$$\Phi^* \boldsymbol{\omega}(\boldsymbol{X}) = (\Phi^* \omega)_\mu X^\mu, \tag{1.3.51}$$

$$\boldsymbol{\omega}(\Phi_* \boldsymbol{X}) = \omega_\nu (\Phi_* X)^\nu = \omega_\nu \frac{\partial y^\nu}{\partial x^\mu} X^\mu, \tag{1.3.52}$$

$$(\Phi^* \omega)_\mu = \omega_\nu \frac{\partial y^\nu}{\partial x^\mu}. \tag{1.3.53}$$

Considering an $(0,2)$ tensor $\boldsymbol{T} \in N$ the pullback $\Phi^* \boldsymbol{T} \in M$ follows simply from demanding that $\boldsymbol{T}\Phi_* \boldsymbol{X}, \Phi_* \boldsymbol{Y} = \Phi^* \boldsymbol{T}(\boldsymbol{X}, \boldsymbol{Y})$ where $\boldsymbol{X}$ and $\boldsymbol{Y}$ are vector fields on M. The components of the pull-back of $\boldsymbol{T}$ are therefore

$$(\Phi^* T)_{\mu\nu} = \frac{\partial y^\rho}{\partial x^\mu} \frac{\partial y^\sigma}{\partial x^\nu} T_{\rho\sigma}. \tag{1.3.54}$$

The pull-back of a generic $(0,q)$ tensor and the push-foreward of a generic $(p,0)$ tensor can be found similarly.

So far we have only discussed the mapping $\Phi : M \to N$, which was required to have a well behaved $\partial y^\nu / \partial x^\mu$. In the case $y^\nu(x^\mu)$ has a smooth inverse $x^\nu(y^\mu)$, and therefore a well behaved $\partial x^\nu / \partial y^\mu$, we have a smooth inverse map $\Phi^{-1} : N \to M$ and the mapping Φ is a diffeomorphism. When Φ is a diffeomorphism we can then also define the pull-back of $(p,0)$ tensors from N to M along with the push-foreward of $(0,q)$ tensors from M to N.

As mentioned, a good use of this formalism is to find the metric on an embedded surface. Starting from an m dimensional manifold M with metric $g_{\mu\nu}$ and coordinates x^μ we consider an embedded n dimensional surface N where $n < m$. We can treat N as a separate n dimensional manifold with metric $h_{\mu\nu}$. MAYBGE PUT THIS LATER AS THIS REQUIRES PROJECTIONS.

We have now discussed the necesary formalism to define the Lie derivative. The Lie derivative at a point is the rate of change of a tensor field with respect to a pull-back from a diffeomorphism Φ mapping infinitessimally close points $p, q \in \mathcal{M}$ like $\Phi : p = x^\mu \to q = x^\mu + \epsilon \xi^\mu$ for some vector field ξ. The simplest example is the Lie derivative of a scalar field ϕ, denoted $\mathcal{L}_\xi \phi$ with respect to vector field $\boldsymbol{\xi}$, is

$$\mathcal{L}_\xi \phi = \lim_{\epsilon \to 0} \left[\frac{\Phi^* \phi|_q - \phi|_p}{\epsilon} \right], \tag{1.3.55}$$

$$= \lim_{\epsilon \to 0} \left[\frac{\phi(x^\mu + \epsilon \xi^\mu) - \phi(x^\mu)}{\epsilon} \right], \tag{1.3.56}$$

$$= \xi^\mu \partial_\mu \phi, \tag{1.3.57}$$

which reduces to the directional derivative of ϕ with respect to $\boldsymbol{\xi}$. Next let's calculate the Lie derivative of a vector field $\boldsymbol{X}$ with respect to vector field $\boldsymbol{\xi}$. Starting with the same definition as Eq. (1.3.58), and

using $y^\mu = x^\mu + \epsilon\xi^\mu$, the Lie derivative of $\boldsymbol{X}$ is

$$(\mathcal{L}_\xi X)^\mu = \lim_{\epsilon \to 0} \left[\frac{(\Phi^* X|_q)^\mu - X|_p{}^\mu}{\epsilon} \right], \tag{1.3.58}$$

$$= \lim_{\epsilon \to 0} \left[\frac{\frac{\partial x^\mu}{\partial y^\nu} X^\nu(x^\rho + \epsilon\xi^\rho) - X^\mu(x^\rho)}{\epsilon} \right], \tag{1.3.59}$$

$$= \lim_{\epsilon \to 0} \left[\frac{(\delta^\mu_\nu - \epsilon\partial_\nu\xi^\mu)X^\nu(x^\rho + \epsilon\xi^\rho) - X^\mu(x^\rho)}{\epsilon} \right], \tag{1.3.60}$$

$$= \lim_{\epsilon \to 0} \left[\frac{-\epsilon\partial_\nu\xi^\mu X^\nu(x^\rho + \epsilon\xi^\rho) + X^\mu(x^\rho + \epsilon\xi^\rho) - X^\mu(x^\rho)}{\epsilon} \right], \tag{1.3.61}$$

$$= \lim_{\epsilon \to 0} \left[\frac{-\epsilon\partial_\nu\xi^\mu X^\nu(x^\rho) + X^\mu(x^\rho + \epsilon\xi^\rho) - X^\mu(x^\rho) + \mathcal{O}(\epsilon^2)}{\epsilon} \right], \tag{1.3.62}$$

$$= \xi^\nu\partial_\nu X^\mu - X^\nu\partial_\nu\xi^\mu. \tag{1.3.63}$$

The Lie derivative for co-vectors and tensors can be derived in the same way, but can be quickly derived from the Liebnitz rule as follows. Define a scalar field ψ, vector field $\boldsymbol{X}$ and co-vector field $\boldsymbol{\omega}$, where $\psi = X^\mu\omega_\mu$, then it follows that

$$\mathcal{L}_\xi\psi = \xi^\mu\partial_\mu\psi = X^\nu\xi^\mu\partial_\mu\omega_\nu + \omega_\nu\xi^\mu\partial_\mu X^\nu, \tag{1.3.64}$$

$$= \mathcal{L}_\xi(X^\mu\omega_\mu), \tag{1.3.65}$$

$$= \omega_\mu(\mathcal{L}_\xi X)^\mu + X^\mu(\mathcal{L}_\xi\omega)_\mu, \tag{1.3.66}$$

$$X^\mu(\mathcal{L}_\xi\omega)_\mu = X^\nu\xi^\mu\partial_\mu\omega_\nu + \omega_\nu\xi^\mu\partial_\mu X^\nu - \omega_\mu(\mathcal{L}_\xi X)^\mu, \tag{1.3.67}$$

$$(\mathcal{L}_\xi\omega)_\mu = \xi^\nu\partial_\nu\omega_\mu + \omega_\nu\partial_\mu\xi^\nu. \tag{1.3.68}$$

As it turns out, any Lie derivative can replace all partial derivatives with covariant derivatives ∇ due to the connection/Christoffel symbols cancelling.

A special example of a Lie derivative is of the metric tensor, $\boldsymbol{g}$, giving

$$(\mathcal{L}_\xi g)_{\mu\nu} = \xi^\rho\partial_\rho g_{\mu\nu} + g_{\rho\nu}\partial_\mu\xi^\rho + + g_{\mu\rho}\partial_\nu\xi^\rho, \tag{1.3.69}$$

$$= \xi^\rho\underbrace{\nabla_\rho g_{\mu\nu}}_{=0} + g_{\rho\nu}\nabla_\mu\xi^\rho + g_{\mu\rho}\nabla_\nu\xi^\rho, \tag{1.3.70}$$

$$\tag{1.3.71}$$

where $\nabla_\rho g_{\mu\nu} = 0$ is assumed from metric compatibility in [REF]. In the case the Lie derivative vanishes we get Killing's equation

$$\nabla_\mu\xi_\nu + \nabla_\nu\xi_\mu = 0 \tag{1.3.72}$$

and a vector field $\boldsymbol{\xi}$ satisfying Killing's equation is called a Killing vector. [MENTION IS MENAS CONSERVATINO OF ENERGY-MOM HERE?]

special case lei metric

1.4 General Relativity

General Relativity is the theory of gravity

Einstein vacuum eqn, then add matter, maybe horizons and black holes stuff. check harvey/tong gr/bh notes for inspiration.

specific solutions like minkowski, gravitational waves, BH's, NS'

1.4.1 The Einstein Equation

[MAYBE SPLIT THE VACUUMMSPACETIME TO ANOTHER SECTION]

At the core of General Relativity is the Einstein Equation

$$G_{\mu\nu} = \frac{8\pi G}{c^4} T_{\mu\nu}, \tag{1.4.1}$$

also called the Einstein Field Equations, relating spacetime curvature encoded in the Einstein tensor $G_{\mu\nu}$ to the matter distribution described by the stress tensor $T_{\mu\nu}$. To be able to solve this equation we also need to insert a curvature dependant equation of motion to dictate how matter moves. This leads nicely to J. Wheeler's insightful one line summary of general relativity:

"Spacetime tells matter how to move; matter tells spacetime how to curve."

In the case of a vacuum spacetime with $T_{\mu\nu} = 0$, or one where the matter distribution is supposed to be so small that it does not cause a spacetime curvature backreaction, the Einstein equation simplifies greatly to

$$G_{\mu\nu} = 0. \tag{1.4.2}$$

Taking the trace of the above equation and the definition of $G_{\mu\nu}$ in Eq. (REF), we can see that

$$g^{\mu\nu} G_{\mu\nu} = 0 = g^{\mu\nu}(R_{\mu\nu} - \frac{1}{2} R g_{\mu\nu}) = R(1 - \frac{D}{2}), \tag{1.4.3}$$

where D is the number of spacetime dimensions. Clearly for $D \neq 2$ a vanishing einstein implies a vanishing Ricci scalar R; if the Ricci scalar vanishes then $G_{\mu\nu} = R_{\mu\nu}$ and the Einstein equation in vacuum simplifies to

$$R_{\mu\nu} = 0. \tag{1.4.4}$$

In the special case of $D = 2$ it can be shown that $R_{\mu\nu} = R g_{\mu\nu}/2$ [MAYBE REF EARLIER SECTION ON RIEMANN TENSOR] and the Einstein tensor $G_{\mu\nu} \equiv 0$ which renders Einstein's equation nonsensical. [CHECK THIS]

1.4.2 Matter in General Relativity

1.4.3 The Cosmological Constant

1.4.4 The Lagrangean Formulation of General Relativity

[ADD SOME MOTIVATION OF WHY WE LIKE LAGRANGEANS, EASY TO QUNATIZE OR ADD MORE MATTER RO INTERACTIONS OF MATTER?

1.4.5 Low Curvature Limit of General Relativity

An important use of General Relativity is it's use in the low curvature limit. The simplest example of this would be Special Relativity; if General Relativity i[DO] reproduce Special Relativity in the limit of vanishing curvature then it is. We work with the assumption of a vacuum spacetime with no Cosmological constant and seek solutions to the Einstein equation with metric $g_{\mu\nu} = \eta_{\mu\nu}$ where

$$\eta_{\mu\nu} = \begin{pmatrix} -1 & 0 & 0 & 0 \\ 0 & 1 & 0 & 0 \\ 0 & 0 & 1 & 0 \\ 0 & 0 & 0 & 1 \end{pmatrix} \tag{1.4.5}$$

in Cartesian coordinates. As seen before, in Eq.[REF]REF the Einstein equation in vacuum simplfies to just a vanishing Ricci tensor,

$$R_{\mu\nu} = 0, \tag{1.4.6}$$

$$= \partial_\rho \Gamma^\rho{}_{\mu\nu} - \partial_\nu \Gamma^\rho{}_{\mu\rho} + \Gamma^\rho{}_{\rho\sigma} \Gamma^\sigma{}_{\mu\nu} - \Gamma^\rho{}_{\mu\sigma} \Gamma^\sigma{}_{\rho\nu}. \tag{1.4.7}$$

Given that the Connection symbols $\Gamma^{\mu}{}_{\nu\rho}$ vanish everywhere for the metric components $\eta_{\mu\nu}$ then Eq. (1.4.6) is trivially satisfied and we have proved that Special Relativity is the zero-curvature limit of GR.

Relaxing the condition $g_{\mu\nu} = \eta_{\mu\nu}$ to $g_{\mu\nu} = \eta_{\mu\nu} + h_{\mu\nu}$, where the components $h_{\mu\nu} \ll 1$, we can create a vacuum spacetime consisting of small curvature fluctuations; this turns out to describe gravitational waves. Ignoring terms of order $\mathcal{O}(h^2)$ we can see that

$$g^{\mu\nu} = \eta^{\mu\nu} - h^{\mu\nu}, \tag{1.4.8}$$

$$h^{\rho\sigma} = \eta^{\mu\rho}\eta^{\nu\sigma}h_{\mu\nu}, \tag{1.4.9}$$

$$g^{\mu\nu}g_{\nu\rho} = \delta^{\mu}_{\rho} = \eta^{\mu\nu}\eta_{\nu\rho} + \eta^{\mu\nu}h_{\nu\rho} - h^{\mu\nu}\eta_{\nu\rho} + \mathcal{O}(h^2), \tag{1.4.10}$$

$$= \delta^{\mu}_{\rho} + \eta^{\mu\nu}h_{\nu\rho} - \eta^{\mu\alpha}\eta^{\nu\beta}h_{\alpha\beta}\eta_{\nu\rho}, \tag{1.4.11}$$

$$= \delta^{\mu}_{\rho} + \underbrace{\eta^{\mu\nu}h_{\nu\rho} - \eta^{\mu\alpha}h_{\alpha\rho}}_{=0}. \tag{1.4.12}$$

Note that we raise/lower the indeces of $h_{\mu\nu}/h^{\mu\nu}$ with $\boldsymbol{\eta}$ and not $\boldsymbol{g}$. Looking at the connection symbols and Ricci tensor while ignoring $\mathcal{O}(h^2)$ terms we get

$$\Gamma^{\rho}{}_{\mu\nu} = \frac{1}{2}\left(\eta^{\rho\sigma} - h^{\rho\sigma}\right)\left(\partial_{\mu}(\eta_{\sigma\nu} + h_{\sigma\nu}) + \partial_{\nu}(\eta_{\mu\sigma} + h_{\mu\sigma}) - \partial_{\sigma}(\eta_{\mu\nu} + h_{\mu\nu})\right), \tag{1.4.13}$$

$$= \frac{1}{2}\eta^{\rho\sigma}\left(\partial_{\mu}h_{\sigma\nu} + \partial_{\nu}h_{\mu\sigma} - \partial_{\sigma}h_{\mu\nu}\right) + \mathcal{O}(h^2), \tag{1.4.14}$$

$$R_{\mu\nu} = \partial_{\rho}\Gamma^{\rho}{}_{\mu\nu} - \partial_{\nu}\Gamma^{\rho}{}_{\mu\rho} + \mathcal{O}(h^2), \tag{1.4.15}$$

$$= \frac{1}{2}\eta^{\rho\sigma}\left(\partial_{\rho}\partial_{\mu}h_{\sigma\nu} - \partial_{\rho}\partial_{\sigma}h_{\mu\nu} - \partial_{\nu}\partial_{\mu}h_{\sigma\rho} + \partial_{\sigma}\partial_{\mu}h_{\rho\mu}\right) + \mathcal{O}(h^2), \tag{1.4.16}$$

$$R = (\eta^{\mu\nu} - h^{\mu\nu})R_{\mu\nu}, \tag{1.4.17}$$

$$= \eta^{\mu\nu}\eta^{\rho\sigma}(\partial_{\mu}\partial_{\rho}h_{\sigma\nu} - \partial_{\sigma}\partial_{\rho}h_{\mu\nu}) + \mathcal{O}(h^2). \tag{1.4.18}$$

To simplify the solving of Einsteins eqn [FIX THIS] we can consider coordinate transformation like $x^{\mu} \to x^{\mu} + \zeta^{\mu}$ where $\zeta^{\mu} \ll 1$. It can easily be shown that to first order in ζ^{μ} and $h_{\mu\nu}$ that $h_{\mu\nu}$ transforms like

$$h_{\mu\nu} \to h_{\mu\nu} + \partial_{\mu}\zeta_{\nu} + \partial_{\nu}\zeta_{\mu} \tag{1.4.19}$$

where raising/lowering the indeces of $\boldsymbol{\zeta}$ is done with $\boldsymbol{\eta}$ as terms of order $\mathcal{O}(h)\mathcal{O}(\zeta)$ are ignored.

Note [TALK ABOUT G PLUS H RATHER THAN ETA PLUS H FOR BH RINGDOWN AND MAYBE BS STABILITY? THIS IS MORE PERTURBATION THEORY THOUGH]

[MENTION : GW'S, PRECESSION, LIGHT DEFLECTION, TIME DILATION AROUND EARTH/-SUN, MAYBE MENTION INTERSTELLAR'S TIME DILATION? ARE THESE REALLY LOW ENERGY LIMIT? MENTION POST NEWTONIAN OTHER THINGS?]

1.5 Stuff

wheeler quote, matter tells space how to curve, adn space tells matter how to move.

GRChombo section?

einstein summation conventions? and upstiars/downstairs incedes in conventions

distinguish between tensors and tensor fields (especially in teh d/dlambda and X bit)

maybe work coordinate transformation into the text earlier with ther introduction of vectors? maybe split the long diff geom section (fucntions curves and tensors) into two sections, functions curves, coords trans, vectors part 1 then covectors, tensors and tensor transformation part 2, forms part 3 then differentiation then calculuas?

mention SR and the fact that GR is based on the equivalence principles (weak and strong?) somewhere
.

maybe make SR as a solution to the Einstein eqation a different section to just SR.

decide when to use SR and GR acronyms

1887 Michelson-Morley to find aether that light moves on. Instead found not true. laws of physics are the same in all frames. Assming these two things Einstein derived the Lorentz group.

connection/christoffel and capitalise or not?

talk about newman penrose scalars for GW extraction?

check capital letters

define trace

Chapter 2

Numerical Relativity

MAYBE PUT SOME STUFF HERE ABOUT NUMERICAL ALGORITHMS LIKE RK4 EULAR STEP LEAPFROG AND DO ERROR GROWTH RATES AND COURANT

2.1 Numerical Relativity

2.1.1 Spacetime Foliation

Einstein's equation is a classical field equation which governs the dynamics of physical objects and spacetime curvature.

$$R_{\mu\nu} - \frac{1}{2}Rg_{\mu\nu} = \frac{8\pi G}{c^4}T_{\mu\nu} \tag{2.1.1}$$

The above version is fully covariant, agnostic of the definition of time, and many solutions are known analytically, for instance Black Hole geometries. When the system of interest becomes more complicated, such as the case of orbiting objects which will be discussed later, finding an analytic expression becomes impossible. For low energy dynamics, Newtonian theory, Post-Newtonian theory and perturbation theory can make more progress; however this report will focus on the highly nonlinear regime where Numerical relativity is truly the only hope to solve Einstein's equations. To do this it is common to split spacetime into 3+1 dimensions, evolving a 3 dimensional manifold (maybe with matter) on a computer along the final 4th dimension. To do this we need to define a suitable hypersurface $\Sigma \in \mathcal{M}$. This is usually done by demanding the hypersurface Σ_t be the set of points $p \in \mathcal{M}$ where some scalar function $f : \mathcal{M} \mapsto \mathbb{R}$ satisfies $f(p) = t$. This hypersurface should be a Cauchy surface, intersecting all causal curves only once, or a partial Cauchy surface which intersects all causal curves at most once. Generally we will choose a partial Cauchy surface due to the finite memory of computers, however by picking certain compactified coordinates it is possible to use a Cauchy surface [ref]. A foliation $\mathcal{F}$ is then the union of a set of Σ_t for some range of the parameter t.

$$\mathcal{F} = \cup_t(\Sigma_t) \subseteq \mathcal{M}$$

This means we should be careful to pick a parameter t such that the foliation is not self intersecting for the parameter range that covers the region of $\mathcal{M}$ that we are interested in simulating. Fortunately the time coordinate in a suitable coordinate system works in all cases covered by this report; it also gives the physical interpretation of Σ_t being an instance of time. Now we should define unit normal vector n to Σ_t.

$$n^\mu = -\frac{\nabla^\mu t}{\sqrt{|g_{\mu\nu}\nabla^\mu t\nabla^\nu t|}} \quad \& \quad n_\mu = -\frac{dt_\mu}{\sqrt{|g_{\mu\nu}\nabla^\mu t\nabla^\nu t|}} \tag{2.1.2}$$

For simplicity we define the lapse function α to be

$$\alpha := \frac{1}{\sqrt{|g_{\mu\nu}\nabla^\mu t\nabla^\nu t|}} \tag{2.1.3}$$

giving us $n_\mu = -\alpha \mathrm{d}t_\mu$ as well as the normal evolution vector $m_\mu = \alpha n_\mu$. Defining two infinitessimaly close points $(p, q) \in (\Sigma_t, \Sigma_{t'})$ where $q^\mu = p^\mu + m^\mu \delta t$ we see

$$t(q) = t(p^\mu + m^\mu \delta t) = t(p) + \frac{\mathrm{d}t}{\mathrm{d}x^\mu} m^\mu \delta t = t(p) + \mathrm{d}t_\mu m^\mu \delta t = t(p) + \delta t$$

showing that m^μ points between neighbouring hypersurfaces; therefore when creating evolution equations we should care about Lie derivates along m^μ, $\mathcal{L}_m$, rather than $\mathcal{L}_n$.

2.1.2 The 3+1 Decomposition

With the notion of a spacetime foliation we should define how to project tensors onto Σ_t; clearly scalars need no projecting. Splitting a vector $X^\mu e_\mu = X^\mu_\parallel e_\mu + X^\mu_\perp e_\mu$ into components tangent or normal to Σ_t we define the orthogonal projector $\perp^\mu_\nu$ and parallel projector $-n^\mu n_\nu$.

$$X^\mu_\parallel = [\delta^\mu_\nu + n^\mu n_\nu] X^\mu = \perp^\mu_\nu X^\nu \tag{2.1.4}$$

$$X^\mu_\perp = -n^\mu n_\nu X^\nu \tag{2.1.5}$$

Considering scalars such as $\phi = w_\mu X^\mu$ or $\psi = T^{\mu\nu} w_\mu w_\nu$, and remembering scalars don't vary under projection, it is simple to show that any tensor T can be projected by contracting a projection operator $\perp$ on any free index.

$$T_\parallel^{ab\ldots}{}_{cd\ldots} = \mathcal{T}^{ab\ldots}{}_{cd\ldots} = \perp^a_A \perp^b_B \perp^C_c \perp^D_d \cdots T^{AB\ldots}{}_{CD\ldots} \tag{2.1.6}$$

We can find the 3 metric $\gamma_{\mu\nu}$ of Σ_t by projecting $g_{\mu\nu}$

$$\gamma_{ij} = \perp^\mu_i \perp^\nu_j g_{\mu\nu} = g_{\mu\nu} + n_\mu n_\nu \quad \rightarrow \quad \gamma^i_j = \perp^i_j \tag{2.1.7}$$

and we find it is equivalent to the projector $\perp$; this had to be the case as $\perp_{ij} \mathrm{d}x^i \mathrm{d}x^j$ gives the line element along Σ_t. With this machinery we can define the extrinsic curvature tensor $\mathcal{K}_{ij}$ representing curvature due to the choice of spacetime foliation; it could be nonzero for certain foliations of Minkowski space. It is not the same as the 3-Ricci tensor $\mathcal{R}_{ij}$ which is due to genuine spacetime curvature of $\mathcal{M}$ regardless of foliation. The extrinsic curvature tensor is defined the following way

$$\mathcal{K}_{ij} = \mathcal{K}_{ji} := - \perp^\mu_i \perp^\nu_j \nabla_\mu n_\nu = - \perp^\mu_i \nabla_\mu n_j = -\nabla_i n_j - n_i a_j \tag{2.1.8}$$

$$\mathcal{K} = \mathcal{K}^i_i = -\nabla \cdot n \tag{2.1.9}$$

where $a_i = n \cdot \nabla n_i$ is called the Eularian acceleration; it should be noted $\mathcal{K}_{ij}$ is symmetric. It can also be shown to take the following form

$$\mathcal{K}_{ij} = -\frac{1}{2} \mathcal{L}_n \gamma_{ij} = -\frac{1}{2\alpha} \mathcal{L}_m \gamma_{ij} \tag{2.1.10}$$

which gives the intuitive explanation of $\mathcal{K}_{ij}$ being the rate of change of the 3-metric γ_{ij} with respect to the foliation. The next object we should discuss is the projected covariant 3-derivative $\mathcal{D}_i$. This is the covariant derivative belonging to Σ_t and hence it's arguments should be tensors belonging to Σ_t. This means we can define it as so

$$T^{ab\ldots}{}_{cd\ldots} = \perp^a_A \perp^b_B \perp^C_c \perp^D_d \cdots T^{AB\ldots}{}_{CD\ldots}, \tag{2.1.11}$$

$$\mathcal{D}_\mu \mathcal{T}^{ab\ldots}{}_{cd\ldots} := \perp^\nu_\mu \perp^a_A \perp^b_B \perp^C_c \perp^D_d \nabla_\nu \mathcal{T}^{AB\ldots}{}_{CD\ldots}. \tag{2.1.12}$$

A simple example is the derivative of a vector $X^i e_i \in \mathcal{T}(\Sigma_t)$

$$\mathcal{D}_i X^j = \partial_i X^j + \Upsilon^i{}_{jk} X^k$$

$$\Upsilon^i{}_{jk} = \frac{1}{2} \gamma^{il} [\partial_j \gamma_{lk} + \partial_k \gamma_{jk} - \partial_l \gamma_{jk}] \tag{2.1.13}$$

where $\Upsilon^i_{\ jk}$ is the Christoffel symbol of Σ_t. Another useful example is a^μ which can be equated to

$$a_\mu = n \cdot \nabla n_\mu = \mathcal{D}_\mu \ln \alpha = \frac{1}{\alpha} \mathcal{D}_\mu \alpha$$

and allows us to evaluate the Lie derivative of the projector $\perp^i_j$.

$$\mathcal{L}_m \perp^i_j = \alpha n^k \nabla_k \perp^i_j + \perp^i_k \nabla_j \alpha n^k - \perp^k_j \nabla_k \alpha m^i = \alpha n^k \nabla_k \left[n^i n_j \right] + \alpha \nabla_j n^i - \left[\alpha K^i_j + n^i \mathcal{D}_j \alpha \right] = 0$$

The result $\mathcal{L}_m \perp^i_j = 0$ is incredibly important, it tells us that the projector commutes with $\mathcal{L}_m$ and as a result any tensor T which when projected onto Σ_t, written $\mathcal{T}$, satisfies

$$\mathcal{L}_m \mathcal{T}^{ab...}_{\quad cd...} = \perp^a_A \perp^b_B \perp^C_c \perp^D_d \ \mathcal{L}_m \mathcal{T}^{AB...}_{\quad CD...}. \tag{2.1.14}$$

or in other words, evolving a projected tensor along integral curves of m leaves the tensor parallel to Σ_t.

2.1.3 Gauss, Codazzi and Ricci Equations

We now have all the results we need to decompose the Riemann and Ricci tensors and scalar. From the definition of the Riemann tensor we know

$$[\mathcal{D}_\alpha \mathcal{D}_\beta - \mathcal{D}_\beta \mathcal{D}_\alpha]v^\gamma = \mathcal{R}^\gamma_{\ \lambda\alpha\beta}v^\lambda,$$
$$[\nabla_\alpha \nabla_\beta - \nabla_\beta \nabla_\alpha]v^\gamma = R^\gamma_{\ \lambda\alpha\beta}v^\lambda,$$

where the vector $v^\lambda = \perp^\lambda_\rho v^\rho$ is tangent to Σ_t. Expanding the $\mathcal{D}$'s into ∇'s gives

$$\mathcal{D}_\alpha \mathcal{D}_\beta v^\gamma = \perp^\mu_\alpha \perp^\sigma_\beta \perp^\gamma_\xi \nabla_\mu (\perp^\nu_\sigma \perp^\xi_\rho \nabla_\nu v^\rho)$$

and using the following properties; impotence of projections $\perp^\alpha_\mu \perp^\mu_\beta = \perp^\alpha_\beta$, null projection of orthogonal vectors $\perp n = 0$, metric compatibility $\nabla_\mu \perp^\alpha_\beta = n_\beta \nabla_\mu n^\alpha + n^\alpha \nabla_\mu n_\beta$ and equation () for $\mathcal{K}_{ij}$ we obtain the Gauss relation.

$$\perp^\mu_\alpha \perp^\nu_\beta \perp^\gamma_\rho \perp^\sigma_\delta \ R^\rho_{\ \sigma\mu\nu} = \mathcal{R}^\gamma_{\ \delta\alpha\beta} + \mathcal{K}^\gamma_\alpha \mathcal{K}_{\delta\beta} - \mathcal{K}^\gamma_\beta \mathcal{K}_{\alpha\delta} \tag{2.1.15}$$

Contracting over α, γ above and relabelling indices we get the contracted Gauss relation.

$$\perp^\mu_\alpha \perp^\nu_\beta \ R_{\mu\nu} + \gamma_{\alpha\mu} n^\nu \perp^\rho_\beta n^\sigma R^\mu_{\ \nu\rho\sigma} = \mathcal{R}_{\alpha\beta} + \mathcal{K}\mathcal{K}_{\alpha\beta} - \mathcal{K}^\mu_\beta \mathcal{K}_{\alpha\mu} \tag{2.1.16}$$

Contracting again and realising $R_{abcd}n^a n^b n^c n^d = 0$ from antisymmetry in indeces 0,1 or 2,3 in the Riemann tensor gives the scalar Gauss equation.

$$R + 2R_{\mu\nu}n^\mu n^\nu = \mathcal{R} + \mathcal{K}^2 - \mathcal{K}_{\mu\nu}\mathcal{K}^{\mu\nu} \tag{2.1.17}$$

The Codazzi relations are derived from a different start point

$$[\nabla_\alpha \nabla_\beta - \nabla_\beta \nabla_\alpha]n^\gamma = R^\gamma_{\ \lambda\alpha\beta}n^\lambda$$

and project down with 3 operators $\perp\perp\perp$. The following relations are used

$$\nabla_\beta n^\gamma = -\mathcal{K}^\gamma_{\ \beta} - a^\gamma n_\beta,$$
$$\perp^\alpha_\mu \perp^\beta_\nu \perp^\rho_\gamma \nabla_\alpha \nabla_\beta n^\gamma = -\mathcal{D}_\alpha \mathcal{K}^\gamma_{\ \beta} + a^\gamma \mathcal{K}_{\alpha\beta},$$

which lead immediately to the Codazzi relation

$$\perp^\mu_\alpha \perp^\nu_\beta \perp^\gamma_\rho \ n^\sigma R^\rho_{\ \sigma\mu\nu} = \mathcal{D}_\beta \mathcal{K}^\gamma_{\ \alpha} - \mathcal{D}_\alpha \mathcal{K}^\gamma_{\ \beta} \tag{2.1.18}$$

and the contracted Codazzi relation.

$$\perp^{\mu}_{\alpha} n^{\nu} R_{\mu\nu} = \mathcal{D}_{\alpha}\mathcal{K} - \mathcal{D}_{\mu}\mathcal{K}^{\mu}_{\alpha} \tag{2.1.19}$$

Finally we turn our attention to the Ricci equation. We start with the Riemann term in the contracted Gauss equation,

$$\gamma_{\alpha\mu} \perp^{\rho}_{\beta} n^{\sigma} R^{\mu}_{\ \nu\rho\sigma} n^{\nu} = \gamma_{\alpha\mu} \perp^{\rho}_{\beta} n^{\sigma} \left[\nabla_{\rho}\nabla_{\sigma} - \nabla_{\sigma}\nabla_{\rho} \right] n^{\nu}$$

and using the following two formulae with equation (D ln a)

$$\nabla_{\sigma} n^{\mu} = -\mathcal{K}^{\mu}_{\ \sigma} - n^{\mu}\mathcal{D}_{\sigma}\ln(\alpha)$$

$$\mathcal{L}_m \mathcal{K}_{ij} = \perp^{a}_{i} \perp^{b}_{j} \mathcal{L}_m \mathcal{K}_{ab} = \perp^{a}_{i} \perp^{b}_{j} \left[\alpha n \cdot \nabla\mathcal{K}_{ab} + 2\mathcal{K}_{k(b}\nabla_{a)}m^k \right]$$

some algebra yields

$$\gamma_{\alpha\mu} n^{\sigma} \gamma^{\nu}_{\beta} R^{\mu}_{\ \rho\nu\sigma} n^{\rho} = -\mathcal{K}_{\alpha\sigma}\mathcal{K}^{\sigma}_{\ \beta} + \frac{1}{\alpha}\mathcal{D}_{\beta}\mathcal{D}_{\alpha}\alpha + \gamma^{\mu}_{\alpha}\gamma^{\nu}_{\beta} n^{\sigma} \nabla_{\sigma}\mathcal{K}_{\mu\nu}.$$

From () we know $\mathcal{L}_m \mathcal{K}_{\alpha\beta} \in \Sigma_t$ and the projected Lie derivative is

$$\mathcal{L}_m \mathcal{K}_{\alpha\beta} = \alpha\gamma^{\mu}_{\alpha}\gamma^{\nu}_{\beta} n^{\sigma} \nabla_{\sigma}\mathcal{K}_{\mu\nu} - 2\alpha\mathcal{K}_{\alpha\mu}\mathcal{K}^{\mu}_{\ \beta}.$$

This is what we need to derive the Ricci equation.

$$\gamma_{\alpha\mu} n^{\sigma} \gamma^{\nu}_{\beta} R^{\mu}_{\ \rho\nu\sigma} = \frac{1}{\alpha}\mathcal{L}_m \mathcal{K}_{\alpha\beta} + \frac{1}{\alpha}\mathcal{D}_{\beta}\mathcal{D}_{\alpha}\alpha + \mathcal{K}_{\alpha\mu}\mathcal{K}^{\mu}_{\ \beta} \tag{2.1.20}$$

2.1.4 Decomposition of Einstein's Equation

To evolve General Relativity numerically we must project the Einstein Equation into 3+1 dimensions. Relations between 3 and 4 dimensional geometric objects have been derived above and will be used to decompose the Einstein tensor $G_{\mu\nu}$ from the left hand side of (). The second component, for simulating non-vacumm spacetimes, is the 3+1 decomposition of the Stress tensor T_{ab}. We contract twice with n, then once with n while projecting onto Σ_t and finally twice projecting onto Σ_t to get an energy, momentum and stress-like split.

$$\mathcal{E} = T(n, n) = T_{ab} n^a n^b \tag{2.1.21}$$

$$\mathcal{S}_i = -T(n, \cdot) = - \perp^{a}_{i} n^b T_{ab} \tag{2.1.22}$$

$$\mathcal{S}_{ij} = \perp^{a}_{i} \perp^{b}_{j} T_{ab} \tag{2.1.23}$$

By construction the following is true.

$$T_{ab} = \mathcal{E}n_a n_b + \mathcal{S}_a n_b + \mathcal{S}_b n_a + \mathcal{S}_{ab}$$

With this and the Gauss-Codazzi equations () we can project the Einstein equation. Lets first look at the scalar equation

$$G_{\mu\nu} n^{\mu} n^{\nu} = R_{\mu\nu} n^{\mu} n^{\nu} + \frac{1}{2}R = 8\pi\mathcal{E}$$

and equating the geometric terms to the scalar Gauss equation () we get the Hamiltonian constraint, $\mathcal{H} = 0$.

$$\mathcal{H} = \mathcal{K}_{\mu\nu}\mathcal{K}^{\mu\nu} - \mathcal{K}^2 - \mathcal{R} + 16\pi\mathcal{E} \tag{2.1.24}$$

Now looking at the once projected part we see

$$\perp^{\mu}_{i} n^{\nu} G_{\mu\nu} = \perp^{\mu}_{i} n^{\nu} R_{\mu\nu} = -8\pi\mathcal{S}_i$$

and substituting the geometric terms for the contracted Codazzi relation we get the Momentum constraint, $\mathcal{P}_i = 0$.

$$\mathcal{P}_i = \mathcal{D}_i \mathcal{K} - \mathcal{D}_j \mathcal{K}_i^j + 8\pi \mathcal{S}_i \tag{2.1.25}$$

Finally, the space-space projection gives the 6 evolution PDE's. This time start with the trace reversed Einstein Equation

$$R_{\mu\nu} = 8\pi \left[T_{\mu\nu} - \frac{1}{2} T g_{\mu\nu} \right]$$

$$\perp_i^\mu \perp_j^\nu R_{\mu\nu} = 8\pi \left[\mathcal{S}_{ij} - \frac{1}{2} T \gamma_{ij} \right]$$

$$T = [\gamma^{\mu\nu} - n^\mu n^\nu] T_{\mu\nu} = \mathcal{S} - \mathcal{E}$$

and to project the Ricci tensor, we use the contracted Gauss equation () but replace the term with $R^a_{\ bcd}$ with the Ricci equation (). Rearranging gives a normal evolution for the extrinsic curvature.

$$\mathcal{L}_m \mathcal{K}_{ij} = -\mathcal{D}_j \mathcal{D}_i \alpha + \alpha \left[\mathcal{R}_{ij} + \mathcal{K}\mathcal{K}_{ij} - 2\mathcal{K}_i^k \mathcal{K}_{kj} + 4\pi \left[\gamma_{ij} \left[\mathcal{S} - \mathcal{E} \right] - 2\mathcal{S}_{ij} \right] \right] \tag{2.1.26}$$

Along with the definition of $\mathcal{K}_{ij}$ in equation (), this gives the normal evolution equations for γ_{ij} and $\mathcal{K}_{ij}$. These contain 6 of the second derivatives in Einstein's equation, with the other 4 being the constraint equations to be satisfied along evolution.

2.1.5 Foliation Adapted Coordinates, CHECK ERORR IN ADM METRIC MATRIX

Picking coordinates in GR introduces a large gauge freedom, this allows us to use a level set of the time coordinate $x^0 = t$ to define our foliation hypersurfaces Σ_t. The other three coordinates x^i for $i \in [1,2,3]$ can be used to span each hypersurface Σ_t however we define. It is conventional to split the normal evolution vector m^μ into time t^μ and space parts β^μ.

$$m^\mu = t^\mu - \beta^\mu = (\partial_0)^\mu - \beta^i (\partial_i)^\mu$$

$$m^\mu = \left(1, -\beta^1, -\beta^2, -\beta^3 \right)$$
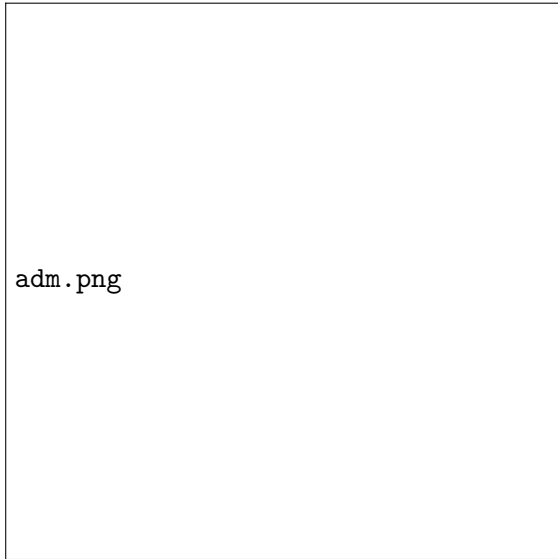
We can view t^μ as the (not necessarily causal) worldline for a simulation gridpoint, hence we would like to evolve our PDE's along t^μ on a computer introducing advection terms like $\mathcal{L}_\beta$. Equations (def of m) specify n^μ and n_μ

$$n^\mu = \frac{1}{\alpha} \left(1, -\beta^1, -\beta^2, -\beta^3 \right) \quad \& \quad n_\mu = -\alpha \left(1, 0, 0, 0 \right) \tag{2.1.27}$$

as well as the decomposed metric, using the property that β is tangent to Σ_t and orthogonal to m.

$$g_{00} = g(\partial_0, \partial_0) = g(m + \beta^i \partial_i, m + \beta^j \partial_j) = g(m, m) + \beta^i \beta_j \langle \partial_i, dx^j \rangle = -\alpha^2 + \beta^i \beta_i$$

$$g_{0i} = \beta_i, \quad g_{ij} = g(\partial_i, \partial_j) = \gamma(\partial_i, \partial_j) = \gamma_{ij}$$

This is commonly called the $3 + 1$ ADM metric and α, β^i are referred to the lapse and shift vector in this context. The metric is commonly written as follows.

$$\mathrm{d}s^2 = -\alpha^2 \mathrm{d}t^2 + \gamma_{ij} \left[\mathrm{d}x^i + \beta^i \mathrm{d}t \right] \left[\mathrm{d}x^j + \beta^j \mathrm{d}t \right] \tag{2.1.28}$$

$$g_{\mu\nu} = \begin{pmatrix} -\alpha^2 + \beta^i \beta_i & \beta_i \\ \beta_j & \gamma_{ij} \end{pmatrix} \quad \leftrightarrow \quad g^{\mu\nu} = \begin{pmatrix} -\alpha^{-2} & -\alpha^{-2} \beta^i \\ -\alpha^{-2} \beta^j & \gamma^{ij} - \alpha^{-2} \beta^i \beta^j \end{pmatrix} \tag{2.1.29}$$

and using Cramers rule for metric determinant

$$g^{00} = \frac{\det\{\gamma_{ij}\}}{\det\{g_{\mu\nu}\}}$$

we get the important relationship

$$\sqrt{-g} = \alpha\sqrt{\gamma}. \tag{2.1.30}$$

2.1.6 ADM Equations

Now that we have some coordinates suitable for the spacetime foliation we can find the ADM evolution equations for $\mathcal{K}_{ij}$ and γ_{ij}. First expand the Lie derivative $\mathcal{L}_m$ using

$$t^\mu = (1, 0, 0, 0) \rightarrow \mathcal{L}_t T^{ab\ldots}{}_{cd\ldots} = \partial_t T^{ab\ldots}{}_{cd\ldots}$$

$$\mathcal{L}_m = \mathcal{L}_t - \mathcal{L}_\beta = \partial_t - \mathcal{L}_\beta$$

and the ADM equations can be written by expanding the $\mathcal{L}_m$ in equations ().

$$\partial_t \mathcal{K}_{ij} = \mathcal{L}_\beta \mathcal{K}_{ij} - \mathcal{D}_j \mathcal{D}_i \alpha + \alpha \left[\mathcal{R}_{ij} + \mathcal{K} \mathcal{K}_{ij} - 2\mathcal{K}_i^k \mathcal{K}_{kj} + 4\pi \left[\gamma_{ij} \left[\mathcal{S} - \mathcal{E} \right] - 2\mathcal{S}_{ij} \right] \right] \tag{2.1.31}$$

$$\partial_t \gamma_{ij} = \mathcal{L}_\beta \gamma_{ij} - 2\alpha \mathcal{K}_{ij} \tag{2.1.32}$$

Unfortunately, these PDE's turn out to be ill-posed []; the resolution comes in the next section.

2.1.7 BSSN

To tackle the ill-posedness of the ADM equations () the Baumgarte-Shapiro-Shibata-Nakamura (BSSN) formalism is introduced []. Another strongly hyperbolic formalism is the generalised harmonic gauge [**?**] with $\Box x^\mu = H^\mu$. The first step in BSSN is to decompose the 3-metric into the conformal metric $\tilde{\gamma}_{ij}$ and the conformal factor χ

$$\tilde{\gamma}_{ij} = \chi \gamma_{ij} \quad \rightarrow \quad \det\{\tilde{\gamma}_{ij}\} = \tilde{\gamma} = \chi^3 \gamma = 1 \tag{2.1.33}$$

with the above being the convention used in GRChombo; other conventions include factors such as

$$\tilde{\gamma}_{ij} = \psi^{-4} \gamma_{ij} \quad \text{or} \quad e^{-\phi} \gamma_{ij}.$$

Along with this the extrinsic curvature $\mathcal{K}_{ij}$ is modified to be trace free, $\mathcal{A}_{ij}$.

$$\tilde{A}_{ij} = \chi \left[\mathcal{K}_{ij} - \frac{1}{3} \mathcal{K} \gamma_{ij} \right] \quad \rightarrow \quad \tilde{A}_{ij} \gamma^{ij} = 0$$

During an evolution the conditions $\operatorname{tr} \tilde{A}_{ij} = 0$ and $\tilde{\gamma} = 1$ are enforced which are observed to improve numerical stability; however it is unclear why beyond heuristic arguments. The definition of $\chi = \gamma^{-1/3}$ is good for black hole simulations where $\gamma \to \infty$ but $\chi \to 0$; for example the isotropic schwarzschild metric has

$$\gamma = \left[1 + \frac{M}{2r} \right]^{12} \quad \rightarrow \quad \chi = \left[\frac{r}{\frac{M}{2} + r} \right]^4.$$

The next step is to introduce the conformal connection functions as auxiliary variables.

$$\tilde{\Upsilon}^i = \tilde{\gamma}^{jk}\tilde{\Upsilon}^i{}_{jk} = -\partial_i\tilde{\gamma}^{ij} \tag{2.1.34}$$

$$\tilde{\Upsilon}^i{}_{jk} = \frac{1}{2}\tilde{\gamma}^{il}\left[\partial_j\tilde{\gamma}_{kl} + \partial_k\tilde{\gamma}_{lj} - \partial_l\tilde{\gamma}_{jk}\right] = \Upsilon^i{}_{jk} + \left[\delta^i_j\partial_k + \delta^i_k\partial_j - \gamma^{il}\gamma_{jk}\partial_l\right]\ln\sqrt{\chi} \tag{2.1.35}$$

Promoting these to evolution variables changes the hyperbolicity of the characteristic matrix and make the system well posed. This reduces the set of vacuum evolution variables to $\{\chi, \tilde{\gamma}_{ij}, \mathcal{K}, \tilde{\mathcal{A}}_{ij}, \tilde{\Upsilon}^i\}$. It is conventional to use $-\partial_i\tilde{\gamma}^{ij}$ to evaluate the conformal connection coefficients when they appear in the RHS of an equation, but $\partial_j\tilde{\Upsilon}^i$ is calculated by differentiating the evolution variable $\tilde{\Upsilon}^i$. One final detail, not included in the CCZ4 formulation discussed later, is to add multiples of the constraints () to the evolution equations to change the characteristic matrix and improve stability.

2.1.8 Z4 Formalism

The Z4 formalism [**?**] generalises the Einstein equation () to include an unphysical field Z_μ, along with damping terms parameterised by κ_1, κ_2.

$$R_{\mu\nu} + \nabla_\mu Z_\nu + \nabla_\nu Z_\mu - \kappa_1\left[n_\mu Z_\nu + n_\nu Z_\mu - [1+\kappa_2]g_{\mu\nu}n^\alpha Z_\alpha\right] = 8\pi G\left[T_{\mu\nu} - \frac{1}{2}Tg_{\mu\nu}\right] \tag{2.1.36}$$

Of course regular General Relativity is returned setting $Z_\mu = 0$. It is shown in [] that achieving $Z_\mu = 0$ whilst dynamically evolving Z_μ is equivalent to solving the constraints. Z_μ is subjected to a wave equation, transporting constraint violation off the computational domain. It can be shown that the system is driven to $Z_\mu = 0$ for $k_1 > 0$ and $k_2 < -1$. It is much cheaper to evolve the variables Z_μ, driven to zero, than do perform four elliptic solves for the constraints $\{\mathcal{H}, \mathcal{M}^i\}$ on each timestep.

2.1.9 CCZ4

Joining BSSN with Z4 gives the CCZ4 formalism. The additional modifications

$$\Theta = -n\cdot Z = -\alpha Z^0 \tag{2.1.37}$$

$$\hat{\Upsilon}^i = \tilde{\Upsilon}^i + \frac{2\gamma^{ij}Z_j}{\chi} \tag{2.1.38}$$

are made, leaving us with the following set of vacuum evolution variables $\{\chi, \tilde{\gamma}_{ij}, \mathcal{K}, \tilde{\mathcal{A}}_{ij}, \hat{\Upsilon}^i, \Theta\}$. Notably the pair of variables $\mathcal{R}_{ij} + \mathcal{D}_{(i}Z_{j)}$, and traced version $\mathcal{R} + \mathcal{D}\cdot Z$, always appear together; separately they ruin strong hyperbolically but together they do not. The Evolution equations can now be found in the CCZ4 scheme using the following equations (list evolution equations and decomposition of Υ). Note the

last two equations () are for the 3+1 Klein-Gordon equation which will be derived later in ().

$$\partial_t \chi = \beta^k \partial_k \chi + \frac{2\chi}{3} \left[\alpha \mathcal{K} - \partial_k \beta^k \right] \tag{2.1.39}$$

$$\partial_t \tilde{\gamma}_{ij} = \beta^k \partial_k \tilde{\gamma}_{ij} + \tilde{\gamma}_{kj} \partial_i \beta^k + \tilde{\gamma}_{ik} \partial_j \beta^k - \frac{2}{3} \tilde{\gamma}_{ij} \partial_k \beta^k - 2\alpha \tilde{\mathcal{A}}_{ij} \tag{2.1.40}$$

$$\partial_t \mathcal{K} = \beta^k \partial_k \mathcal{K} + \alpha \left[\mathcal{R} + 2\mathcal{D} \cdot Z + \mathcal{K} \left[\mathcal{K} - 2\Theta \right] \right] - 3\alpha\kappa_1 \left[1 + \kappa_2 \right] \Theta \tag{2.1.41}$$
$$- \chi \tilde{\gamma}^{kl} \mathcal{D}_k \mathcal{D}_l \alpha + 4\pi G \alpha \left[\mathcal{S} - 3\mathcal{E} \right]$$

$$\partial_t \tilde{\mathcal{A}}_{ij} = \beta^k \partial_k \tilde{\mathcal{A}}_{ij} + \chi \left[\alpha \left[\mathcal{R}_{ij} + 2\mathcal{D}_{(i} Z_{j)} - 8\pi G \mathcal{S}_{ij} \right] - \mathcal{D}_i \mathcal{D}_j \alpha \right]^{TF} \tag{2.1.42}$$
$$+ \tilde{\mathcal{A}}_{ij} \left[\alpha \left[\mathcal{K} - 2\Theta \right] - \frac{2}{3} \mathcal{K}^2 \right] + 2\tilde{\mathcal{A}}_{k(i} \partial_{j)} \beta^k - 2\alpha \tilde{\gamma}^{kl} \tilde{\mathcal{A}}_{ik} \tilde{\mathcal{A}}_{lj}$$

$$\partial_t \Theta = \beta^k \partial_k \Theta + \frac{1}{2} \alpha \left[\mathcal{R} + 2\mathcal{D} \cdot Z - \tilde{\mathcal{A}}_{kl} \tilde{\mathcal{A}}^{kl} + \frac{2}{3} \mathcal{K}^2 - 2\Theta\mathcal{K} \right] - \kappa_1 \alpha \Theta \left[2 + \kappa_2 \right] - Z^k \partial_k \alpha - 8\pi G \alpha \mathcal{E} \tag{2.1.43}$$

$$\partial_t \hat{\Upsilon}^i = \beta^k \partial_k \hat{\Upsilon}^i + \frac{2}{3} \left[\partial_k \beta^k \left[\tilde{\Upsilon}^i + 2\kappa_3 \frac{Z^i}{\chi} \right] - 2\alpha \mathcal{K} \frac{Z^j}{\chi} \right] - 2\alpha\kappa_1 \frac{Z^i}{\chi} \tag{2.1.44}$$
$$+ 2\tilde{\gamma}^{ij} \left[\alpha \partial_j \Theta - \Theta \partial_j \alpha \right] - 2\tilde{\mathcal{A}}^{ij} \partial_j \alpha - \alpha \left[\frac{4}{3} \tilde{\gamma}^{ij} \partial_j \mathcal{K} + 3\tilde{\mathcal{A}}^{ij} \frac{\partial_j \chi}{\chi} \right]$$
$$- \left[\tilde{\Upsilon}^j + 2\kappa_3 \frac{Z^j}{\chi} \right] \partial_j \beta^i + 2\alpha \tilde{\Upsilon}^i{}_{jk} \tilde{\mathcal{A}}^{jk} + \tilde{\gamma}^{jk} \partial_j \partial_k \beta^i + \frac{1}{3} \tilde{\gamma}^{ij} \partial_k \partial_j \beta^k - 16\pi G \alpha \tilde{\gamma}^{ij} \mathcal{S}_j$$

$$\partial_t \varphi = \beta^k \partial_k \varphi - \alpha \Pi \tag{2.1.45}$$

$$\partial_t \Pi = \beta^k \partial_k \Pi - \chi \tilde{\gamma}^{ij} \partial_i \varphi \partial_j \alpha + \alpha \left[\chi \tilde{\Upsilon}^k \partial_k \varphi + \frac{1}{2} \tilde{\gamma}^{lk} \partial_k \chi \partial_l \varphi - \chi \tilde{\gamma}^{ij} \partial_i \partial_j \varphi + \mathcal{K} \Pi + V' \varphi \right] \tag{2.1.46}$$

Also used was the lie derivative for a tensor density $\mathcal{T}$ of weight n.

$$\mathcal{L}_X \mathcal{T} = \widetilde{\mathcal{L}}_X \mathcal{T} + n \mathcal{T} \partial_k X^k$$

Here $\widetilde{\mathcal{L}}_X$ represents the differential operator that is equivalent to $\mathcal{L}_X$ if it didn't act on a tensor density. Also to be noted, in the CCZ4 equations there is an additional parameter κ_3 premultiplying terms in the evolution of $\hat{\Upsilon}^i$ which experimentally were found to ruin numerical stability for black hole simulations []. Setting $\kappa_3 < 1$ stabilises the simulation but at the cost of covariance. Later on it was realised that setting $\kappa_3 = 1$ and $\alpha\kappa_1 \to \kappa_1$ retains covariance as well as numerical stability [].

The CCZ4 scheme proves useful in my simulations for a few reason. Firstly, any initial data that does not satisfy the constraints will not do so along evolution either when using BSSN. Given that superposition of solutions in GR does not generally give a new solution, but does approximate one for separated compact objects, all the simulated binaries considered in the report will have non constraint satisfying initial data. The boosted stars I use later are an exact solution of GR though, being a coordinate transformation from the exact resting soliton. The use of CCZ4 will help simulations satisfy the constraints even if they initially satisfy them; one reason being that finite resolution imposes some small deviation from the continuum solution. More importantly, the use of adaptive mesh refinement AMR introduces large interpolation errors into the simulation at the boundary of the different grid resolution levels. Finally, the Sommerfeld boundary conditions used are inexact in GR and will introduce small errors at the boundary that ruin constraint satisfaction. In all above cases, the CCZ4 system forces the evolution towards constraint satisfaction, despite the numerical errors and approximations.

2.1.10 Gauge Conditions

In GR, the lapse α and shift β^i are freely specifiable being gauge variables, however they must be chosen carefully along with a suitable initial Cauchy surface Σ_{t_0} for sensible foliations and numerical

accuracy. Figure 1 (left) shows how a poor initial Cauchy surface could extend to the singularity for ingoing Eddington-Finkelstein coordinates; likely causing a simulation crash. In my work Σ_{t_0} is chosen to be isotropic as in Figure 1 (right); not only does this allow trivial swapping between spherical polar and Cartesian (used in simulation) coordinates but also provides an initial Cauchy surface that's free of singularities and easy to compute. For a poor choice of lapse function, even a well chosen Σ_{t_0} can advance to the singularity in finite simulation time.
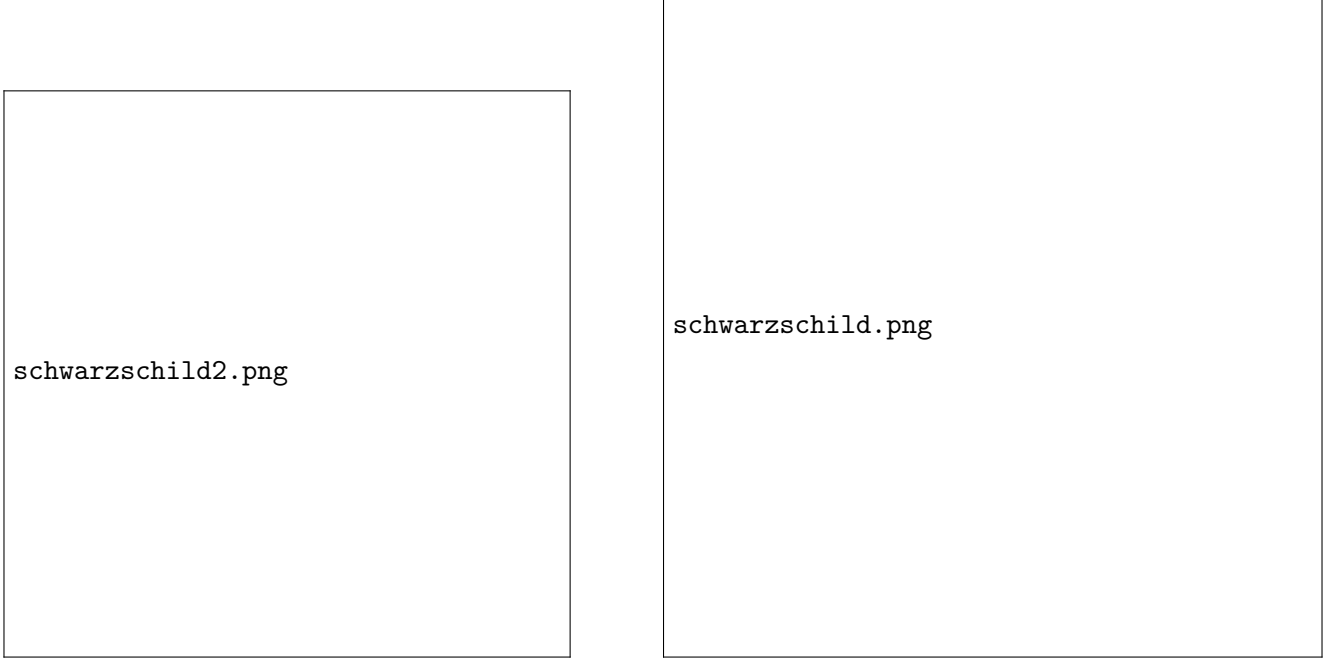

Figure 2.1: Penrose Diagrams, Σ_{t_0} dashed, Left: Ingoing Eddington-Finkelstein Coordinates, Right: Isotropic Coordinates.

The simplest lapse choice would be to enforce $\alpha = 1$, which is geodesic slicing, with the hypersurface following geodesics; given that geodesics can converge this can lead to hypersurface self-intersection which breaks the definition of a Cauchy surface and the simulation will likely fail. Another problem is that a black hole singularity can be reached in finite simulation time. This can be modified to the maximal slicing condition which keeps the volume element $\sqrt{-g}$ constant along geodesics. This means as $\gamma \to \infty$ nearing a singularity $\alpha \to 0$ using equation (), causing the hypersurface to advance more slowly before a singularity is reached. This property is called singularity avoiding and is crucial for numerical stability (unless using excision?). Maximal slicing can be implemented by forcing $\mathcal{K} = \partial_t \mathcal{K} = 0 \ \forall t$ which requires a slow elliptic solve for α at each timestep. Instead α is promoted to an evolution variable and is evolved along with every other simulation variable. To do this we can pick an algebraic slicing condition of the following type.

$$\mathcal{L}_m \alpha = -\alpha^2 f(\alpha) \mathcal{K}$$

This is used with $f = 2\alpha^{-1}$ in GRChombo giving

$$\mathcal{L}_m \alpha = -2\alpha \mathcal{K}$$

and using normal coordinates $\beta^i = 0$ it reduces to

$$\alpha = 1 + \ln \gamma$$

which is called 1+log slicing; this is very common in Numerical Relativity codes. In practice 1+log slicing is strongly singularity avoiding reaching $\alpha = 0$ before the singularity. This is modified in the

CCZ4 scheme to

$$\partial_t \alpha = -2\alpha \left[\mathcal{K} - 2\Theta \right] + \beta^i \partial_i \alpha \tag{2.1.47}$$

which is very similar to before; it should be noted that the advection term is important for black hole simulations.

So far the shift vector β^i has been ignored, the simplest choice for it would be $\beta^i = 0$. Using 1+log slicing causes great stretching and shearing of Σ_t in the neghbourhood of a singularity and choosing $\beta^i = 0$ causes this shear to mean neighbouring gridpoints have large differences in field values leading to inaccurate and unstable evolutions. Another negative side effect is that the computational domain can fall inside an event horizon in black hole simulations. To counteract this we want to pick a shift vector that minimises hypersurface shear σ_{ij} which can be defined as [ref 1977 smarr and york]

$$\sigma_{ij} := \perp_i^\mu \perp_j^\nu \left[\nabla_{(\mu} n_{\nu)} - \frac{1}{3} \gamma^{ab} \nabla_{(a} n_{b)} \gamma_{\mu\nu} \right]$$

where σ_{ij} is tracefree corresponding to shearing rather than inflation or expansion. Minimising total shear, Σ,

$$\Sigma = \int \sigma_{ij} \sigma^{ij} \sqrt{\gamma} \, \mathrm{d}x^3$$

with respect to β^i leads to an elliptic PDE to be solved for each β^i at each time step that minimises shear.

$$\delta\Sigma = 0 \to \mathcal{D}_i \sigma^{ij} = 0$$

This is known as the minimal shift condition. As before, promoting β^i to be evolution variables is computationally cheaper. A very common choice is to promote the elliptic PDE for β^i into a hyperbolic equation via introducing a $\partial_t^2 \beta^i$ term and an artificial damping term parameterised by η. This becomes a damped wave equation and is supposed to transport away any part of β^i which does not satisfy $\mathcal{D}_i \sigma^{ij} = 0$. This requires Sommerfeld (outgoing wave) boundary conditions. In GRChombo the standard gamma driver shift condition is used.

$$\partial_t \beta^i = FB^i \tag{2.1.48}$$

$$\partial_t B^i = \partial_t \tilde{\Gamma}^i - \eta B^i \tag{2.1.49}$$

Here $F = 3/4$ and $\eta = 1$ are used in GRChombo.

Chapter 3

Boson Stars

3.1 Mathematical Modelling of Boson Stars

3.1.1 Action

The Boson Stars considered are a complex Klein Gordon Scalar field, φ, minimally coupled to gravity. The action is the Einstein Hilbert vacuum action plus the matter action for curved space.

$$S = \int_{\mathcal{M}} [\mathcal{L}_{EH} + \mathcal{L}_M] \sqrt{-g}\, \mathrm{d}x^4 \tag{3.1.1}$$

$$\mathcal{L}_{EH} = \frac{1}{16\pi G} R \tag{3.1.2}$$

$$\mathcal{L}_M = -\frac{1}{2} g^{\mu\nu} \nabla_\mu \varphi^* \nabla_\nu \varphi - \frac{1}{2} V(|\varphi|^2) \tag{3.1.3}$$

Here V is the Klein-Gordon potential and it's effect on boson stars is discussed in [].

$$V = \frac{m^2 c^2}{\hbar^2} |\varphi|^2 \to m^2 |\varphi|^2 \tag{3.1.4}$$

$$V = \frac{m^2 c^2}{\hbar^2} |\varphi|^2 + \frac{1}{2}\Lambda|\varphi|^4 \to m^2|\varphi|^2 + \frac{1}{2}\Lambda|\varphi|^4 \tag{3.1.5}$$

$$V = \frac{m^2 c^2}{\hbar^2} |\varphi|^2 \left(1 - \frac{|\varphi|^2}{2\sigma^2}\right)^2 \to m^2|\varphi|^2 \left(1 - \frac{|\varphi|^2}{2\sigma^2}\right)^2 \tag{3.1.6}$$

Considering only the m^2 term, which corresponds to the squared mass of the particle in the quantum theory, we get a massive wave equation linear in φ, leading to so called mini Boson stars. Having $\Lambda \neq 0$ gives self-interacting stars which have a nonlinear wave equation corresponding to particle creation and annihilation at the quantum level. Finally, equation 3.6 describes the solitonic potential, giving rise to boson stars with compactnesses comparable to neutron stars.

Varying the action with respect to the metric and scalar field return the Einstein Field equations and the Klein Gordon equation of curved space respectively.

$$R_{\mu\nu} - \frac{1}{2} R g_{\mu\nu} = \frac{8\pi G}{c^4} T_{\mu\nu} \tag{3.1.7}$$

$$g^{\mu\nu} \nabla_\mu \nabla_\nu \varphi = \frac{\partial V}{\partial |\varphi|^2} \varphi \tag{3.1.8}$$

Collectively these are known as the Einstein-Klein-Gordon (EKG) equations. The definition and boson-specific stress energy tensors are as follows.

$$T_{\mu\nu} := -2\frac{\delta\mathcal{L}_M}{\delta g^{\mu\nu}} + g_{\mu\nu}\mathcal{L}_M \tag{3.1.9}$$

$$T_{\mu\nu} = \frac{1}{2}\nabla_\mu\varphi^*\nabla_\nu\varphi + \frac{1}{2}\nabla_\nu\varphi^*\nabla_\mu\varphi - \frac{1}{2}g_{\mu\nu}\left[g^{\alpha\beta}\nabla_\alpha\varphi^*\nabla_\beta\varphi + V\right] \tag{3.1.10}$$

Studying neutron stars requires the fermionic, or ordinary fluid, stress tensor; this is given below.

$$T_F^{\mu\nu} = \left[\rho c^2 + P\right]\frac{u^\mu u^\nu}{c^2} + Pg^{\mu\nu} + 2u^{(\mu}q^{\nu)} + \pi^{\mu\nu}$$

The vanishing of the divergence, $\nabla_\nu T^{\mu\nu} = 0$, returns the highly nonlinear relativistic Navier-Stokes equations of curved space. The viscosity term $\pi^{\mu\nu}$ and heat flux q^μ are often omitted for simplicity. The remaining variables ρ, P and u^μ are the fluid density [and enthalpy?], pressure and worldline tangent. Note here the use of sophisticated shock capturing schemes are required, unlike the linear Klein-Gordon equation.

3.1.2 Solitons

A soliton is a wave that exhibits particle-like behaviour. More precisely, in classical field theory, a soliton is a field or set of fields in a localised configuration that can travel at constant speed but not disperse. Some examples of solitons in General Relativity are fluid stars, black holes, wormholes and exotic stars [refernece]. [check are they solitons if they cannot pass though each other (e.g. black holes ...)]. For our purposes, we look for solitons in the Einstein-Klein Gordon (EKG) system which are localised scalar field configurations with accompanying metric. In the case of the real scalar field it was shown by [] that there are no long lived stars; however promoting the field to a complex scalar we can find a spherically symmetric stationary soliton with the following scalar field.

$$x^\mu \in \{t, r, \theta, \phi\}$$
$$\varphi = \Phi(r)e^{i\omega t} \tag{3.1.11}$$

Traditionally, the polar areal gauge has been used [] for the metric's ansatz.

$$g_{\mu\nu}\mathrm{d}x^\mu\mathrm{d}x^\nu = -a^2(r)\mathrm{d}t^2 + b^2(r)\mathrm{d}r^2 + r^2\left[\mathrm{d}\theta^2 + \sin^2\theta\mathrm{d}\phi^2\right]$$

The boundary condition $b^2(0) = 1$ is demanded to avoid a conical singularity at the origin. However an isotropic gauge is more useful for simulations due to easier conversion to cartesian space-coordinates. The polar areal solution must then be transformed into an isotropic solution. Alternatively, the approach taken in this report, is to start with an isotropic ansatz

$$g_{\mu\nu}\mathrm{d}x^\mu\mathrm{d}x^\nu = -\Omega^2(r)\mathrm{d}t^2 + \Psi^2(r)\mathrm{d}\boldsymbol{x}^2$$

where $\mathrm{d}\boldsymbol{x}^2$ denotes the euclidean 3D line element; this changes between spherical polar or cartesian coordinates trivially. This ends up being slightly harder to integrate numerically, but no conversion to isotropic coordinates is needed afterwards.

To get a set of ODE's to solve for the functions $\{\Omega(r), \Psi(r), \Phi(r)\}$ we must turn to the Einstein Equation and Klein Gordon Equation. The Einstein Equations for $\{\mu, \nu\} = \{0,0\}, \{1,1\}, \{2,2\}$ are the only components that give unique non-zero equations; they are given below.

$$\frac{\Omega^2\left[r\Psi'^2 - 2\Psi\left[r\Psi'' + 2\Psi'\right]\right]}{r\Psi^4} = 4\pi G\left[\Omega^2\left[\frac{P'^2}{\Psi^2} + V\right] + \omega^2 P^2\right] \tag{3.1.12}$$

$$\frac{2\Psi\Psi'\left[r\Omega' + \Omega\right] + r\Omega\Psi'^2 + 2\Psi^2\Omega'}{r\Psi^2\Omega} = 4\pi G\left[P'^2 - \Psi^2 V + \frac{\omega^2 P^2\Psi^2}{\Omega^2}\right] \tag{3.1.13}$$

$$r\left[-\frac{r\Psi'^2}{\Psi^2} + \frac{r\Psi'' + \Psi'}{\Psi} + \frac{r\Omega'' + \Omega'}{\Omega}\right] = -4\pi Gr^2\Psi^2\left[\frac{P'^2}{\Psi^2} + V - \frac{\omega^2 P^2}{\Omega^2}\right] \tag{3.1.14}$$

The Einstein tensor $G_{\mu\nu} = R_{\mu\nu} - \frac{1}{2}Rg_{\mu\nu}$ (left above) and the stress tensor (right above) were obtained with a self written Mathematica notebook. The Klein Gordon equation (3.6) becomes

$$\frac{1}{\sqrt{-g}}\partial_\mu\left[\sqrt{-g}g^{\mu\nu}\partial_\nu\Phi(r)e^{i\omega t}\right] = \frac{\partial V}{\partial|\varphi|^2}\Phi(r)e^{i\omega t}$$

$$\Phi'' = \Phi\Psi^2\left[V' - \frac{\omega^2}{\Omega^2}\right] - \Phi'\left[\frac{\Omega'}{\Omega} + \frac{\Psi'}{\Psi} + \frac{2}{r}\right]$$

Simplifying the Einstein Equations and combinig with the Klein Gordon equation we get 3 ODE's to solve.

$$\Omega' = \frac{\Omega}{r\Psi' + \Psi}\left[2\pi Gr\Psi\left[\Phi'^2 - \Psi^2 V + \frac{\omega^2\Phi^2\Psi^2}{\Omega^2}\right] - \Psi' - \frac{r\Psi'^2}{2\Psi}\right] \tag{3.1.15}$$

$$\Psi'' = \frac{\Psi'^2}{2\Psi} - \frac{2\Psi'}{r} - 2\pi G\left[V\Psi^3 + \Phi'^2\Psi + \frac{\omega^2\Phi^2\Psi^3}{\Omega^2}\right] \tag{3.1.16}$$

$$\Phi'' = \Phi\Psi^2\left[V' - \frac{\omega^2}{\Omega^2}\right] - \Phi'\left[\frac{\Omega'}{\Omega} + \frac{\Psi'}{\Psi} + \frac{2}{r}\right] \tag{3.1.17}$$

This is turned into a set of five first order ODE's to numerically integrate. Note that if we had used the polar areal ansatz () the equation for Φ would also be first order; reducing the EKG system to four first order ODE's.

3.1.3 3+1 Klein Gordon System

Now let's project the Klein Gordon equation in a 3+1 split to get an evolution equation. The first step is to turn the second order (in time) differential equation into two first order ones

$$\mathcal{L}_m\{\varphi, \Pi\} = ...$$

where Π is the foliation dependant definition of conjugate momentum to the complex scalar field.

$$\Pi := -\mathcal{L}_n\varphi \tag{3.1.18}$$

Now decompose the Klein Gordon Equation.

$$\nabla^\mu\nabla_\mu\varphi = V'\varphi = \frac{1}{\sqrt{-g}}\partial_\mu\left[\sqrt{-g}\left[\gamma^{\mu\nu} - n^\mu n^\nu\right]\partial_\nu\varphi\right] = \frac{1}{\sqrt{-g}}\partial_\mu\left[\sqrt{-g}\left[\mathcal{D}^\mu\varphi - n^\mu\mathcal{L}_n\varphi\right]\right]$$

The term with $\mathcal{D}^\mu$ simplifies like

$$\frac{1}{\sqrt{-g}}\partial_\mu\left[\sqrt{-g}\mathcal{D}^\mu\varphi\right] = \frac{1}{\alpha\sqrt{\gamma}}\partial_\mu\left[\alpha\sqrt{\gamma}\mathcal{D}^\mu\varphi\right] = \mathcal{D}_\mu\mathcal{D}^\mu\varphi + \mathcal{D}^\mu\varphi\,\partial_\mu\ln\alpha$$

and the remainder becomes

$$-\frac{1}{\sqrt{-g}}\partial_\mu\left[\sqrt{-g}n^\mu\mathcal{L}_n\varphi\right] = -\left[\nabla\cdot n + n\cdot\partial\right]\mathcal{L}_n\varphi = -\mathcal{K}\Pi + \mathcal{L}_n\Pi$$

then the full Klein Gordon system is constructed.

$$\mathcal{L}_m\Pi = -\mathcal{D}^\mu\varphi\,\partial_\mu\alpha + \alpha\left[\mathcal{K}\Pi - \mathcal{D}_\mu\mathcal{D}^\mu\varphi + V'\varphi\right] \tag{3.1.19}$$

$$\mathcal{L}_m\varphi = -\alpha\Pi \tag{3.1.20}$$

The final matter term we must decompose is the Klein-Gordon stress tensor with equations ().

$$E = n^\mu n^\nu T_{\mu\nu} = \frac{1}{2}|\Pi|^2 + \frac{1}{2}\gamma^{ij}\mathcal{D}_i\varphi^*\mathcal{D}_j\varphi + \frac{1}{2}V(|\varphi|^2) \tag{3.1.21}$$

$$S_i = -\perp_i^\mu n^\nu T_{\mu\nu} = \frac{1}{2}\left[\Pi^*\mathcal{D}_i\varphi + \Pi\mathcal{D}_i\varphi^*\right] \tag{3.1.22}$$

$$S_{ij} = \perp_i^\mu\perp_j^\nu T_{\mu\nu} = \mathcal{D}_{(i}\varphi\mathcal{D}_{j)}\varphi^* - \frac{1}{2}\left[\gamma^{ij}\mathcal{D}_i\varphi\mathcal{D}_j\varphi^* - |\Pi|^2 + V(|\varphi|^2)\right] \tag{3.1.23}$$

3.1.4 Klein Gordon's Noether Charge

For the complex scalar field, we have the U(1) symmetry

$$\varphi \to \varphi e^{i\epsilon} \approx \varphi + i\epsilon\varphi, \quad \varphi^* \to \varphi^* e^{-i\epsilon} \approx \varphi^* - i\epsilon\varphi*.$$

This leaves the Lagrangian unchanged and therefore the total action. The associated conserved current j and current density $\mathcal{J}$ are then

$$j^\mu = \frac{\delta\mathcal{L}}{\delta\nabla_\mu\varphi}\delta\varphi + \frac{\delta\mathcal{L}}{\delta\nabla_\mu\varphi^*}\delta\varphi*, \quad \nabla_\mu j^\mu = 0,$$

$$j^\mu = ig^{\mu\nu}\left[\varphi\nabla_\nu\varphi^* - \varphi^*\nabla_\nu\varphi\right], \quad \mathcal{J}^\mu = \sqrt{-g}j^\mu.$$

The total integral over a manifold $\mathcal{M}$ gives a conserved charge $\mathcal{Q}$ associated with the conserved current J^μ, assuming $\mathcal{J}^i \to 0$ sufficiently fast towards the boundary $\partial\Sigma_t$ of Σ.

$$\int_{\mathcal{M}} \left[\nabla \cdot j\right] \star 1 = 0 = \int_{\phi(\mathcal{M})} \nabla_\mu j^\mu \sqrt{-g}\,\mathrm{d}x^4 = \int_{\phi(\mathcal{M})} \partial_\mu\left[\sqrt{-g}j^\mu\right]\mathrm{d}x^4 = \int_{\phi(\mathcal{M})} \partial_\mu\mathcal{J}^\mu \mathrm{d}x^4$$

$$\int_{t_0}^{t_1}\left[\int_{\phi(\Sigma_t)} \partial_0\mathcal{J}^0\mathrm{d}x^3\right]\mathrm{d}t = -\int_{t_0}^{t_1}\left[\int_{\phi(\Sigma_t)} \partial_i\mathcal{J}^i\mathrm{d}x^3\right]\mathrm{d}t = 0$$

The term containing $\partial_i\mathcal{J}^i$ integrates to zero over Σ_t due to the divergence theorem. The left hand term can be simplified by permuting the time derivative using

$$\partial_0\int_{\phi(\Sigma_t)} \mathcal{J}^0\mathrm{d}x^3 = \int_{\phi(\Sigma_t)} \partial_0\mathcal{J}^0\mathrm{d}x^3 + \lim_{\Delta x^0 \to 0}\left[\frac{1}{\Delta x^0}\int_{\phi(\Delta\Sigma_t)}\left[\mathcal{J}^0 + \Delta x^0\partial_0\mathcal{J}^0\right]\mathrm{d}x^3\right]$$

where the last term vanishes as $\mathcal{J}$ vanishes near $\partial\Sigma$, and we get a formula for the conserved charge.

$$\partial_0\int\mathcal{Q} = 0, \quad \mathcal{Q} = \int_{\phi(\Sigma_t)} \mathcal{J}^0\mathrm{d}x^3$$

Finally we get an expression for the total Noether charge $\mathcal{N} = \mathcal{Q}[\varphi]$

$$\mathcal{N} = i\int_{\Sigma_t} \sqrt{-g}\left[\varphi\nabla^0\varphi^* - \varphi^*\nabla^0\varphi\right]\mathrm{d}x^3$$

and using $\sqrt{-g} = \alpha\sqrt{\gamma}$, $n_\mu\nabla^\mu = -\alpha\nabla^0$ we get the following neat formula.

$$\mathcal{N} = i\int_{\Sigma_t} \left[\varphi\Pi^* - \varphi^*\Pi\right]\sqrt{\gamma}\,\mathrm{d}x^3 \tag{3.1.24}$$

3.1.5 Boosted Boson Stars and Black Holes

Let us now consider a moving star, this corresponds to making a stationary soliton and boosting it. There is no unique way of doing this as any coordinate transformation that reduces to a Minkowski spacetime boost at large radius will do the job. All the degrees of freedom we have can be absorbed into a coordinate gauge choice, so it makes sense to choose the trivial boost, with rapidity χ, from Special Relativity.

$$\chi = \operatorname{arctanh}\frac{v}{c}$$

$$\Lambda^\mu_\nu = \exp\begin{pmatrix} 0 & -\chi & 0 & 0 \\ -\chi & 0 & 0 & 0 \\ 0 & 0 & 1 & 0 \\ 0 & 0 & 0 & 1 \end{pmatrix} = \begin{pmatrix} \cosh(\chi) & -\sinh(\chi) & 0 & 0 \\ -\sinh(\chi) & \cosh(\chi) & 0 & 0 \\ 0 & 0 & 1 & 0 \\ 0 & 0 & 0 & 1 \end{pmatrix}$$

$$\tilde{x}^\mu = \Lambda^\mu_\nu x^\nu \quad \& \quad \tilde{g}_{\mu\nu} = [\Lambda^{-1}]^\alpha_\mu [\Lambda^{-1}]^\beta_\nu g_{\alpha\beta}(\tilde{x})$$

Declaring the rest and boosted frame to have coordinates x^μ and $\tilde{x}^\mu$ we choose the boosted soliton's initial Cauchy surface to be the level set of $\tilde{t} = 0$. The coordinates and metric transform as follows.

$$x^\mu = \{t, x, y, z\} = \{\tilde{t}\cosh(\chi) + \tilde{x}\sinh(\chi), \tilde{x}\cosh(\chi) + \tilde{t}\sinh(\chi), \tilde{y}, \tilde{z}\}$$

$$g_{\mu\nu} = \mathrm{diag}\{-\Omega^2, \Psi^2, \Psi^2, \Psi^2\}$$

$$\tilde{g}_{\mu\nu} = \begin{pmatrix} -\Omega^2\cosh^2(\chi) + \Psi^2\sinh^2(\chi) & \sinh(\chi)\cosh(\chi)\left[\Omega^2 - \Psi^2\right] & 0 & 0 \\ \sinh(\chi)\cosh(\chi)\left[\Omega^2 - \Psi^2\right] & \Psi^2\cosh^2(\chi) - \Omega^2\sinh^2(\chi) & 0 & 0 \\ 0 & 0 & \Psi^2 & 0 \\ 0 & 0 & 0 & \Psi^2 \end{pmatrix}$$

Comparing this boosted metric to the $3+1$ decomposed metric () we can read off the shift vector $\tilde{\beta}_i$, the 3 metric $\tilde{\gamma}_{ij}$ and obtain the lapse and metric determinant.

$$\tilde{\alpha}^2 = \frac{\Psi^2\Omega^2}{\Psi^2\cosh^2(\chi) - \Omega^2\sinh^2(\chi)} \tag{3.1.25}$$

$$\tilde{\gamma} = \det\tilde{\gamma}_{ij} = \Psi^4\left[\Psi^2\cosh^2(\chi) - \Omega^2\sinh^2(\chi)\right] \tag{3.1.26}$$

Finally, the conformal 3-metric with unit determinant is

$$\bar{\gamma}_{ij} = \tilde{\gamma}^{-\frac{1}{3}}\begin{pmatrix} \Psi^2\cosh^2(\chi) - \Omega^2\sinh^2(\chi) & 0 & 0 \\ 0 & \Psi^2 & 0 \\ 0 & 0 & \Psi^2 \end{pmatrix}. \tag{3.1.27}$$

Note normally $\tilde{\gamma}_{ij}$ is the conformal 3-metric, but to avoid confusion with the boosted frame it is denoted $\bar{\gamma}_{ij}$. Turning our attention to the matter fields now we only need to change the coordinate dependance, like $\varphi(x) \to \varphi(\tilde{x})$, and remembering $\tilde{t} = 0$ defines our boosted frame, which implies $t = \tilde{x}\sinh(\chi)$, we get the following boosted complex scalar field.

$$\varphi = \Phi(\tilde{x}^2\cosh^2(\chi) + \tilde{y}^2 + \tilde{z}^2)e^{i\omega\tilde{x}\sinh(\chi)} \tag{3.1.28}$$

Note the field is modulated by an oscillatory phase now with wavenumber $k = \omega\tilde{x}\sinh(\chi)$; nodal planes in $\mathrm{Re}(\varphi)$ appear perpendicular to velocity. The conjugate momentum $\tilde{\Pi}$ () in the boosted frame it becomes

$$\tilde{\Pi}(\tilde{x}^\mu) = -\mathcal{L}_{\tilde{n}}\varphi(\tilde{x}^\mu) = -\frac{1}{\tilde{\alpha}}\tilde{m}\cdot\tilde{\partial}\varphi = -\frac{1}{\tilde{\alpha}}\left[\tilde{\partial}_0 - \tilde{\beta}^i\tilde{\partial}_i\right]\Phi(r)e^{i\omega t}.$$

Inconveniently we cannot simply evaluate $\tilde{\Pi}$ in the rest frame as this has a different spacetime foliation and the normal vector $n \neq \tilde{n}$ is genuinely changed; not just transforming components under coordinate transformation. Explicitly writing the contravariant components of the shift vector

$$\tilde{\beta}^i = \left(\frac{\sinh(\chi)\cosh(\chi)\left[\Omega^2 - \Psi^2\right]}{\Psi^2\cosh^2(\chi) - \Omega^2\sinh^2(\chi)}, 0, 0\right)$$

and the partial derivatives of φ in the boosted frame

$$\tilde{\partial}_0 = \cosh(\chi)\partial_t + \sinh(\chi)\partial_x, \quad \tilde{\partial}_1 = \cosh(\chi)\partial_x + \sinh(\chi)\partial_t$$

$$\partial_t\varphi = \Phi\partial_t e^{i\omega t} = i\omega\Phi e^{i\omega t}, \quad \partial_x\varphi = \frac{\partial r}{\partial x}\Phi' e^{i\omega t} = \frac{x}{r}\Phi' e^{i\omega t}$$

we get an expression for the boosted conjugate momentum; explicitly setting $\tilde{t} = 0$ gives the momentum on the surface $\tilde{t} = 0$ to be used as initial conditions in GRChombo.

$$\widetilde{\Pi} = -\frac{1}{\tilde{\alpha}}\left[\left[\sinh(\chi) - \tilde{\beta}^1\cosh(\chi)\right]\frac{\tilde{x}\cosh(\chi)}{r}\Phi' + i\omega\left[\cosh(\chi) - \tilde{\beta}^1\sinh(\chi)\right]\Phi\right]e^{i\omega\tilde{x}\sinh(\chi)} \tag{3.1.29}$$

Our final ingredient is the intrinsic curvature, defined in ().

$$\widetilde{\mathcal{K}}_{\mu\nu} := -\frac{1}{2}\mathcal{L}_{\tilde{n}}\tilde{\gamma}_{\mu\nu} = -\frac{1}{2\tilde{\alpha}}\mathcal{L}_{\tilde{m}}\tilde{\gamma}_{\mu\nu} = -\frac{1}{2\tilde{\alpha}}\left[\tilde{m}\cdot\tilde{\partial}\tilde{\gamma}_{ij} + \tilde{\gamma}_{ik}\tilde{\partial}_j\tilde{m}^k + \tilde{\gamma}_{jk}\tilde{\partial}_i\tilde{m}^k\right]$$

A self written mathematica script gives the following expansion.

$$\alpha^{-1}\widetilde{\mathcal{K}}_{xx} = \cosh^2(\chi)\sinh(\chi)\frac{x\left[v^2\Omega^2\Omega' + \Psi\Omega\Psi' - 2\Psi^2\Omega'\right]}{r\Psi^2\Omega} \tag{3.1.30}$$

$$\alpha^{-1}\widetilde{\mathcal{K}}_{xy} = \cosh(\chi)\sinh(\chi)\frac{y\left[\Omega\Psi' - \Psi\Omega'\right]}{r\Psi\Omega} \tag{3.1.31}$$

$$\alpha^{-1}\widetilde{\mathcal{K}}_{xz} = \cosh(\chi)\sinh(\chi)\frac{z\left[\Omega\Psi' - \Psi\Omega'\right]}{r\Psi\Omega} \tag{3.1.32}$$

$$\alpha^{-1}\widetilde{\mathcal{K}}_{yy} = -\sinh(\chi)\frac{x\Psi'}{r\Psi} \tag{3.1.33}$$

$$\widetilde{\mathcal{K}}_{zz} = \widetilde{\mathcal{K}}_{yy} \tag{3.1.34}$$

Clearly we can apply this to the Black Hole spacetime by an identical procedure, but ignoring φ and Π and setting the isotropic solutions

$$\Omega = \frac{1-\frac{M}{2r}}{1+\frac{M}{2r}}, \qquad \Psi = \left[1+\frac{M}{2r}\right]^2.$$

3.1.6 Spherical Harmonics in Curved Space

Spherical harmonics are an orthonormal function basis for the surface of a sphere. They arise when looking for solutions to the 3D spherical polar laplacian

$$\nabla^2\varphi = \frac{1}{\sqrt{|g|}}\partial_\mu\left(\sqrt{|g|}g^{\mu\nu}\partial_\nu\varphi\right), \quad \mu,\nu\in\{1,2,3\}.$$

On the hypersurface $r = 1$ we get the following metric

$$g_{\mu\nu} = \begin{pmatrix} 1 & 0 \\ 0 & \sin^2\theta \end{pmatrix},$$

and on this surface the spherical harmonics $Y_{lm}(\theta,\phi)$ satisfy the following condition.

$$\mathcal{D}_\mu\mathcal{D}^\mu Y_{lm}(\theta,\phi) = -l(l+1)Y_{lm}(\theta,\phi), \quad x^\mu\in\{\theta,\phi\}$$

This means we can take any spherically symmetric and static metric with $g_{\phi\phi} = \sin^2\theta g_{\theta\theta}$ and replace the angular part of the wave equation with $l(l+1)$. For a spherically symmetric spacetime this gives the Klein Gordon equation for scalar hair.

$$\nabla_\mu\nabla^\mu\varphi = V'\varphi, \quad \varphi = T(t)R(r)Y_{lm}(\theta,\phi)$$

$$\varphi^{-1}\nabla_\mu\nabla^\mu\varphi = g^{tt}\frac{\ddot{T}}{T} + \frac{1}{R\sqrt{|g|}}\partial_r\left(\sqrt{|g|}g^{rr}\partial_r R\right) - l(l+1)g^{\theta\theta}$$

This is a second order ODE for the radial profile R and is an eigenvalue problem for ω if we assume $T = e^{i\omega t}$. Assuming $T = e^{-kt}$ can be done on-top of the black hole metric () and requires the assumption of no back reaction of the scalar field on the metric; this gives an eigenvalue problem in k instead. This leads to the following ODE for the radial profile.

$$\frac{1}{R\sqrt{|g|}}\partial_r\left(\sqrt{|g|}\Psi^{-4}\partial_r R\right) = k^2\frac{\Omega^2}{\Psi^2} + \frac{l(l+1)}{r^2\Psi^4} + V' \tag{3.1.35}$$

Simulations shown later involve boson stars of mass M and black holes of mass $M \to 10M$; these simulations often produce scalar hair about these black holes that is orders of magnitude less massive than the boson stars. In this regime the above equation is assumed relevant.

3.2 Boson Star Numerical Simulations

3.2.1 Simulation Units

GRChombo defaults to geometric units, as described in section (1.2). The scalar field φ appears in the action as

$$S = \int_{\mathcal{M}} [g^{\mu\nu} \partial_\mu \varphi \partial_\nu \varphi^* + ...] \, \mathrm{d}x^4$$

and given S and the metric are dimensionless, dimensional analysis tells us φ has units of inverse length in natural units, or units of energy. The Klein-Gordon mass m

$$\Box \varphi = m^2 \varphi$$

can be absorbed into new dimensionless spatial coordinates $\tilde{x}^i = x^i m$ changing the KG equation to the scale invariant form.

$$\Box \varphi = \varphi$$

3.2.2 GRChombo

GRChombo [] is a recently developed Numerical Relativity code built on top of Chombo [], a PDE solver with fully adaptive mesh refinement (AMR). The advantage of AMR is that regridding, and subsequently sub-volumes of high resolution, is calculated during runtime. This is especially useful for simulating fluids in GR as they can develop features requiring higher resolution in places a human may not expect making pre-specified mesh refinement hard to use. GRChombo uses the CCZ4 system with 1+log slicing and the Gamma driver shift condition, discussed in sections (). GRChombo also supports vectorisation and parallelisation with OpenMP and MPI making it suitable for use on supercomputer clusters.

So far I have implemented initial data for a single or binary system of compact objects which can be either a Schwarzschild black hole or a boson star. The initial data uses isotropic coordinates and can be boosted along coordinate axes, but not yet general directions, giving the possibility of single boosted objects, accelerated head on collisions, grazing collisions and inspirals/quasi-orbits. It should be noted that my implementation was built on top of the pre-existing complex scalar field class (written by Miren). The remainder of this section will cover the numerical aspects of my work.

3.2.3 Initial Data

Following on from the EKG ODE's () we now seek to solve them numerically to obtain initial data for a single static boson star. The system can be reduced to a set of five first order ODE's so we have 5 boundary conditions. Intuitively, for a physical star we would like to impose $\Phi(0) = \Phi_c$, $\Phi'(0) = 0$, $\Phi(r \to \infty) \to 0$, $\Omega'(0) = 0$, $\Omega(r \to \infty) \to 1$, $\Psi'(0) = 0$ and $\Psi(r \to \infty) \to 1$ to be regular at the origin and match the Schwarzschild vacuum solution at large radius; however this is 7 boundary conditions. One of these can be removed by asking for asymptotic flatness, $\sqrt{\Psi(\infty)}\,(1 + \Omega(\infty)) = 2$, rather than $\Omega(\infty) = \Psi(\infty) = 1$, which is inspired by the isotropic black hole metric. One final point of importance is the frequency ω turns the Klein-Gordon ODE () into an eigenvalue problem, admitting only discrete values of ω.

The first attempt to find the radial profile $\{\Phi(r), \Omega(r), \Psi(r)\}$ of the boson star was to use a relaxation method as it trivially incorporates the above two-point boundary conditions. The modification of promoting equation () to a second order ODE like

$$\Omega''(r) = f(g_{\mu\nu}, \partial g_{\mu\nu}, \Phi, \partial\Phi)$$

is one way we can get an extra degree of freedom to allow 6 boundary conditions; it also means all the EKG ODE's can be written in a parabolic (heat/diffusion equation like) form

$$\frac{\partial H}{\partial t} = \nabla^2 H + f(H, ...)$$

by introducing an imaginary time t and solved iteratively via evolving in t to a final state where $\dot{H} = 0$ thus solving the ODE; this is a relaxation method. In practice this method did not work well with the eigenvalue problem in ω. Unlike with a shooting method, there was no obvious way of telling whether the guess ω was bigger or smaller than the correct value. Even if this problem were overcome, numerical solution with relaxation takes far longer than than a simple shooting method, even with Chebychev acceleration [], hence a shooting method was chosen over relaxation.

To find the initial data for a single Boson star, a private c++ script was written using RK4 to integrate the EKG system taking 5 initial conditions, and eigenvalue guess ω_0.

$$\{\Phi(0), \Phi'(0), \Psi(0), \Psi'(0), \Omega(0); \omega\} = \{\Phi_c, 0, \Psi_c, 0, \Omega_c; \omega_0\}$$

Unfortunately we do not know Ω_c and Ψ_c apriori, but it turns out that guessing any values, such as $\Omega_c = 0.5$ and $\Psi_c = 2$, still give a boson star. This will generally result in the following asymptotic metric, for constant A and B.

$$g_{\mu\nu}(r \to \infty) \to \text{diag}(-A^2, B^2, B^2, B^2) \tag{3.2.1}$$

However the eigenvalue ω must be chosen very carefully. It can be shown [], using asymptotics, that the Klein-Gordon equation has a second solution

$$\varphi_2 \approx r^{-1} \exp\left[r\sqrt{1 - \frac{\omega^2}{m^2}} \right]$$

which eventually dominates for any numerical integration at large radii. Interval bisection was used to find the best value of ω to machine precision, and at a radius r_* when the large radius mode is deemed to be growing ($\Phi(r_*) = 0$ or $\Phi'(r_*) = 0$) the conditions $\Phi(r > r_*) = \Phi'(r > r_*) = 0$ are enforced during integration. This creates a vacuum for $r > r_*$ and the spacetime is pure Schwarzschild. After this point, an exponentially growing stepsize was used to reach radii of order 10^8 times larger than desired for evolutions and the values $A = \Omega_\infty = \sqrt{-g_{00}}$ and $B = \Psi_\infty = \sqrt{g_{ii}}$ can be read off. These values are then used iteratively to improve the initial guesses for the metric functions as such $\Omega_c \to \Omega_c / \Omega_\infty$ and $\Psi_c \to \Psi_c / \Psi_\infty$ and the interval bisection for ω is restarted, but with better initial conditions. This is iterated 5 times which leaves $A = B = 1$ to extreme precision and the isotropic boson star is created, requiring a few seconds runtime for a high resolution 200,000 grid-point simulation on a laptop.

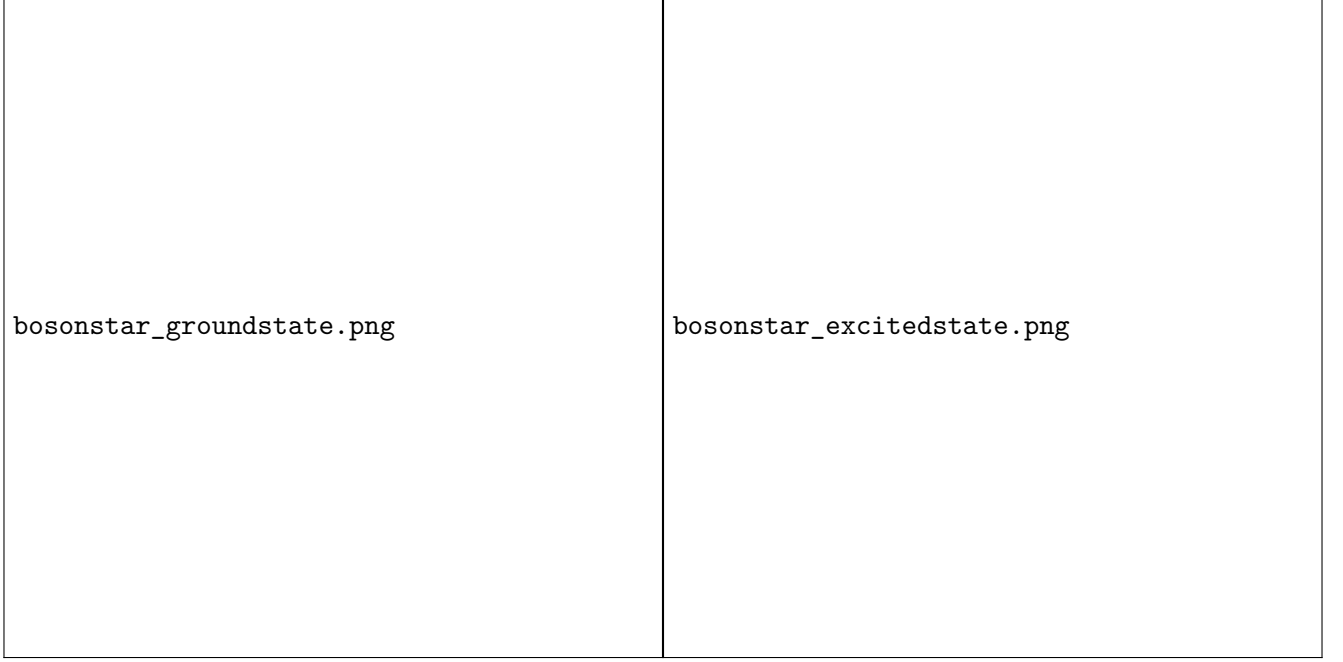|	
bosonstar_groundstate.png	bosonstar_excitedstate.png

Figure 3.1: Boson Star radial profile, Left: Ground state, Right: 1st Excited state

Figures () show the numerical result for the radial profile of a mini boson star ($\Lambda = 0$) and an excited mini boson star. Note two mass definitions are plotted; the ADM mass (calculated as a function of finite r) and the aspect mass $M_A(r)$ which corresponds to assuming the metric's solution is Schwarzschild with $M_A(r)$ rather than M. Polytropic fluid stars were also simulated as a preliminary test of the code; they are much easier to create not needing to solve an eigenvalue problem and don't have an asymptotically growing mode. Figures () show how the ADM mass of boson stars varies with central amplitude $\Phi(0)$ and r_{99}, the radius which $\Phi(r_{99}) = \Phi(0)/100$. It should be noted that the $\Lambda = 0$ case agrees with the known maximum mass, the Kaup limit [] $M_{max} \approx 0.633 M_{PL}^2 m^{-1}$ with the highest measured mass being $M_{max} = 0.63299(3) M_{PL}^2 m^{-1}$ corresponding to a central amplitude of $\sqrt{4\pi G}\Phi(0)_{max} = 0.271(0)$.
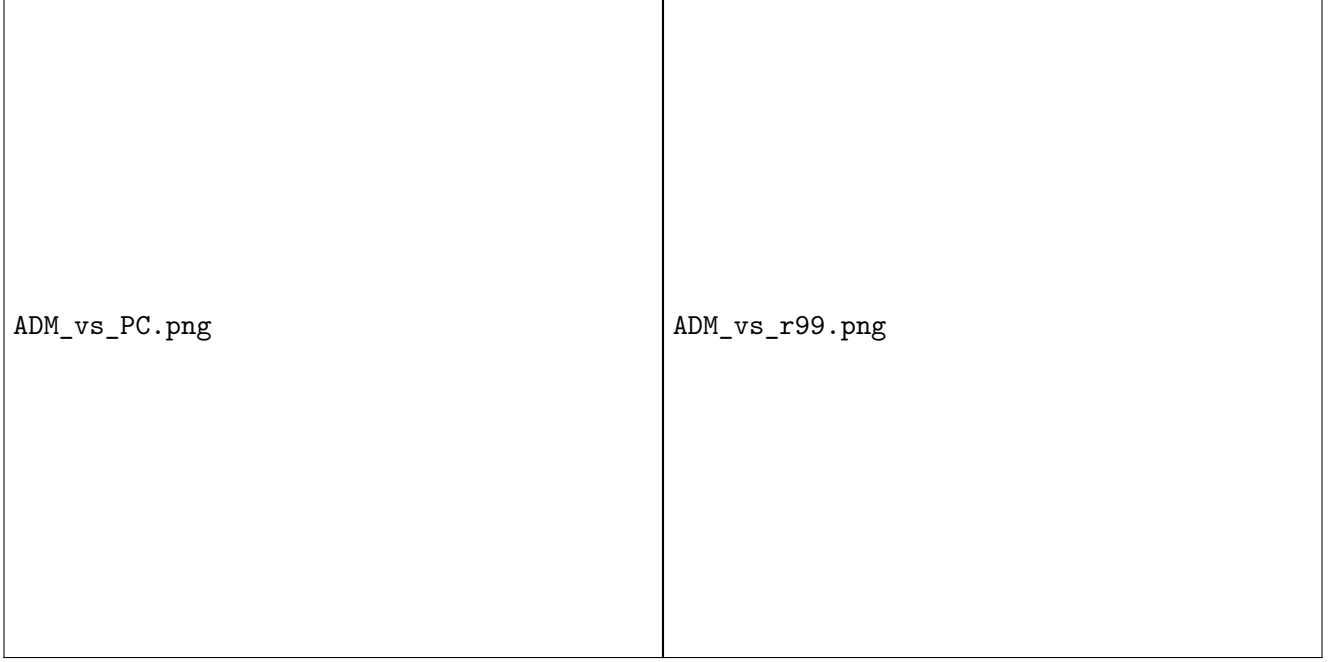
Figure 3.2: Boson star trends, Left: ADM mass vs $\Phi(0)$, Right: ADM mass vs r_{99}

While many different boson stars have been made to test the initial data code, all the following evolutions use the same boson star with parameters $\Lambda = 0$, $\sqrt{4\pi G}\Phi(0) = 0.1 \to \Phi(0) \approx 0.0282$ and ADM mass $M = 0.532(7)$. This is as the stars are heavy enough to form black holes under collisions and large deformations, but stable enough to not collapse to a black hole for moderate perturbations.
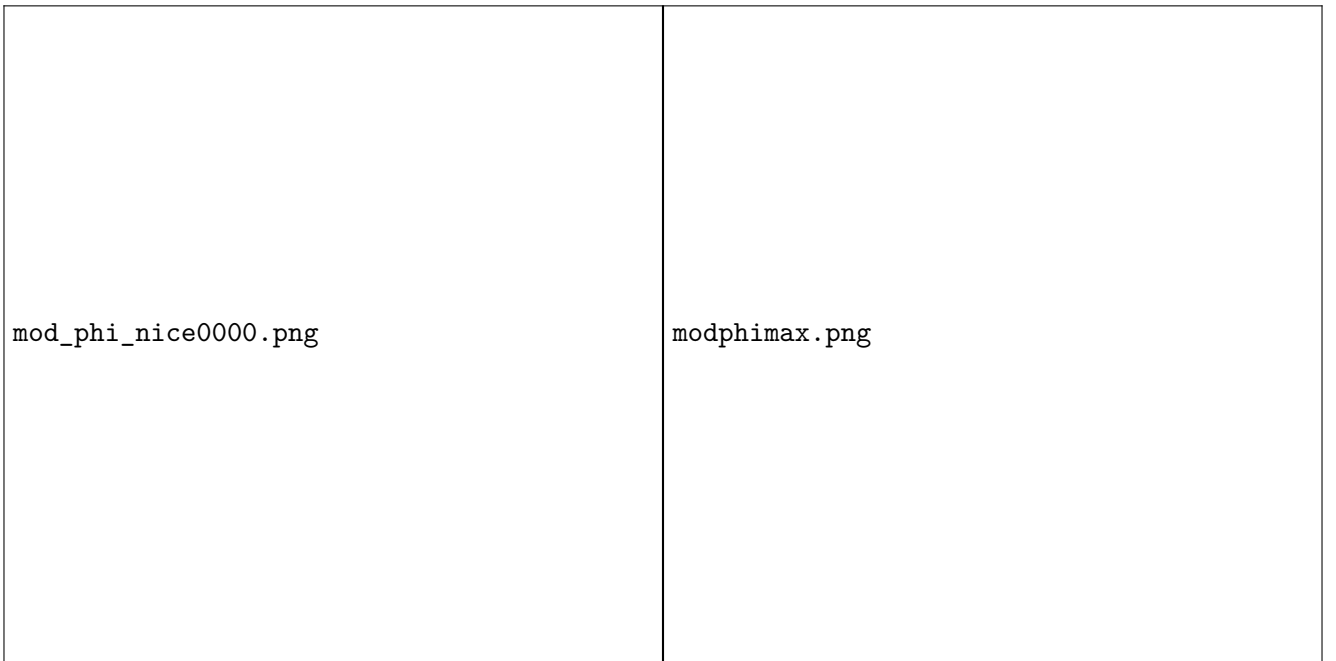
3.2.4 Single Star Evolutions

Figure 3.3: Left: 2D slice of initial $|\varphi|$, Right: Maximum of $|\varphi|$ during evolution.

The first simulation done was of the $\Phi(0) = 0.02820$ mini boson star; as mentioned before all simulations are done with this star. The star is supposed to remain in the centre of the grid and not change as it is a rest frame soliton; this is observed through evolution with GRChombo. Figure () shows a rough initial phase in $|\varphi|$ which changes significantly upon changing the AMR regridding, hence it is likely only a side effect of the interpolation errors at the boundary of AMR regions. Figure () shows that the star conserves $\mathcal{N}$ upto 4 figures and the constraint $\mathcal{H}$ is driven towards zero as desired.
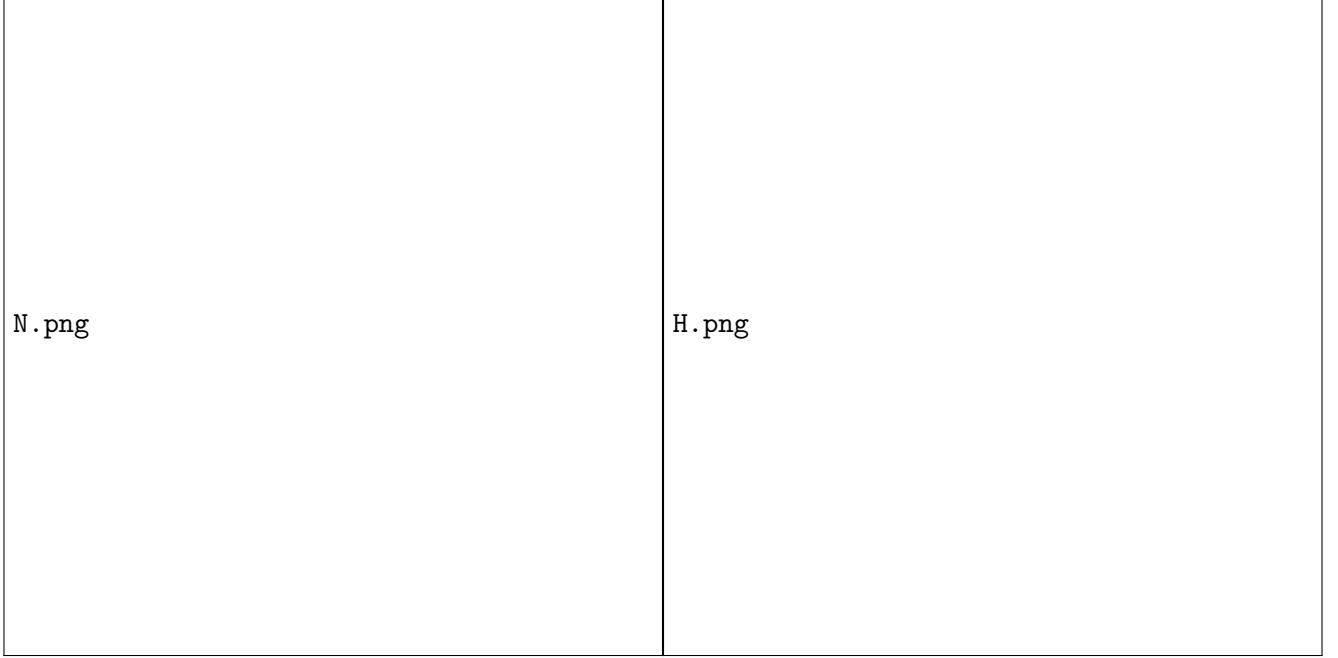
Figure 3.4: Left: Total Noether charge $\mathcal{N}$ during evolution, Right: $||\mathcal{H}||_2$ during evolution.

3.2.5 Superposition of Initial Data

Suppose we have two compact objects with fields φ, Π, γ_{ij}, $\mathcal{K}_{ij}$, α and β^i. The chosen scheme to superpose solutions is below.

$$\varphi = \varphi^{(1)} + \varphi^{(2)}$$
$$\Pi = \Pi^{(1)} + \Pi^{(2)}$$
$$\mathcal{K}^i_j = \mathcal{K}^{(1)i}_{j} + \mathcal{K}^{(2)i}_{j}$$
$$\gamma_{\mu\nu} = \gamma^{(1)}_{\mu\nu} + \gamma^{(2)}_{\mu\nu}$$
$$\beta_i = \beta^{(1)}_i + \beta^{(2)}_i$$
$$\alpha = \sqrt{\alpha^2_{(1)} + \alpha^2_{(2)} - 1} \quad \text{or} \quad \left[\alpha^{-1}_{(1)} + \alpha^{-1}_{(2)} - 1\right]^{-1}$$
$$\chi = \det\left\{\gamma^{(1)}_{\mu\nu} + \gamma^{(2)}_{\mu\nu}\right\}^{-1/3}$$

When a black hole is involved $\Omega(r = \frac{2}{M}) = 0$ so the event horizon causes the lapse to cross through zero; this is circumvented by setting

$$\alpha = \sqrt{\chi}$$

and the lapse is real, non-negative for a spacelike hypersurface Σ. Superposing the scalar field φ is exact for the mini boson star (); for every other variable and type of star case superposition is inexact. Luckily, for sufficiently separated compact objects, superposition gives a very close approximation to the exact numerical solution. The use of CCZ4 also forces the evolution towards a constraint satisfying one.

3.2.6 Head-on Collisions

All the cases studied here are for stationary initial data $\tilde{\mathcal{A}}_{ij} = 0, \mathcal{K} = 0$ in-falling from an initial separation of $d \cdot m = 32$ due to gravitational attraction. Firstly we consider the equal mass Boson star binary, initial data in figure (). At first they slowly infall creating a short lived object with three maxima, shown in figure (,left), then collapse to a black hole with a decaying spherical harmonic cloud (figures) outside. As with all the simulations from now on we assume a black hole forms if $\chi \ll 16^{-1}$ where $\chi = 16^{-1}$ is the value taken on the horizon for the isotropic Schwarzschild metric.

Figure 3.5: Initial Data, Left: χ, Right: $|\varphi|$.

headon_bs/modphi0003.png

headon_bs/modphi0004.png

Figure 3.6: Scalar field amplitude before and after black hole formation, Left: Time $t \cdot m = 150$, Right: Time $t \cdot m = 200$.

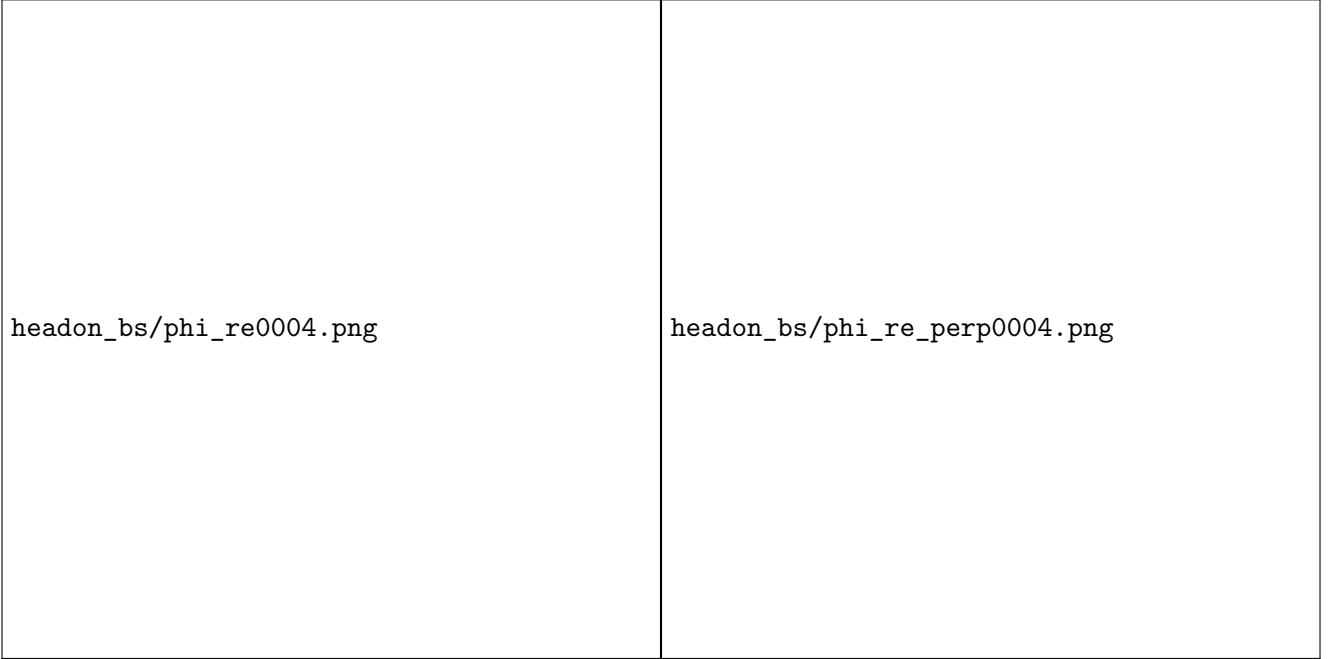headon_bs/phi_re0004.png

headon_bs/phi_re_perp0004.png

Figure 3.7: Real part of scalar field after black hole formation, Left: xy plane, Right: yz plane, perpendicular to initial star separation.

The second case considered is the same Boson star outside a black hole parameterised by $M = 10M_{BS}$ where M_{BS} is the ADM mass of the Boson star. The scalar field tidally deforms into an ellipsoid with high central density, well beyond Kaup limit of $\varphi(0) \sim 0.0764$, and spontaneous collapse to a smaller external black hole is observed. After collapse, figure (), there is an elongated cloud about the new small black hole; there are many nodal lines in $\mathrm{Re}(\varphi)$ which focus on the large black hole showing the cloud is
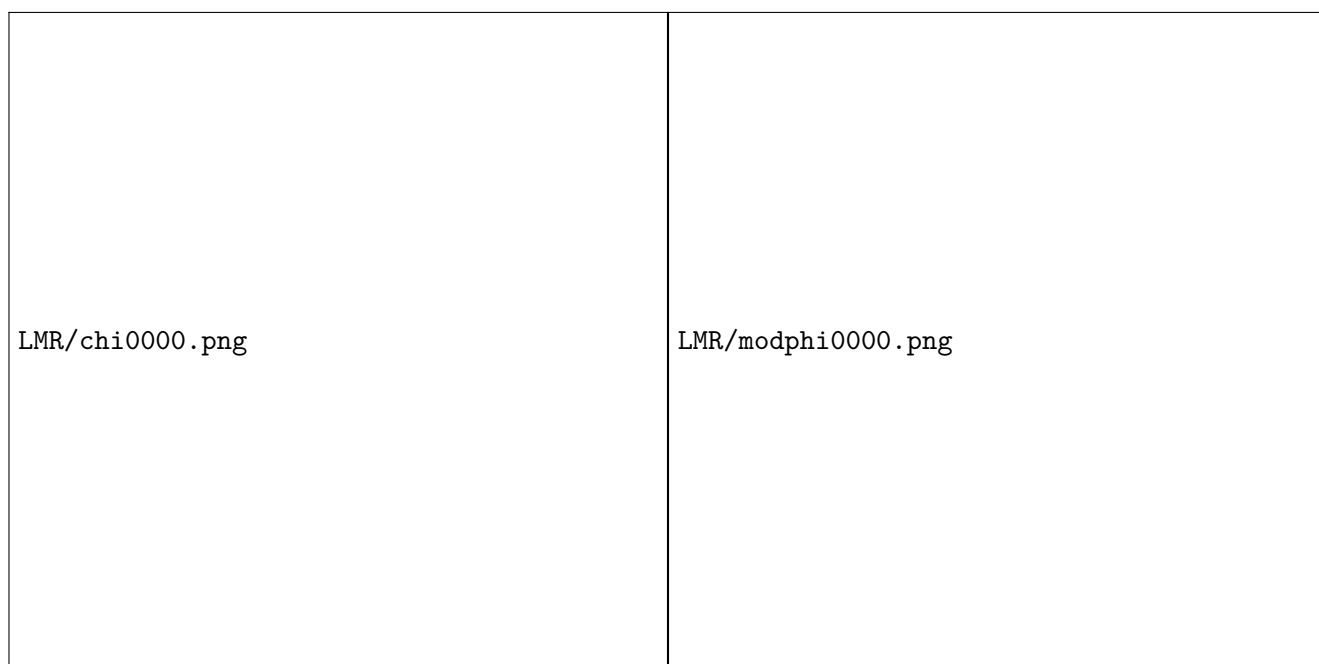
in-falling.

Figure 3.8: Initial Data, Left: χ, Right: $|\varphi|$.

LMR/chi0005.png

LMR/modphi0005.png

LMR/phi_re0000.png

Figure 3.9: Final Data at time $t \cdot m = 125$, Left: Conformal factor χ, Right: Scalar field modulus $|\varphi|$, Bottom: Real part of scalarfield $\mathrm{Re}(\varphi)$.

Final case consists of an equal mass Black Hole and Boson Star, initial configuration in Figure 11. As can be seen from the plot of $\mathrm{Re}(\phi)$ and $|\phi|$, in Figure 12, most of the star falls into the black hole, however some scalar field manages to excite an intricate spherical harmonic cloud pattern.

| headon/chi0000.png | headon/mod_phi0000.png |

Figure 3.10: Initial data for equal mass Boson Star and Black Hole, Left: χ, Right: $|\varphi|$

| headon/phi_re0000.png | headon/mod_phi0007.png |

Figure 3.11: Time $t \cdot m = 905$ for equal mass Boson Star and Black Hole, Left: $\text{Re}(\varphi)$, Right: $|\varphi|$

In all three cases, the Noether charge drops rapidly upon the formation of a black hole; this will be explained in the next section. However some scalar field lingers after collapse, in each case the hair takes the form of spherical harmonics discussed in (). Also observed is the decay of the spherical harmonics to zero amplitude in these simulations with no angular momentum.

3.2.7 Binary Inspiral

The only considered case here is the Quasi-circular orbit and inspiral of two equal mass boson stars. The initial boosts were determined by a newtonian calculation yielding

$$v^2 = \frac{M}{2d}$$

where $M = 0.53(29)$ is the ADM mass of the Boson Star and d is the initial separation. For a relatively low separation of $d \cdot m = 32$ code units, shown in Figures 13,14 (Left), we get $v \sim 0.0915$. The boson stars are observed to complete roughly half an orbit before merging and collapse, forming a black hole. Here a Kerr black hole is assumed to have formed as the spacetime has a significant angular momentum which should partially infall with the scalar field.
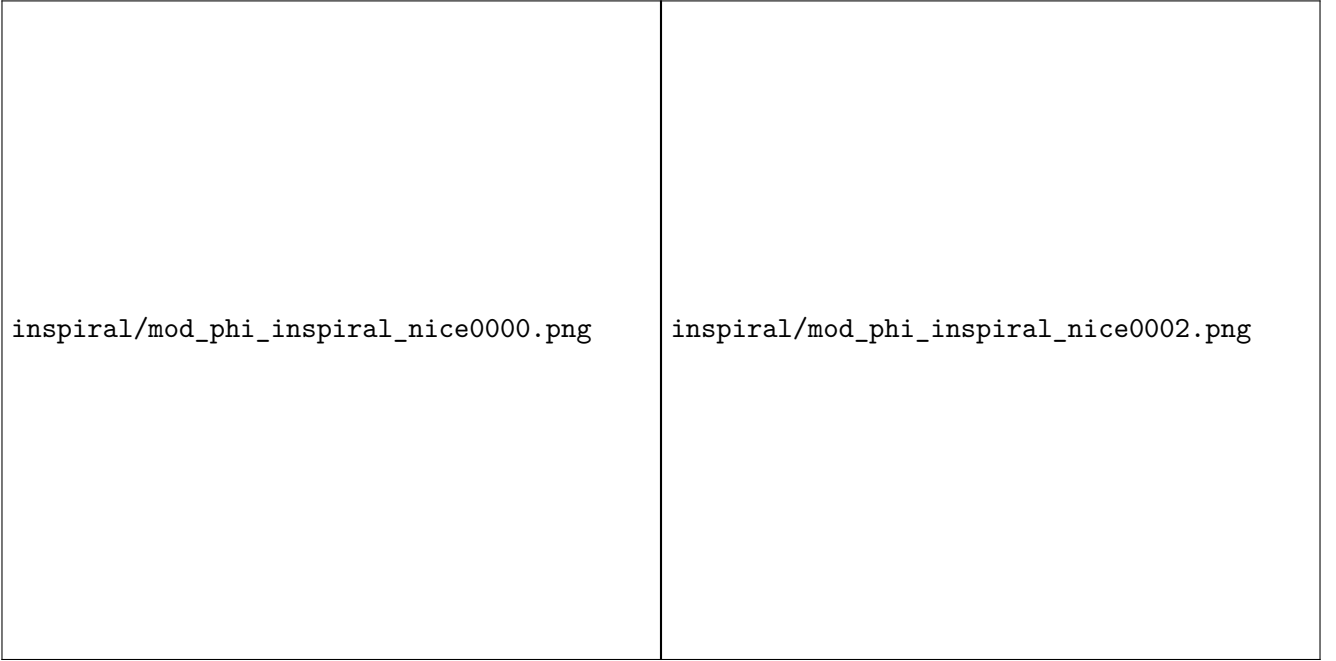
inspiral/mod_phi_inspiral_nice0000.png	inspiral/mod_phi_inspiral_nice0002.png

Figure 3.12: Boson Star $|\varphi|$. Left: initial data, Right: later time $t \cdot m = 700$

inspiral/phi_inspiral_nice0000.png

inspiral/phi_inspiral_nice0002.png

Figure 3.13: Boson Star $\text{Re}(\varphi)$. Left: initial data, Right: later time $t \cdot m = 700$
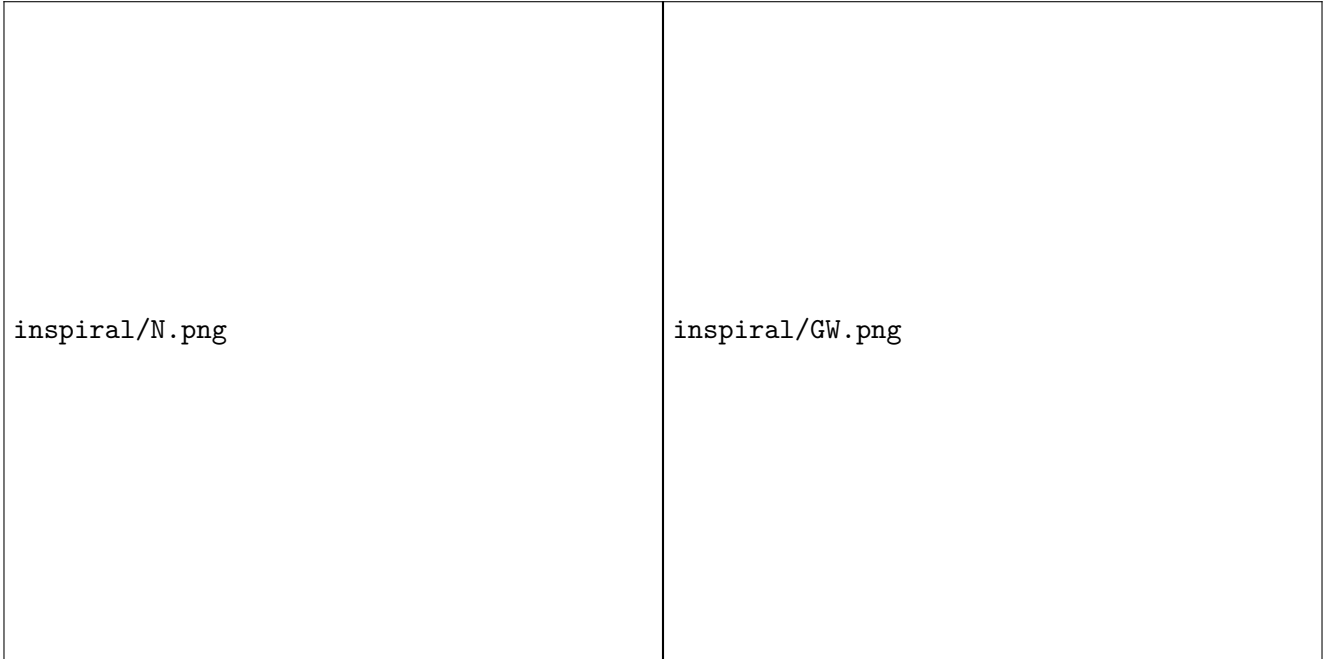

inspiral/N.png

inspiral/GW.png

Figure 3.14: Left: Total Noether charge $\mathcal{N}$ during evolution, Right: Ψ_4 over 22 harmonic during evolution.

Figure 15 shows the total Noether charge, which is no longer conserved. When the black hole forms, the in-falling scalar field moves towards zero radius and gets hugely compressed. The huge compression causes extreme field gradients which induces continuous regridding in the AMR, but this is capped at 7 layers in this simulation to make runtime feasible. When the 8th AMR level is needed it is simply not added and resolution becomes low enough that any Noether charge near the centre is so under-resolved that it seems to fall between the gridpoints. Interestingly, Figures 13,14 (Right) show a scalar field

configuration lingering around the black hole, mostly outside the contour $\chi = 0.7$, looking like scalar hair. Also Figure 15 (Left) of the Noether charge appears to take significantly longer to decay than in the linear collision simulations. It can be seen in Figure 14 in the plot of $\text{Re}(\varphi)$ that the cloud has angular nodes corresponding to angular momentum similarly to boosted stars picking up nodal planes perpendicular to momentum and Figure 10 (Bottom) of the infalling cloud.

The gravitational wave (GW) signal can be seen in Figure 15 (Right), extracted at a radius $r \cdot m = 90$. At the time $t \cdot m \approx 700$ the gravitational wave signal due to the merger appears; in order to record a longer inspiral simulations with larger initial separations need to be simulated. Currently there appears to be some small problem with the initial data, also observed in the collisions with no angular momentum, that manifests itself in noisy GW extraction and the Hamiltonian constraint initially sharply rising.

3.3   Future Work

The first thing that needs to be done is to fix the small error in initial data discussed in section 4.7. After this, the natural extension to work done is to perform binary inspirals with larger radii and inspirals containing an initial black hole. Apart from inspirals, grazing collisions should be studied. A collision with no angular momentum that needs to be looked at is the case of a very small black hole near a large boson star.

Other avenues of study could include exploration of the boson star parameter space, for instance changing central densities, eigenstates, parameters in the potential () and total phase offsets. Binary systems with asymmetric stars are also possible a possibility.

Finally I plan on studying long lived scalar hair. In general it is difficult to create near extremal Kerr black holes in collisions so it could be useful to create new initial data for this. Maybe collisions with high angular momentum can also produce long lived hair; section 4.7's inspiral shows what appears to be very slowly decaying scalar hair. The study of Proca Stars (spin-1) is another way to study scalar hair and super radiance, here the timescales are often shorter than that for the spin-0 Klein Gordon stars.

Chapter 4

Local Continuity of Angular Momentum and Noether Charge

Conservation laws have many applications in numerical relativity. However, it is not straightforward to define local conservation laws for general dynamic spacetimes due the lack of coordinate translation symmetries. In flat space, the rate of change of energy-momentum within a finite spacelike volume is equivalent to the flux integrated over the surface of this volume; for general spacetimes it is necessary to include a volume integral of a source term arising from spacetime curvature. In this work a study of continuity of matter in general relativity is extended to include angular momentum of matter and Noether currents associated with gauge symmetries. Expressions for the Noether charge and flux of complex scalar fields and complex Proca fields are found using this formalism. Expressions for the angular momentum density, flux and source are also derived which are then applied to a numerical relativity collision of boson stars in 3D with non-zero impact parameter as an illustration of the methods.

Conventions

Throughout this work the metric has sign $\{-, +, +, +\}$ and physical quantities will be expressed as a dimensionless ratio of the Planck length L_{pl}, time T_{pl} and mass M_{pl} unless stated otherwise; for example Newtons equation of gravity would be written as

$$F = \frac{GMm}{r^2} \quad \rightarrow \quad \left(\frac{F}{F_{pl}} \right) = \frac{\left(\frac{M}{M_{pl}} \right) \left(\frac{m}{M_{pl}} \right)}{\left(\frac{r}{L_{pl}} \right)^2}, \tag{4.0.1}$$

where $F_{pl} = M_{pl} L_{pl} T_{pl}^{-2}$ is the Planck force. Consequently c, G and $\hbar$ take the numerical value of 1. Additionally, tensor fields will be denoted using bold font for index free notation and normal font for the components. The dot product between two vector fields will be written interchangeably as $\boldsymbol{A} \cdot \boldsymbol{B} \leftrightarrow A^\mu B_\mu$ for readability. Additionally, ∇_μ denotes the covariant derivative and ∂_μ is the partial derivative, both with respect to coordinate x^μ. Finally, unless stated otherwise, Greek indices such as $\{\alpha, \beta, ..., \mu, \nu, ...\}$ label four dimensional tensor components whereas late Latin indices such as $\{i, j, k, ...\}$ label three dimensional tensor components and early Latin indices such as $\{a, b, ...\}$ label two dimensional ones.

4.1 Introduction

Conservation laws play an important role in many areas of physics. For a general Lagrangian density $\mathcal{L}$, dependant on fields ϕ_i and derivatives $\partial_k \phi_i$ for $i \in \{1, 2, ..., m\}$ and $k \in \{1, 2, ..., n\}$, if a field transformation $\phi_i \rightarrow \phi_i + \delta\phi_i$ leaves the Lagrangian constant the Euler-Lagrange equations imply there is a

conserved current $\boldsymbol{J}$, with zero divergence, given by

$$J^k = \sum_i \frac{\partial \mathcal{L}}{\partial(\partial_k \phi_i)} \delta \phi_i. \tag{4.1.1}$$

In curved space a conserved current $\boldsymbol{J}$ satisfies $\nabla_\mu J^\mu = 0$. A charge Q within 3-volume V and a flux F though ∂V, the boundary of V, can be associated with $\boldsymbol{J}$ as described later in Eqs. (4.2.16) and (4.2.17). If $\boldsymbol{J}$ is conserved then Q is a conserved charge satisfying

$$\partial_t Q = F. \tag{4.1.2}$$

This says the rate of change of a charge in a volume V is equal to the flux across the boundary ∂V of V. In the case that $\boldsymbol{J}$ has a non-zero divergence, $\nabla_\mu J^\mu \neq 0$, Eq. (4.1.2) generalises to the continuity equation

$$\partial_t Q = F - S, \tag{4.1.3}$$

where S is defined in Eq. (4.2.18); S is the source of $\boldsymbol{J}$ in V which can be understood as the destruction or creation of charge Q. Eq. (4.1.3) is a simplified version of Eq. (4.2.12), later referred to as the QFS system.

Evaluation of the continuity equations above, and their corresponding charges Q, have many uses in the study of fundamental fields in Numerical Relativity. One such use is the measurement of the Noether current $\boldsymbol{J}$ of a complex scalar/vector field which arises from a $U(1)$ gauge symmetry of the matter fields ψ_j of the form $\psi_j \to \psi_j e^{ia} \sim \psi_j + ia\psi_j$ for some small constant a and $j \in \{1, 2, ..., n\}$. The total charge Q, also called Noether charge in this case, is useful to track during numerical simulations as it gives insight into the numerical quality of a simulation. A violation of Noether charge conservation can arise from insufficient resolution in some region of the simulation or due to boundary conditions in a finite volume simulation. In the case of Sommerfeld (outgoing wave) boundary conditions [?] we might expect charge to be transported out of a finite computational domain and the total charge Q in the simulation should decrease. Monitoring only Q within some volume V, it is impossible to tell whether Noether charge violation is due to a flux F through the surface ∂V or undesirable numerical inaccuracies such as dissipation. It is more useful to check whether the continuity Eq. (4.1.2) (or equivalently Eq. (4.1.3) if there were a non-zero source term) is obeyed for a finite domain V; if this fails there is likely a problem as the continuity equations should be exactly observed for general spacetimes.

Another use of the continuity equations is to measure the amount of energy-momentum belonging to matter fields within a volume V. This has many possible applications such as calculating the total energy or momentum of compact objects such as boson stars and neutron stars. The energy-momentum of matter obeys a conservation law in General Relativity as given by Penrose [?] where the considered spacetime is assumed to admit a Killing vector. In the case a Killing vector exists then a conserved current $\boldsymbol{J}$ associated with the energy-momentum tensor $\boldsymbol{T}$ can be identified. The current is $J^\mu = T^\mu_\nu \xi^\nu$ for some Killing vector $\boldsymbol{\xi}$ and satisfies $\nabla_\mu J^\mu = 0$. If $\boldsymbol{\xi}$ is a Killing vector then Eq. (4.1.2) is the correct continuity equation and the charge Q is conserved. In General Relativity the existence of Killing vectors is rare, reserved for spacetimes with special symmetries. Generic dynamic spacetimes with no symmetries, such as inspirals and grazing collisions of compact objects, have no easily identifiable Killing vector fields. If there is no Killing vector the divergence of $\boldsymbol{J}$ becomes $\nabla_\mu J^\mu = T^{\mu\nu} \nabla_\mu \xi_\nu$ and the source term S is non-zero. Now Eq. (4.1.3) is the correct continuity equation and the charge Q is no longer conserved. In section 4.5 we will show how the choice of $\boldsymbol{\xi}$ affects the type of current $\boldsymbol{J}$, and therefore charge Q, obtained. While measures of energy or momentum are interesting in their own right, the measure of Eq. (4.1.3) within some volume V can be a good measure of numerical quality of a simulation in a similar fashion to the measure of Noether charge mentioned already.

When dealing with black hole spacetimes resolution requirements typically become very strict towards the singularity and lead to a local violation of Eqs. (4.1.2) and (4.1.3). This might not doom a simulation as for most physical applications in GR singularities are contained by an event horizon and are therefore

causally disconnected from the rest of the simulation; a resolution problem in the vicinity of a singularity therefore may not propagate to the exterior. It could be helpful instead to consider a volume $\bar{V}$ equal to V but removing a set of finite volumes $\tilde{V}_i$ which surround any singularities. Testing Eqs. (4.1.2) and (4.1.3) in volume $\bar{V}$ would then give a measure of the simulation resolution untainted by the resolution issues at a singularity.

Currently in Numerical Relativity it is common to measure energy-momentum in a localised region with with Eq. (4.2.16) for the charge Q where the charge density $\mathcal{Q}$ is given in section 4.5. Examples of this can be seen in [?], [?], [?] and [?]. While this is a good measure it neglects any radiation and the transfer of energy-momentum between matter and spacetime curvature; if the spacetime does not contain the corresponding Killing vector the charge cannot be treated as a conserved quantity. Instead the combination of variables $Q - S$, where S is defined in Eq. (4.2.18) and $\mathcal{S}$ in section 4.5, should be treated as a conserved quantity. Other popular methods to obtain the energy-momentum of a system include integrating asymptotic quantities such as the ADM mass and momentum, however these can not be used locally as they are defined in the limit of large radii only.

Recent work by Clough [?] evaluates Q, F and S for energy and linear momentum with the assumption that the approximate Killing vector $\boldsymbol{\xi}$ is a coordinate basis vector satisfying $\partial_i \xi^j = 0$. Successful numerical tests of Eq. (4.1.3) are given for fixed and dynamic background simulations.

This paper builds on the work of [?] and generalises the system to measure angular momentum conservation and the conservation of Noether charges of complex scalar fields and spin-1 complex Proca fields. The assumption that the approximate Killing vector $\boldsymbol{\xi}$ is a basis vector satisfying $\partial_i \xi^j = 0$ is dropped and leads to a more general source term $\mathcal{S}$. The QFS system for angular momentum is also tested using fully non-linear numerical Relativity simulations of a spacetime consisting of two boson stars colliding in a grazing fashion.

This paper is organised as follows. In section 4.2 the QFS system for a general non-conserved current is derived and section 4.3 explicitly expands the results for use with a spherical extraction surface. Even though no other extraction surfaces are considered, the results of 4.3 are easily adaptable to other shapes. Section 4.4 is a standalone derivation of the well known Noether charge density from the QFS perspective and goes on to find the flux variable; results for complex scalar fields and complex Proca fields are given. The application of the QFS system to energy momentum currents, angular momentum and energy are given in section 4.5. A fully non-linear test of the QFS system for angular momentum, using [?, ?] to perform Numerical Relativity simulations, is presented in section 4.6 along with a convergence analysis.

4.2   Derivation of the QFS System

For a spacetime $(\mathcal{M}, \boldsymbol{g})$ we start by defining a vector field $\boldsymbol{J}$ and subjecting it to the following continuity equation,

$$\nabla_\mu J^\mu = S, \tag{4.2.1}$$

where S is a source term and describes the non-conservation of $\boldsymbol{J}$. In the case $S = 0$ the current is conserved. We are interested in the charge density $\mathcal{Q}$ and source density $\mathcal{S}$ associated with $\boldsymbol{J}$ in a spatial 3-volume $V \in \Sigma$. Here Σ is the usual 3-dimensional spacelike manifold Σ consisting of the set of all points with constant time coordinate t, equipped with metric $\boldsymbol{\gamma}$. We are also interested in the flux density $\mathcal{F}$ through ∂V, the boundary of V with metric $\boldsymbol{\sigma}$. Σ is spanned by spatial coordinates x^i related to the full spacetime coordinates x^μ by $x^\mu = \{t, x^i\}$. The normal to Σ is the unit co-vector $\mathbf{n}$ defined as,

$$n_\mu := \frac{\nabla_\mu t}{\sqrt{g^{\rho\sigma} \nabla_\rho t \nabla_\sigma t}} = -(\alpha, 0, 0, 0), \tag{4.2.2}$$

$$n^\mu = \frac{1}{\alpha} (t^\mu - \beta^\mu) = \frac{1}{\alpha}(1, -\beta^i), \tag{4.2.3}$$

where (α, β^i) are the usual lapse and shift from the ADM 3+1 spacetime decomposition [**?**]. The reader is directed to [**?**] for a comprehensive introduction to the 3+1 decomposition. In Eq. (4.2.3), $t^\mu = (1, 0, 0, 0)$ is the future directed vector and is distinct from n^μ. Time vector $\boldsymbol{t}$ is useful as its integral curves form lines of constant spatial coordinates. With this knowledge we can define the 4-volume M, the spatial 3-volume V evolved along integral curves of $\boldsymbol{t}$ between times $t_0 \leq t \leq t_0 + \delta t$ in the limit $\delta t \to 0$. Finally we define the 3-dimensional volume H, with metric $\boldsymbol{h}$. H is the evolution of ∂V along integral curves of $\boldsymbol{t}$ between times $t_0 \leq t \leq t_0 + \delta t$ and is the 3-volume the flux crosses; clearly our definition of H will affect our definition of flux density. There is no reason to choose the timelike vector $\boldsymbol{t}$, rather than $\boldsymbol{n}$, to evolve V and ∂V in time and both will result in a different definition of flux density. However, it is shown in appendix .2 that these two choices result in the same total integrated flux. A diagram summarising the relevant geometry can be found in Fig. 4.1.

With the relevant geometry discussed we can derive the QFS system, Eq. (4.1.3), by integrating Eq. (4.2.1) over M;

$$\int_M \boldsymbol{\nabla} \cdot \boldsymbol{J} \sqrt{-g} \, \mathrm{d}x^4 = \int_M S \sqrt{-g} \, \mathrm{d}x^4. \tag{4.2.4}$$

Let us start by using Gauss' theorem for curved space [**?**] on the left hand side,

$$\int_M \boldsymbol{\nabla} \cdot \boldsymbol{J} \sqrt{-g} \, \mathrm{d}x^4 = \int_{\partial M} \hat{\boldsymbol{s}} \cdot \boldsymbol{J} \sqrt{^{(3)}g} \, \mathrm{d}x^3, \tag{4.2.5}$$

with $\sqrt{^{(3)}g}$ being the volume element of a generic 3-surface and $\hat{\boldsymbol{s}}$ being the corresponding unit normal. Note that $\hat{\boldsymbol{s}}$ is outward directed when spacelike and inward directed when timelike. The integral of $\boldsymbol{\nabla} \cdot \boldsymbol{J}$ over M is now transformed to a surface integral of $\boldsymbol{J}$ over the compound 3-volume ∂M. This surface is split into an integral over H and two integrals over V at times t_0 and $t_0 + \delta t$. The integrals over V give,

$$\left(\int_V^{(t=t_0)} - \int_V^{(t=t_0+\delta t)} \right) \boldsymbol{n} \cdot \boldsymbol{J} \sqrt{\gamma} \, \mathrm{d}^3 x,$$

$$= -\int_V \left[(\boldsymbol{n} \cdot \boldsymbol{J} \sqrt{\gamma})_{t+\delta t} - (\boldsymbol{n} \cdot \boldsymbol{J} \sqrt{\gamma})_t \right] \mathrm{d}^3 x, \tag{4.2.6}$$

$$= -\delta t \, \partial_t \int_V \boldsymbol{n} \cdot \boldsymbol{J} \sqrt{\gamma} \, \mathrm{d}^3 x, \tag{4.2.7}$$

where we made use of the fact that the coordinate volume V is constant for all times due to it evolving in time with t^μ. Here $\sqrt{\gamma}$ is the volume element on the spacelike manifold Σ. Now let us evaluate the integral over H, with metric $\boldsymbol{h}$ of signature $\{-, +, +\}$,

$$\int_H \boldsymbol{N} \cdot \boldsymbol{J} \sqrt{-h} \, \mathrm{d}^2 x \, \mathrm{d}t,$$

$$= \int_{\partial V} \boldsymbol{N} \cdot \boldsymbol{J} \sqrt{-h} \, \mathrm{d}^2 x \int_t^{t+\delta t} \mathrm{d}t, \tag{4.2.8}$$

$$= \delta_t \int_{\partial V} \boldsymbol{N} \cdot \boldsymbol{J} \sqrt{-h} \, \mathrm{d}^2 x, \tag{4.2.9}$$

where $\boldsymbol{N}$ is the unit normal to H as shown in Fig. 4.1. Given that $\boldsymbol{n}$ is not tangent to H (but the time vector $\boldsymbol{t}$ is) we have $\boldsymbol{N} \cdot \boldsymbol{n} \neq 0$ and $\boldsymbol{N} \cdot \boldsymbol{t} = 0$. This means we must normalise $\boldsymbol{N}$ with metric $\boldsymbol{g}$ and not γ as $\boldsymbol{N}$ is not tangent to Σ and $\boldsymbol{g}(\boldsymbol{N}, \boldsymbol{N}) \neq \gamma(\boldsymbol{N}, \boldsymbol{N})$. In other words, $\boldsymbol{N}$ is a 4-vector in the case we time evolve V with time vector $\boldsymbol{t}$ but $\boldsymbol{N}$ is a 3-vector if we time evolve with $\boldsymbol{n}$. Finally the right hand

side source integral from (4.2.4) becomes,

$$\int_M S\sqrt{-g}\,\mathrm{d}x^4,$$

$$= \int_V S\sqrt{-g}\,\mathrm{d}x^3 \int_t^{t+\delta t} \mathrm{d}t, \tag{4.2.10}$$

$$= \delta t \int_V S\alpha\sqrt{\gamma}\,\mathrm{d}x^3. \tag{4.2.11}$$

Combining Eqs. (4.2.7), (4.2.9) and (4.2.11) transforms Eq. (4.2.4) into,

$$\partial_t \int_V \mathcal{Q}\sqrt{\gamma}\,\mathrm{d}^3 x = \int_{\partial V} \mathcal{F}\sqrt{\sigma}\,\mathrm{d}^2 x - \int_V \mathcal{S}\sqrt{\gamma}\,\mathrm{d}^3 x, \tag{4.2.12}$$

where the density, flux density and source density $(\mathcal{Q}, \mathcal{F}, \mathcal{S})$ of angular momentum are defined as,

$$\mathcal{Q} := J^\mu n_\mu, \tag{4.2.13}$$

$$\mathcal{F} := \frac{\sqrt{-h}}{\sqrt{\sigma}} J^\mu N_\mu, \tag{4.2.14}$$

$$\mathcal{S} := \alpha S. \tag{4.2.15}$$

The integrated version of these quantities can be written as

$$Q := \int_V \mathcal{Q}\sqrt{\gamma}\,\mathrm{d}^3 x, \tag{4.2.16}$$

$$F := \int_{\partial V} \mathcal{F}\sqrt{\sigma}\,\mathrm{d}^2 x, \tag{4.2.17}$$

$$S := \int_V \mathcal{S}\sqrt{\gamma}\,\mathrm{d}^3 x. \tag{4.2.18}$$

For later sections it is useful to split the normal vector $\boldsymbol{N}$ into its spacelike and timelike parts,

$$N_\mu =_\mu -\boldsymbol{n}\cdot\boldsymbol{N} n_\mu, \tag{4.2.19}$$

where $_\mu =\perp_\mu^\nu N_\nu$ is the projected part of $\boldsymbol{N}$ onto Σ with $\boldsymbol{n}\cdot = 0$ and $\perp$ is the projection operator onto Σ,

$$\perp_\mu^\nu = \delta_\mu^\nu + n^\mu n_\nu. \tag{4.2.20}$$

Using Eqs. (4.2.19) and (4.2.20) the flux term becomes,

$$\mathcal{F} = \frac{\sqrt{-h}}{\sqrt{\sigma}} J^\mu (_\mu -\boldsymbol{n}\cdot\boldsymbol{N} n_\mu), \tag{4.2.21}$$

$$= \frac{\sqrt{-h}}{\sqrt{\sigma}} (\gamma^{\mu\nu} J_\mu N_\nu - \boldsymbol{n}\cdot\boldsymbol{N}\mathcal{Q}). \tag{4.2.22}$$

The term on the left arises from flux through the surface ∂V and the term on the right is a consequence of the coordinate volume V moving with respect to a normal observer with worldline traced by $\boldsymbol{n}$. Writing the flux term as above makes it obvious how the definition of flux depends on the 3-volume H which determines $\sqrt{-h}$, $\sqrt{\sigma}$ and $\boldsymbol{N}$. Equivalently it can be seen that the density (4.2.13) and source (4.2.15) terms do not depend on the extraction surface.

4.3 Application to Spherical extraction

The numerical application of the QFS system in section 4.6 chooses a spherical volume V to extract the angular momentum flux. Using standard Cartesian and spherical polar coordinates, $x^i_{\text{cart}} = \{x, y, z\}$ and $x^i_{\text{polar}} = \{r, \theta, \phi\}$ respectively, we can define H as the coordinate volume $r = r_0$, $t_0 \leq t \leq t + \delta t$. Thus, the normal $\boldsymbol{N}$ to H is proportional to $\boldsymbol{\nabla}(r - r_0) = \boldsymbol{\nabla}(\sqrt{x^2 + y^2 + z^2} - r_0)$. Explicitly calculating the components N_μ, and normalising to unity, with spherical polar spacelike coordinates gives,

$$N_\mu = \frac{\nabla_\mu r}{\sqrt{g^{\rho\sigma}\nabla_\rho r \nabla_\sigma r}}, \tag{4.3.1}$$

$$= \frac{1}{\sqrt{g^{rr}}}(0, 1, 0, 0). \tag{4.3.2}$$

Note that if we had chosen H, the future evolution of ∂V, to be evolved along the unit vector $\boldsymbol{n}$ rather than time vector $\boldsymbol{t}$ then we would have obtained a different definition of $\boldsymbol{N}$ perpendicular to $\boldsymbol{n}$ rather than $\boldsymbol{t}$. The consequences of the alternate choice of H are explored in appendix .2.

The density and source terms $\mathcal{Q}$ and $\mathcal{S}$ do not depend on the integration domain V, but the flux term $\mathcal{F}$ does. The calculation of the Flux term requires the evaluation of the volume element $\sqrt{-h}$ of H. Due to the choice that H is the surface of constant radial coordinate, finding the metric of this surface is straightforward. Here we define spherical polar coordinates $x^\mu = \{t, r, \theta, \phi\}$ on $\mathcal{M}$ and $X^m = \{t, \theta, \phi\}$ spanning H. Projecting the 4-metric $\boldsymbol{g}$ onto H we can write

$$^{(4)}h_{\mu\nu} = g_{\mu\nu} - N_\mu N_\nu, \tag{4.3.3}$$

where $^{(4)}\boldsymbol{h}$ belongs to $\mathcal{M}$. The line element of a curve residing in H can be equivalently evaluated in $\mathcal{M}$ or H; the pullback of $^{(4)}\boldsymbol{h}$ from $\mathcal{M}|_{r=r_0}$ to H gives the 3-metric $\boldsymbol{h}$ belonging to H,

$$h_{mn} = {}^{(4)}h_{\mu\nu} \frac{\partial x^\mu}{\partial X^m} \frac{\partial x^\nu}{\partial X^n}, \tag{4.3.4}$$

$$= \begin{pmatrix} g_{tt} & g_{t\theta} & g_{t\phi} \\ g_{\theta t} & g_{\theta\theta} & g_{\theta\phi} \\ g_{\phi t} & g_{\phi\theta} & g_{\phi\phi} \end{pmatrix}. \tag{4.3.5}$$

A similar argument can be made for ∂V, the set of all points satisfying $r = r_0$ and $t = t_0$, with metric $\boldsymbol{\sigma}$. The metric components and volume element are

$$\sigma_{ab} = \begin{pmatrix} g_{\theta\theta} & g_{\theta\phi} \\ g_{\phi\theta} & g_{\phi\phi} \end{pmatrix}, \tag{4.3.6}$$

$$\sqrt{\sigma} = \sqrt{g_{\theta\theta}g_{\phi\phi} - g_{\phi\theta}g_{\theta\phi}}. \tag{4.3.7}$$

Using Cramer's rule for the inverse of a matrix with Eqs. (4.3.5) and (4.3.6) we get

$$h^{tt} = \frac{\sigma}{h}, \tag{4.3.8}$$

and reading from Eq. (4.3.3) gives

$$^{(4)}h^{tt} = g^{tt} - N^t N^t, \tag{4.3.9}$$

$$= -\frac{1}{\alpha^2}\left(\frac{\gamma^{rr}}{g^{rr}}\right). \tag{4.3.10}$$

Similarly to Eq. (4.3.4), the pushforward of $\boldsymbol{h}$ on H to $^{(4)}\boldsymbol{h}$ on $\mathcal{M}|_{r=r_0}$ gives

$$^{(4)}h^{\mu\nu} = h^{mn} \frac{\partial x^\mu}{\partial X^m} \frac{\partial x^\nu}{\partial X^n}, \tag{4.3.11}$$

$$= \begin{pmatrix} h^{tt} & 0 & h^{t\theta} & h^{t\phi} \\ 0 & 0 & 0 & 0 \\ h^{\theta t} & 0 & h^{\theta\theta} & h^{\theta\phi} \\ h^{\phi t} & 0 & h^{\phi\theta} & h^{\phi\phi} \end{pmatrix}, \tag{4.3.12}$$

which shows that $h^{tt} = {}^{(4)}h^{tt}$. Combining Eqs. (4.3.8) and (4.3.10) it can be shown that

$$\sqrt{-h} = \alpha\sqrt{\sigma}\sqrt{\frac{g^{rr}}{\gamma^{rr}}}. \tag{4.3.13}$$

Using this with Eq. (4.3.2) we can expand Eq. (4.2.14) for the flux term $\mathcal{F}$,

$$\mathcal{F} = \frac{\sqrt{-h}}{\sqrt{\sigma}}J^{\mu}N_{\mu} = \frac{\alpha}{\sqrt{\gamma^{rr}}}J^{r}, \tag{4.3.14}$$

but for practical purposes it is helpful to decompose this in terms of 3+1 variables as in Eq. (4.2.22),

$$\mathcal{F} = \alpha\frac{\sqrt{g^{rr}}}{\sqrt{\gamma^{rr}}}\left(\gamma^{\mu\nu}J_{\nu}N_{\mu} - \boldsymbol{n}\cdot\boldsymbol{N}\mathcal{Q}\right), \tag{4.3.15}$$

$$= \alpha\frac{\sqrt{g^{rr}}}{\sqrt{\gamma^{rr}}}\left(\gamma^{r\nu}J_{\nu}\frac{1}{\sqrt{g^{rr}}} + \alpha^{-1}\beta^{r}\frac{1}{\sqrt{g^{rr}}}\mathcal{Q}\right), \tag{4.3.16}$$

$$= \frac{1}{\sqrt{\gamma^{rr}}}\left(\alpha\gamma^{r\nu}J_{\nu} + \beta^{r}\mathcal{Q}\right). \tag{4.3.17}$$

It is straightforward to re-derive the results of this section for other extraction volume shapes, such as cylinders or cubes/rectangles, with a redefinition of spacelike volume V giving rise to different $\boldsymbol{N}$, H and ∂V. It is wise to pick suitable coordinates adapted to the symmetry of the problem.

4.4 Noether Currents

In this section we apply the previous results of the QFS system Eq. (4.2.12) to the continuity of Noether charge for both a complex scalar and the Proca field. The charge $\mathcal{Q}$ represents the number density of particles. Since the total particle number minus antiparticle number is always conserved the conservation law is exact and the source term $\mathcal{S}$ vanishes.

Globally the total Noether charge should be conserved, however in numerical simulation this might not always be the case. Two common ways for non-conservation to occur are for the matter to interact with the simulation boundary conditions (often unproblematic) or some region of the simulation being insufficiently resolved (often problematic). Without knowledge of the Noether flux it is difficult to know what a change in Noether charge should be attributed to. If a large extraction volume containing the relevant physics shows a violation of Eq. (4.2.12) then the change in total Noether charge being due to boundary conditions can be ruled out and resolution is likely the culprit.

When considering black hole spacetimes it is common for Noether charge to be dissipated as matter approaches the singularity; this is due to resolution requirements typically becoming very high in this region. The violation of Eq. (4.2.12) inside a black hole horizon might not cause any resolution problems for the black hole exterior however due to causal disconnection. If the extraction volume is modified to exclude finite regions containing any black hole singularities then Eq. (4.2.12) could be used to monitor the conservation of Noether charge away from troublesome singularities. This would be a good way of checking the resolution of a matter field in situations such as boson/Proca stars colliding with black holes or scalar/vector accretion onto a black hole.

Complex Scalar Fields

In this section we consider the conserved Noether current associated with a complex scalar field φ with Lagrangian

$$\mathcal{L} = \left(\frac{1}{16\pi}R - \frac{1}{2}g^{\mu\nu}\nabla_{\mu}\bar{\varphi}\nabla_{\nu}\varphi - \frac{1}{2}V(\varphi\bar{\varphi})\right)\sqrt{-g}, \tag{4.4.1}$$

where V is some real potential function. There is a U(1) symmetry where a complex rotation of the scalar field $\varphi \to \varphi e^a$, for constant a, leaves the action unchanged. The associated Noether current $\boldsymbol{J}$ can be found in [**?**],

$$J^\mu = g^{\mu\nu}(\varphi \partial_\nu \bar{\varphi} - \bar{\varphi} \partial_\nu \varphi), \tag{4.4.2}$$

and satisfies $\boldsymbol{\nabla} \cdot \boldsymbol{J} = 0$. The conservation is exact here which tells us the source term vanishes. In this case the Noether charge density (4.2.13) and flux density (4.2.22) are,

$$\mathcal{Q} = n_\mu J^\mu, \tag{4.4.3}$$
$$= (\varphi n^\mu \partial_\mu \bar{\varphi} - \bar{\varphi} n^\mu \partial_\mu \varphi), \tag{4.4.4}$$
$$= (\bar{\varphi}\Pi - \bar{\Pi}\varphi), \tag{4.4.5}$$
$$\mathcal{F} = \frac{\sqrt{-h}}{\sqrt{\sigma}}(\gamma^{\nu\mu} N_\mu(\varphi \partial_\nu \bar{\varphi} - \bar{\varphi}\partial_\nu\varphi) - \boldsymbol{n} \cdot \boldsymbol{N}\mathcal{Q}), \tag{4.4.6}$$

where $\Pi = -\boldsymbol{n} \cdot \boldsymbol{\nabla}\varphi$ is the conjugate momentum of the scalar field. Using Eq. (4.3.17) for a spherical extraction surface, and spherical polar spacelike coordinates $\{r, \theta, \phi\}$, this explicitly becomes

$$\mathcal{F} = \frac{1}{\sqrt{\gamma^{rr}}}(\alpha\gamma^{\nu r}(\varphi\partial_\nu\bar{\varphi} - \bar{\varphi}\partial_\nu\varphi) + \beta^r \mathcal{Q}). \tag{4.4.7}$$

Complex Vector Fields

The Complex vector field $\boldsymbol{A}$, also called a Proca field, has Lagrangian

$$\mathcal{L} = \left(\frac{1}{16\pi}R - \frac{1}{4}F^{\mu\nu}\bar{F}_{\mu\nu} - \frac{1}{2}V(A^\mu \bar{A}_\mu) \right) \sqrt{-g}, \tag{4.4.8}$$

where $F_{\mu\nu} = \nabla_\mu A_\nu - \nabla_\nu A_\mu$. Again V is some real potential function. The action is invariant under a similar $U(1)$ complex rotation of the vector field $A^\mu \to A^\mu e^a$ for constant a. Following [**?**] this leads to the following Noether current $\boldsymbol{J}$,

$$J_\mu = \left(\bar{A}^\nu F_{\mu\nu} - A^\nu \bar{F}_{\mu\nu} \right), \tag{4.4.9}$$

which again satisfies $\boldsymbol{\nabla} \cdot \boldsymbol{J} = 0$ and the source term vanishes. Defining a $3+1$ decomposition compatible with [**?**] gives,

$$A_\mu := n_\mu \Phi + a_\mu, \tag{4.4.10}$$
$$\Phi = -A_\mu n^\mu, \tag{4.4.11}$$
$$a_\mu = \perp_\mu^\nu A_\nu, \tag{4.4.12}$$
$$F_{\mu\nu} := n_\mu E_\nu - n_\nu E_\mu + B_{\mu\nu}, \tag{4.4.13}$$
$$E_\mu = \perp_\mu^\nu F_{\nu\alpha}n^\alpha, \tag{4.4.14}$$
$$B_{\mu\nu} = \perp_\mu^\alpha \perp_\nu^\beta F_{\alpha\beta} = D_\mu a_\nu - D_\nu a_\mu, \tag{4.4.15}$$

where ϕ, $\boldsymbol{E}$, $\boldsymbol{a}$ and $\boldsymbol{B}$ all belong to Σ. Additionally $\boldsymbol{D}$ is the covariant 3-derivative of Σ. Note that $\boldsymbol{F}$ has no time-time component as $n_\mu n_\nu F^{\mu\nu} = 0$ from the anti-symmetry of $\boldsymbol{F}$. Using these, the Noether charge (4.2.13) becomes,

$$\mathcal{Q} = n_\mu J^\mu, \tag{4.4.16}$$
$$= \left(n^\mu \bar{A}^\nu F_{\mu\nu} - n^\mu A^\nu \bar{F}_{\mu\nu} \right), \tag{4.4.17}$$
$$= \left(n^\mu \bar{a}^\nu n_\mu E_\nu - n^\mu a^\nu n_\mu \bar{E}_\nu \right), \tag{4.4.18}$$
$$= \left(a^\nu \bar{E}_\nu - \bar{a}^\nu E_\nu \right). \tag{4.4.19}$$

Using Eq. (4.2.22), the Noether flux is,

$$\mathcal{F} = \frac{\sqrt{-h}}{\sqrt{\sigma}}(\vec{N}^\mu j_\mu - \boldsymbol{n} \cdot \boldsymbol{N}\mathcal{Q}), \tag{4.4.20}$$

$$= \frac{\sqrt{-h}}{\sqrt{\sigma}}(\vec{N}^\mu(\bar{A}^\nu F_{\mu\nu} - A^\nu \bar{F}_{\mu\nu}) - \boldsymbol{n} \cdot \boldsymbol{N}\mathcal{Q}). \tag{4.4.21}$$

Expanding $\vec{N}^\mu \bar{A}^\nu F_{\mu\nu}$ using the 3+1 split,

$$\vec{N}^\mu \bar{A}^\nu F_{\mu\nu} = \vec{N}^\mu \bar{a}^\nu B_{\mu\nu} - \vec{N}^\mu \bar{\Phi} n^\nu n_\nu E_\mu, \tag{4.4.22}$$

$$= \gamma^{\mu\rho} N_\rho(\bar{a}^\nu B_{\mu\nu} + \bar{\Phi} E_\mu), \tag{4.4.23}$$

$$= \gamma^{\mu\rho} N_\rho(\bar{a}^\nu(\partial_\mu a_\nu - \partial_\nu a_\mu) + \bar{\Phi} E_\mu), \tag{4.4.24}$$

where the Christoffel symbols from D_μ in $B_{\mu\nu}$ cancel out. Putting this into the expression for the Proca Noether flux we get,

$$\mathcal{F} = \frac{\sqrt{-h}}{\sqrt{\sigma}}\{\gamma^{\mu\rho} N_\rho[\bar{\Phi} E_\mu - \Phi \bar{E}_\mu + \bar{a}^\nu(\partial_\mu a_\nu - \partial_\nu a_\mu)$$
$$- a^\nu(\partial_\mu \bar{a}_\nu - \partial_\nu \bar{a}_\mu)] - \boldsymbol{n} \cdot \boldsymbol{N}\mathcal{Q}\}, \tag{4.4.25}$$

and equation (4.3.17) gives the flux term for a spherical extraction surface,

$$\mathcal{F} = \frac{1}{\sqrt{\gamma^{rr}}}(\alpha\gamma^{\mu r}(\bar{\Phi} E_\mu - \Phi \bar{E}_\mu + \bar{a}^\nu(\partial_\mu a_\nu - \partial_\nu a_\mu)$$
$$- a^\nu(\partial_\mu \bar{a}_\nu - \partial_\nu \bar{a}_\mu)) + \beta^r \mathcal{Q}), \tag{4.4.26}$$

where spherical polar spacelike coordinates $\{r, \theta, \phi\}$ used.

4.5 Energy-Momentum Currents

To find the current associated with energy-momentum we consider a vector field $\boldsymbol{J}$ defined with respect to a second vector field $\boldsymbol{\xi}$ and the stress tensor $\boldsymbol{T}$ by

$$J^\mu := T^\mu_\nu \xi^\nu. \tag{4.5.1}$$

Calculating the divergence of this vector leads to the following continuity equation,

$$\nabla_\mu J^\mu = \underbrace{(\nabla_\mu T^\mu_\nu)}_{=0}\xi^\nu + T^\mu_\nu \nabla_\mu \xi_\nu, \tag{4.5.2}$$

$$\nabla_\mu J^\mu = T^{\mu\nu}\nabla_{(\mu}\xi_{\nu)}, \tag{4.5.3}$$

where (4.5.3) shows the divergence vanishes if $\boldsymbol{\xi}$ is a Killing vector of the spacetime; a vanishing divergence corresponds to a conserved current with a zero source term. For more general spacetimes where $\boldsymbol{\xi}$ is not Killing, the right hand side of (4.5.3) leads to a non-zero source term accounting for the transfer of energy-momentum between matter and spacetime curvature [?]. The choice of $\boldsymbol{\xi}$ dictates the type of energy-momentum current retrieved; for instance $\boldsymbol{\xi} = \boldsymbol{\partial_t}$ will correspond to an energy current $J^\mu = T^\mu_\nu(\partial_t)^\nu = T^\mu_t$ and the spacelike choice $\boldsymbol{\xi} = \boldsymbol{\partial_i}$ gives a momentum current $J^\mu = T^\mu_\nu(\partial_i)^\nu = T^\mu_i$ corresponding to the coordinate x^i. For an account of energy and linear momentum continuity see [?].

Angular Momentum

The numerical test of the QFS system (4.2.12) in section 4.6 measures the conservation of angular momentum. To do this we choose $\boldsymbol{\xi} = \boldsymbol{\partial_\phi}$, used in Eq. (4.5.1), which is the coordinate basis vector of some azimuthal coordinate ϕ. The angular momentum current is

$$J^\mu = T^\mu_\nu (\partial_\phi)^\nu = T^\mu_\phi. \tag{4.5.4}$$

Any spacetime with azimuthal symmetry (e.g. the Kerr spacetime) will have a vanishing source term as $\boldsymbol{\partial_\phi}$ is a Killing vector. This includes numerical simulations of matter in a fixed background. The example simulation in section 4.6 is the fully nonlinear grazing collision of two boson stars and $\boldsymbol{\xi}$ is not a Killing vector for finite distances from the collision centre. In this case the source term is non-zero. Using the standard 3+1 decomposition of the stress tensor [?], [?] and explicitly expanding the density term from Eq. (4.2.13) gives,

$$\mathcal{Q} = T^\mu_\nu n_\mu (\partial_\phi)^\nu, \tag{4.5.5}$$

$$= (S^\mu_\nu + S^\mu n_\nu + S_\nu n^\mu + n_\nu n^\mu) n_\mu (\partial_\phi)^\nu, \tag{4.5.6}$$

$$= S_\nu n^\mu n_\mu (\partial_\phi)^\nu, \tag{4.5.7}$$

$$= -S_\phi, \tag{4.5.8}$$

$$= y S_x - x S_y, \tag{4.5.9}$$

where x and y are Cartesian coordinates related to spherical polar coordinates in the usual way. Combining Eqs. (4.2.22), (4.5.4) and (4.5.8) we can get the angular momentum flux through a spherical extraction surface,

$$\mathcal{F} = \frac{\sqrt{-h}}{\sqrt{\sigma}} (\gamma^{\mu\nu} T_{\rho\mu} (\partial_\phi)^\rho N_\nu + \boldsymbol{n} \cdot \boldsymbol{N} S_\phi), \tag{4.5.10}$$

$$= \frac{\sqrt{-h}}{\sqrt{\sigma}} (\gamma^{\mu\nu} S_{\phi\mu} N_\nu + \boldsymbol{n} \cdot \boldsymbol{N} S_\phi). \tag{4.5.11}$$

Using Eq. (4.3.17), for a spherical extraction surface, the flux term becomes,

$$\mathcal{F} = \alpha \frac{\sqrt{g^{rr}}}{\sqrt{\gamma^{rr}}} (\gamma^{\mu r} S_{\phi\mu} N_r - \frac{\beta^r}{\alpha} N_r S_\phi), \tag{4.5.12}$$

$$= \alpha \frac{\sqrt{g^{rr}}}{\sqrt{\gamma^{rr}}} (\gamma^{\mu r} S_{\phi\mu} N_r - \frac{\beta^r}{\alpha} N_r S_\phi), \tag{4.5.13}$$

$$= \frac{1}{\sqrt{\gamma^{rr}}} (\alpha \gamma^{\mu r} S_{\phi\mu} - \beta^r S_\phi) \tag{4.5.14}$$

in spherical polar coordinates. The explicit expansion of the source term $\mathcal{S}$ is left for the appendix .1, but the result is given here,

$$\mathcal{S} = \alpha S^{\mu(3)}_\nu \partial_\mu \xi^\nu + \alpha S^{\mu(3)}_\nu \Gamma^\nu_{\mu\sigma} \xi^\sigma \\ - S_\nu \beta^i \partial_i \xi^\nu + S_\nu \xi^\mu \partial_\mu \beta^\nu - \rho \xi^\mu \partial_\mu \alpha. \tag{4.5.15}$$

As noted in appendix .1, when choosing a coordinate system to evaluate $\mathcal{S}$, if $\boldsymbol{\xi}$ is a coordinate basis vector then the $\partial_i \xi^j$ terms vanish.

It would be simple to re-derive these results for linear momentum, by using $\boldsymbol{\xi} = \boldsymbol{\partial_i}$ for momentum in the x^i direction for example, where x^i is some Cartesian spatial coordinate. Results for linear momentum can be found in [?].

Energy

A local conservation system can also be applied to energy with the choice of an approximate Killing vector $\boldsymbol{\xi}$, $\xi^\mu = (\partial_t)^\mu = t^\mu = (1,0,0,0)$, and energy current

$$J^\mu = T^\mu_\nu t^\nu = T^\mu_t. \tag{4.5.16}$$

Using the standard 3+1 decomposition of the stress-energy tensor from [**?**] or [**?**] the energy density $\mathcal{Q}$ is,

$$\mathcal{Q} = T^\mu_\nu n_\mu \xi^\nu, \tag{4.5.17}$$
$$= T^\mu_\nu n_\mu (\alpha n^\nu + \beta^\nu), \tag{4.5.18}$$
$$= \alpha\rho - S_\mu \beta^\mu, \tag{4.5.19}$$

from Eq. (4.2.13). Similarly, combining Eqs. (4.2.14) and (4.2.19), the energy flux is,

$$\mathcal{F} = \frac{\sqrt{-h}}{\sqrt{\sigma}} T^\mu_\nu N_\mu \xi^\nu, \tag{4.5.20}$$

$$= \frac{\sqrt{-h}}{\sqrt{\sigma}} T^\mu_\nu (_\mu - \boldsymbol{n} \cdot \boldsymbol{N} n_\mu)(\alpha n^\nu + \beta^\nu), \tag{4.5.21}$$

$$\begin{aligned} = \frac{\sqrt{-h}}{\sqrt{\sigma}} (-\boldsymbol{n} \cdot \boldsymbol{N} \alpha\rho -_\mu S^\mu \alpha \\ + \boldsymbol{n} \cdot \boldsymbol{N} S_\mu \beta^\mu +^\mu \beta^\nu S_{\mu\nu}), \end{aligned} \tag{4.5.22}$$

and Eqs. (4.3.2) and (4.3.13) can be used for a spherical extraction surface,

$$\mathcal{F} = \frac{1}{\sqrt{\gamma^{rr}}}(\alpha\rho\beta^r - \alpha^2 S^r + \alpha S^r_\mu \beta^\mu - \beta^\mu S_\mu \beta^r). \tag{4.5.23}$$

The source term is omitted here as the expression derived in appendix .1 assumes that $\boldsymbol{\xi}$ is spacelike. For energy continuity a timelike approximate Killing vector $\boldsymbol{\xi}$ is used and leads to a different expression for the source term that can be found in [**?**] along with the above density $\mathcal{Q}$ and flux term $\mathcal{F}$.

4.6 Numerical Application

To numerically test the QFS system, given in Eq. (4.2.12), for angular momentum an example spacetime consisting of colliding boson stars is simulated in 3D using [**?**, **?**]. is a modern, open source, Numerical Relativity code with fully Adaptive Mesh Refinement (AMR) using the Berger-Rigoutsos block-structured adaptive mesh algorithm [**?**]. The CCZ4 constraint damping formulation [**?**, **?**] is used with the moving puncture gauge [**?**, **?**]. Time integration is done with 4th order Runge-Kutta method of lines.

Numerical Setup of Simulations

The boson stars are composed of a complex scalar field φ, minimally coupled to gravity with the Lagrangian given in Eq. (4.4.1). Boson stars are stable self-gravitating spherically symmetric solutions of the Einstein-Klein-Gordon system in curved space; for a detailed review see [**?**]. In this work, the Klein-Gordon potential is chosen to be $V = m^2\varphi\bar\varphi$, where m is the mass of a bosonic particle, leading to so called *mini boson stars*. The Kaup limit for the maximum mass of a mini boson star can be found numerically as approximately

$$M_{\text{Kaup}} \sim 0.633 \frac{\hbar c}{Gm} = 0.633 M_{pl}^2 m^{-1}, \tag{4.6.1}$$

where the physical constants are included for completeness, but have numerical value 1 in Planck units. Notably, the maximum mass of a mini boson star scales inversely with the boson particle mass m.

The Lagrangian in Eq. (4.4.1) with potential $V = m^2 \varphi \bar{\varphi}$ is unchanged up to an overall constant under a rescaling of the boson mass like $m \to bm$, for some dimensionless constant b, while simultaneously rescaling $x^\mu \to b^{-1} x^\mu$ for coordinates with dimension length/time. Consequently a mini boson star solution, categorised by the central scalar field amplitude φ_c, represents a one parameter family of solutions with ADM mass and radius inversely proportional to m. To keep the choice of m arbitrary the coordinates used in the simulation are mx^μ, which are exactly Planck units in the case $m = 1$ (i.e. the Planck mass).

To measure the charge associated with angular momentum, the following angular momentum measures are considered,

$$Q := \int_V \mathcal{Q} \sqrt{\gamma} \, \mathrm{d}^3 x, \tag{4.6.2}$$

$$F := \int_{\partial V} \mathcal{F} \sqrt{\gamma} \, \mathrm{d}^2 x, \tag{4.6.3}$$

$$S := \int_V \mathcal{S} \sqrt{\gamma} \, \mathrm{d}^3 x, \tag{4.6.4}$$

$$\tilde{Q} := Q(t = 0) + \int_0^t F \, \mathrm{d}t, \tag{4.6.5}$$

$$\delta Q_S := \int_0^t S \, \mathrm{d}t, \tag{4.6.6}$$

$$\hat{Q} := Q + \delta Q_S, \tag{4.6.7}$$

$$\bar{Q} := \tilde{Q} - \delta Q_S, \tag{4.6.8}$$

where $\mathcal{Q}$, $\mathcal{F}$ and $\mathcal{S}$ are defined in Eqs. (4.5.5), (4.5.14) and (4.5.15) respectively. $\hat{Q}$ is the angular momentum modified by δQ_S; this is equivalent to absorbing the source term into Q. $\tilde{Q}$ is the initial angular momentum modified by the time integrated total flux. Equation (4.2.12) implies $\hat{Q} = \tilde{Q}$ exactly, and we define the relative numerical error measure e_1 by

$$e_1 := \frac{\hat{Q} - \tilde{Q}}{\hat{Q}}, \tag{4.6.9}$$

which converges to zero in the continuum limit. We can alternatively define a different relative error

$$e_2 := \frac{Q - \bar{Q}}{Q}, \tag{4.6.10}$$

where the source term is not absorbed into Q. Again, Eq. (4.2.12) implies that $Q = \bar{Q}$, or $e_2 = 0$, in the continuum limit.

The initial data of the numerical simulations consists of two boson stars, each with mass $M = 0.395(0) \, m^{-1}$, boosted towards each other in a grazing configuration. The data for two single boosted stars are superposed as in Ref. [?] to minimise errors in the Hamiltonian and momentum constraints and spurious oscillations in the scalar field amplitudes of the stars. The physical domain is a cube of size $L = 1024 \, m^{-1}$, the centre of this domain locates the origin of the Cartesian coordinates x, y and z. The stars are placed at $x_0^i = \pm(40, 4, 0) \, m^{-1}$ with respect to the centre of the physical domain, giving an initial impact parameter $d = 8 \, m^{-1}$, and the boost velocity is $v^i = \mp(0.1, 0, 0)$ along the x axis. The stars travel towards each other and undergo a grazing collision to form a short lived dense object at time $t \sim 375 \, m^{-1}$. Afterwards, much of the scalar field (and angular momentum) leaves the extraction radii as it is ejected to spatial infinity. Figures. 4.2, 4.3 and 4.4 show the angular momentum within radii $r = \{20, 40, 60\} \, m^{-1}$. The Newtonian angular momentum for this configuration is

$$Mdv = 0.316(0) m^{-2} \tag{4.6.11}$$

which is in close agreement with Q and $\hat{Q}$ in Figs. 4.2, 4.3 and 4.4 while the matter is contained by the extraction radii. Given that we are dealing with a fully non-linear spacetime in general relativity there is no reason why the naive Newtonian angular momentum should agree so well with the numerically integrated values Q or $\hat{Q}$; this could be due to the mass of the stars being $M = 0.395(0)\ m^{-1}$, well below the Kaup limit $M_{\mathrm{Kaup}} \sim 0.633\ m^{-1}$ and the mild boost velocities $v = 0.1$. In the case that the star masses/densities and velocities tend to zero we expect general relativity to approach the Newtonian limit; conversely for large masses/densities and boost velocities the Newtonian estimate likely becomes less accurate.

Finally we note in Figs. 4.2, 4.3 and 4.4 that the source-corrected density variable $\hat{Q}$ is less prone to oscillations than Q and is closer to being constant at early times when no angular momentum flux is radiated. $\hat{Q}$ has another advantage over Q; at extraction radii sufficiently far from any matter $\hat{Q}$ will remain constant due to the flux $\mathcal{F}$ vanishing. Q will only remain constant if the source term integral δQ_S also remains constant which does not happen in general dynamic spacetimes, even for large extraction radii.

Convergence Analysis

Three numerical simulations are used to test the convergence of the angular momentum measures as the continuum limit is approached. They have $N \in \{320, 384, 448\}$ gridpoints on the coarsest level, named level 0 with grid spacing $\Delta x_0 = L/N$. Each finer level, named level n, has grid spacing $\Delta x_n = 2^{-n}\Delta x_0$. Any gridpoints that fall inside radius $r = 200\ m^{-1}$ are forced to be resolved by at least AMR level 1. Similarly, any points within radius $r < 60\ m^{-1}$ are resolved by at least AMR level 3; this modification quadruples the default resolution for $r < 60\ m^{-1}$ compared to level 1. These two radii have a 20% extra buffer zone to ensure that AMR boundaries are outside and away from the desired radii. On top of this the AMR is triggered to regrid when a tagging criterion is exceeded; a description of the algorithm can be found in section 2.2.2 of [**?**]. The tagging criteria used in this paper involve gradients of the scalar field and spatial metric determinant; this loosely means as a region of spacetime becomes more curved, or matter becomes denser, the region is resolved with higher resolution. Figs. 4.5 and 4.6 show the relative errors e_1 and e_2 for the convergence sequence; it can be seen that e_1, the relative error of $\hat{Q}$, is less prone to oscillations than e_2, the relative error of Q. The choice of enforcing AMR regridding to level 3 within $r < 60\ m^{-1}$ is very problem specific and the grid structure has been chosen carefully for the particular physical scenario to give higher resolution around the late time scalar field configuration at the origin; this enables accurate simulation of the extended object after merger. Simulations prior to this modification showed approximately five times higher relative error e_1 and much worse Noether charge conservation. The highest resolution simulation, with $N = 448$, shows that the relative error e_1 is 3% after 8000 m^{-1} time units.

We now obtain the order of convergence ω of e_1. It is convenient to express e_1 as three functions $\{f_1, f_2, f_3\}$ corresponding to the three different resolution simulations with $N = \{320, 384, 448\}$ and f_∞ to denote the continuum limit solution. A traditional convergence analysis, as in [**?**], assumes that the numerical error of a function (i.e. difference from f_∞) is dominated by a term proportional to Δx_i^ω for an order of convergence ω; thus we can write

$$f_i + E(\Delta x_i)^\omega = f_\infty \tag{4.6.12}$$

for some constant coefficient E for all resolutions i. Equation (4.6.12) with $i = \{1, 2, 3\}$ can be used to eliminate both E and f_∞ giving the well known result

$$\frac{f_3 - f_2}{f_2 - f_1} = \frac{\Delta x_3^\omega - \Delta x_2^\omega}{\Delta x_2^\omega - \Delta x_1^\omega} \tag{4.6.13}$$

for ideal convergence. Figure 4.7 shows $f_3 - f_2$ and $(f_2 - f_1)(\Delta x_3^\omega - \Delta x_2^\omega)/(\Delta x_2^\omega - \Delta x_1^\omega)$ for three orders of convergence $\omega = \{2, 3, 4\}$; the two expressions should be equal for an ideal order of convergence ω. It can be seen by eye that $\omega = 3$ is the best estimate.

To quantify the order of convergence, rather than guessing, we define the deviation factor $\mathcal{D}$ as

$$\mathcal{D}(\omega) = \int_{t_0}^{t_1} \left(\frac{f_3 - f_2}{f_2 - f_1} - \frac{\Delta x_3^\omega - \Delta x_2^\omega}{\Delta x_2^\omega - \Delta x_1^\omega} \right)^2 \mathrm{d}t, \tag{4.6.14}$$

which averages the violation of Eq. (4.6.13) between times $t_0 \leq t \leq t_1$. Figure 4.8 plots $\mathcal{D}$ versus ω with a red curve and the order of convergence can be estimated by minimising $\mathcal{D}(\omega)$ with respect to ω. As can be seen in Fig. 4.8, the traditional order of convergence is approximately 3.2.

Given that e_1 vanishes in the continuum limit we can set $f_\infty = 0$ to find the order of convergence to zero. Using Eq. (4.6.12) with the two highest resolutions $i = \{2, 3\}$, and setting $f_\infty = 0$, E can be eliminated to give

$$\frac{f_3}{f_2} = \frac{\Delta x_3^\omega}{\Delta x_2^\omega}. \tag{4.6.15}$$

Similarly to before, we can define a deviation factor $\tilde{\mathcal{D}}$,

$$\tilde{\mathcal{D}}(\omega) = \int_{t_0}^{t_1} \left(\frac{f_3}{f_2} - \frac{\Delta x_3^\omega}{\Delta x_2^\omega} \right)^2 \mathrm{d}t, \tag{4.6.16}$$

which time averages the violation of Eq. (4.6.15). The black curve in Fig. 4.8 plots Eq. (4.6.16) versus ω and the order of convergence to zero can be estimated by minimising $\tilde{\mathcal{D}}(\omega)$ with respect to ω. As can be seen in Fig. 4.8, the order of convergence convergence to zero is approximately 1.9.

4.7 Conclusion

A derivation of the QFS system (4.2.12) for continuity equations, valid locally for general spacetimes, is derived and applied to spherical integration surfaces. Although spherical extraction surfaces are used, the methods of section 4.3 can be applied to general extraction surfaces with minor adjustments. The QFS system is used to calculate the well known Noether charge densities for complex scalar and complex vector (Proca) fields along with novel expressions for the flux variable $\mathcal{F}$ in section 4.4. Next the QFS system for energy momentum currents associated with matter are found and the main result of this paper is the explicit derivation of the angular momentum QFS variables $\mathcal{Q}$, $\mathcal{F}$ and $\mathcal{S}$. The three variables can be used to measure the angular momentum of matter within a region, the flux of angular momentum of matter through the boundary of that region and the transfer of angular momentum between matter and curvature; they can also be used with Eq. (4.2.12) to determine the numerical quality of a simulation as the QFS system is exactly satisfied in the continuum limit. In section 4.6 the combination of variables $\mathcal{Q}$ and $\mathcal{S}$ is shown to be a superior measure of angular momentum than integrals of only the charge density $\mathcal{Q}$ in two ways; firstly its measurement is less prone to oscillations and secondly it is conserved in the large radius limit.

The QFS system for angular momentum is numerically tested on a dynamic non-linear spacetime consisting of two colliding boson stars; the collision has a small impact parameter giving rise to a non-zero total angular momentum. The stars promptly collide and form a highly perturbed, localised scalar field configuration partially retaining angular momentum. The total angular momentum of the spacetime is measured using the QFS variables (Eqs. (4.5.8), (4.5.14) and (4.5.15)) and is shown to agree well with the Newtonian approximation. This is a good check on the normalisation of the QFS variables as they should return the Newtonian calculation in the low energy limit; even though we simulate a fully non-linear spacetime the density and boost velocity of the stars are mild. The final numerical result is the convergence test of the QFS system which measures the relative error described in 4.6. The relative error converges to zero with order $\omega \approx 1.9$ in the continuum limit and the highest resolution simulation gives a fractional error of approximately 3% in the total angular momentum after 8000 time units.

The QFS system is straightforward to implement and it is hoped these results will be useful to the Numerical Relativity community for better measurement of local energy-momentum of matter and Noether charge aswell as powerful check on simulation resolution.

Acknowledgements

.1 Source Term Calculation

Here we expand the source term $\mathcal{S}$ from section 4.2,

$$\mathcal{S} = \alpha T_{\mu\nu}\nabla^\mu\xi^\nu. \tag{.1.1}$$

Note that $\boldsymbol{\xi}$ is assumed spacelike, $\xi^\mu n_\mu = 0 \rightarrow \xi^0 = 0$. If the reader is interested in a timelike $\boldsymbol{\xi}$, for calculating the source term of energy, it can be found in [**?**]. Expanding the stress tensor with the usual 3+1 components [**?**], [**?**] $(S_{\mu\nu}, S_\mu, \rho)$, gives

$$\frac{1}{\alpha}\mathcal{S} = S_{\mu\nu}\nabla^\mu\xi^\nu + S_\mu n_\nu\nabla^\mu\xi^\nu + S_\nu n_\mu\nabla^\mu\xi^\nu + \rho n_\mu n_\nu\nabla^\mu\xi^\nu. \tag{.1.2}$$

Let us decompose each piece separately. Starting with the spacelike tensor $S_{\mu\nu}$ term,

$$S_{\mu\nu}\nabla^\mu\xi^\nu = (S_{\rho\sigma} \perp_\mu^\rho \perp_\nu^\sigma)\nabla^\mu(\perp_n^\nu \xi^n), \tag{.1.3}$$
$$= S_{\rho\sigma}(\perp_\mu^\rho \perp_\nu^b \nabla^\mu(\perp_n^\nu \xi^n)), \tag{.1.4}$$
$$= S_{\mu\nu}D^\mu\xi^\nu, \tag{.1.5}$$
$$= S_j^i\partial_i\xi^j + S_j^{i\,(3)}\Gamma^j{}_{ik}\xi^k, \tag{.1.6}$$

where we used the idempotence of the projector $\perp$ on components $S_{\mu\nu}$ and ξ^μ which are already projected onto Σ. Here $\boldsymbol{D}$ and ${}^{(3)}\Gamma^j{}_{ik}$ are the covariant derivative and Christoffel symbol components of Σ. Some algebra shows that the terms containing S_μ become

$$S_\nu n^\mu\nabla_\mu\xi^\nu + S^\mu n_\nu\nabla_\mu\xi^\nu = S_\nu\mathcal{L}_n\xi^\nu, \tag{.1.7}$$

where we used the fact that $S^0 = 0$, $n_{i\neq 0} = 0$ and that the we are free to swap between $\partial_\mu \leftrightarrow \nabla_\mu$ derivatives in a Lie derivative. Finally the ρ term simplifies, using $\nabla_\mu(n^\nu n_\nu) = 0$, to

$$\rho n_\mu n_\nu\nabla^\mu\xi^\nu = \rho n_\nu\mathcal{L}_n\xi^\nu. \tag{.1.8}$$

Combining Eqs. (.1.6), (.1.7) and (.1.8) we can write the source term as,

$$\frac{1}{\alpha}\mathcal{S} = S_j^i\partial_i\xi^j + S_j^{i\,(3)}\Gamma^j{}_{ik}\xi^k + S_\nu\mathcal{L}_n\xi^\nu + \rho n_\nu\mathcal{L}_n\xi^\nu, \tag{.1.9}$$

We can expand the Lie derivatives to partial derivatives, for ease of numerical implementation, with the following assumptions $n_\mu S^\mu = 0$, $\xi^0 = 0$, $n_{i\neq 0} = 0$ and $\partial\xi^0 = 0$.

$$S_\nu\mathcal{L}_n\xi^\nu = -\frac{1}{\alpha}S_\nu\beta^i\partial_i\xi^\nu + \frac{1}{\alpha}S_\nu\xi^\mu\partial_\mu\beta^\nu \tag{.1.10}$$

$$\rho n_\nu\mathcal{L}_n\xi^\nu = -\frac{1}{\alpha}\rho\xi^\mu\partial_\mu\alpha \tag{.1.11}$$

This gives us our final form for the angular momentum source density,

$$\begin{aligned}\mathcal{S} = {}&\alpha S_\nu^{\mu\,(3)}\partial_\mu\xi^\nu + \alpha S_\nu^{\mu\,(3)}\Gamma^\nu{}_{\mu\sigma}\xi^\sigma \\ &- S_\nu\beta^i\partial_i\xi^\nu + S_\nu\xi^\mu\partial_\mu\beta^\nu - \rho\xi^\mu\partial_\mu\alpha.\end{aligned} \tag{.1.12}$$

If we pick a coordinate basis vector as our approximate Killing vector, for example with components $\xi^\mu = (\partial_\phi)^\mu = (0,0,0,1)^\mu$ in polar coordinates, then the $\partial_\mu \xi^\nu$ terms will vanish. However if we wish to work in Cartesian coordinates, which is very common for numerical codes, then the vector components $\tilde{\xi}^\mu$ become,

$$\tilde{\xi}^\mu = (\partial_\phi)^\nu \frac{\partial \tilde{x}^\mu}{\partial x^\nu} = (0, -y, x, 0), \tag{.1.13}$$

where $\tilde{x}^\mu$ are Cartesian coordinates and x^μ are spherical polar coordinates.

.2 Generality of Result

Here we demonstrate that the choice of 4-volume M integrated in Eq. (4.2.4) does not change the resulting QFS system (4.1.3). We start by defining the extraction 3-volume $V_1 \in \Sigma$ at time $t = t_0$. The boundary of V_1 is the 2-volume ∂V_1 with metric $\boldsymbol{\sigma}$. As in section 4.2, Σ is the 3-manifold defined by the set of all points with constant time coordinate t, equipped with metric $\boldsymbol{\gamma}$ and unit normal $\boldsymbol{n}$ like Eq. (4.2.2). We now choose to define a 4-volume $\tilde{M}$, different to M, as the evolution of V_1 along integral curves of $\boldsymbol{n}$ between times $t_0 \leq t \leq t_0 + \delta t$ in the limit $\delta t \to 0$. The boundary of $\tilde{M}$, $\partial \tilde{M}$, is composed of three coordinate 3-volumes, $V_1 \in \Sigma_t$, $V_2 \in \Sigma_{t+\delta t}$ and $\tilde{H}$. Here $V_2 = V_1 + \delta V$ and is the future of V_1, at time $t = t_0 + \delta t$, found by following integral curves of $\boldsymbol{n}$. $\tilde{H}$ is the 3-volume defined by the time evolution of 2-volume ∂V_1 with $\boldsymbol{n}$. A diagram showing the differences between the choices of time evolution vectors $\boldsymbol{n}$ and $\boldsymbol{t}$ is given in Fig. 9.

We start again by using Gauss' theorem like in Eq. (4.2.5) which results in three surface integrals over $V_1 \in \Sigma_t$, $V_2 \in \Sigma_{t+\delta t}$, and $\tilde{H}$,

$$\int_{\tilde{M}} \boldsymbol{\nabla} \cdot \boldsymbol{J} \sqrt{-g}\, \mathrm{d}^4 x = -\int_{V_2}^{t=t_0+\delta t} \boldsymbol{n} \cdot \boldsymbol{J} \sqrt{\gamma}\, \mathrm{d}^3 x$$
$$+ \int_{V_1}^{t=t_0} \boldsymbol{n} \cdot \boldsymbol{J} \sqrt{\gamma}\, \mathrm{d}^3 x \tag{.2.1}$$
$$+ \int_{\tilde{H}} \tilde{\boldsymbol{N}} \cdot \boldsymbol{J} \sqrt{-\tilde{h}}\, \mathrm{d}x^2 \mathrm{d}t,$$

where $\tilde{\boldsymbol{N}}$ is the unit normal to $\tilde{H}$. Starting with the integrals over V_1 and $V_2 = V_1 + \delta V$ we get,

$$-\int_{V_2}^{t=t_0+\delta t} \boldsymbol{n} \cdot \boldsymbol{J} \sqrt{\gamma}\, \mathrm{d}^3 x + \int_{V_1}^{t=t_0} \boldsymbol{n} \cdot \boldsymbol{J} \sqrt{\gamma}\, \mathrm{d}^3 x, \tag{.2.2}$$
$$= -\delta t\, \partial_t \int_{V_1} \boldsymbol{n} \cdot \boldsymbol{J} \sqrt{\gamma}\, \mathrm{d}^3 x - \int_{\delta V} \boldsymbol{n} \cdot \boldsymbol{J} \sqrt{\gamma}\, \mathrm{d}^3 x, \tag{.2.3}$$

with the new integral over δV appearing because $V_1 \neq V_2$ as V_1 is evolved along integral curves of $\boldsymbol{n}$ rather than time basis vector $\boldsymbol{t} = \boldsymbol{\partial_t}$; this is demonstrated in Fig. 9. In the limit that $\delta t \to 0$ it can be seen that,

$$\int_{\delta V} \boldsymbol{n} \cdot \boldsymbol{J} \sqrt{\gamma}\, \mathrm{d}^3 x = -\delta t \int_{\partial V_1} \beta^i s_i\, \boldsymbol{n} \cdot \boldsymbol{J} \sqrt{\gamma}\, \mathrm{d}^2 x, \tag{.2.4}$$

where s_i are the components of the unit normal to the coordinate surface ∂V_1 in $\mathbb{R}^3$ rather than Σ_t. The overall negative sign in Eq. (.2.4) comes from the defined direction of the shift vector $\boldsymbol{\beta}$ as seen Fig. 9. Addressing the integral over $\tilde{H}$ gives,

$$\int_{\partial V_1} \int_{t_0}^{t_0+\delta t} \tilde{\boldsymbol{N}} \cdot \boldsymbol{J} \sqrt{-\tilde{h}}\, \mathrm{d}x^2 \mathrm{d}t,$$
$$= \delta t \int_{\partial V_1} \tilde{\boldsymbol{N}} \cdot \boldsymbol{J} \sqrt{-\tilde{h}}\, \mathrm{d}x^2. \tag{.2.5}$$

Combining Eqs. (.2.3), (.2.4) and (.2.5) and a source term like in (4.2.4) we get,

$$\partial_t \int_{V_1} \boldsymbol{n} \cdot \boldsymbol{J} \sqrt{\gamma} \, \mathrm{d}^3 x =$$

$$\int_{\partial V_1} \left(\beta^i s_i \, \boldsymbol{n} \cdot \boldsymbol{J} \sqrt{\gamma} + \tilde{\boldsymbol{N}} \cdot \boldsymbol{J} \sqrt{-\tilde{h}} \right) \mathrm{d}x^2$$

$$- \int_{V_1} S\alpha \sqrt{\gamma} \, \mathrm{d}^3 x, \tag{.2.6}$$

which is in the same form as Eq. (4.2.12) with definitions,

$$\mathcal{Q} := J^\mu n_\mu, \tag{.2.7}$$

$$\mathcal{F} := \frac{\sqrt{-\tilde{h}}}{\sqrt{\sigma}} J^\mu \tilde{N}_\mu + \frac{\sqrt{\gamma}}{\sqrt{\sigma}} \beta^i s_i \, \mathcal{Q}, \tag{.2.8}$$

$$\mathcal{S} := \alpha S, \tag{.2.9}$$

where we used $\boldsymbol{n} \cdot \boldsymbol{J} = \mathcal{Q}$ for the flux term. The density term $\mathcal{Q}$ and source term $\mathcal{S}$ are agnostic to our choice of extraction surface and its time evolution so have turned out the same as Eqs. (4.2.13) and (4.2.15). At first glance the flux term $\mathcal{F}$ seems different to Eq. (4.2.22) but evaluating this term in a coordinate basis will show otherwise.

Choosing a spherical extraction surface as in Section 4.3 and using spherical polar coordinates, $x^\mu = \{t, r, \theta, \phi\}$, V_1 becomes the coordinate 3-volume $r \leq r_0$, $t = t_0$. The unit normal $\tilde{\boldsymbol{N}}$ satisfies $\tilde{\boldsymbol{N}} \cdot \boldsymbol{n} = 0$ so $\tilde{N}^\mu = (0, \tilde{N}^i)$ where,

$$\tilde{N}_i = \frac{\nabla_i (r - r_0)}{\sqrt{\gamma^{jk} \nabla_j (r - r_0) \nabla_k (r - r_0)}}, \tag{.2.10}$$

$$= (\frac{1}{\sqrt{\gamma^{rr}}}, 0, 0), \tag{.2.11}$$

and the flat space normal has components is $s^i = s_i = (1, 0, 0)$ with respect to spherical polar coordinates over a different flat manifold. Using Eqs. (4.3.6) and (4.3.7) with Cramer's rule for matrix inverse, it can be shown that,

$$\gamma^{rr} = \frac{\det \sigma_{ab}}{\det \gamma_{ij}} = \frac{\sqrt{\sigma}^2}{\sqrt{\gamma}^2}, \tag{.2.12}$$

$$\tilde{h}^{tt} = \frac{\det \sigma_{ab}}{\det \tilde{h}_{ij}} = -\frac{\sqrt{\sigma}^2}{\sqrt{-\tilde{h}}^2}, \tag{.2.13}$$

where it should be noted that $\tilde{h} < 0$ and $\sigma > 0$. Deriving Eq. (.2.13) uses the fact that $\tilde{H}$ intersects Σ on ∂V_1 and therefore must have the same line element for variations in angular coordinates; hence $g_{\theta\theta} = \tilde{h}_{\theta\theta}$, $g_{\theta\phi} = \tilde{h}_{\theta\phi}$ and $g_{\phi\phi} = \tilde{h}_{\phi\phi}$. The final component we need is to calculate $\tilde{h}^{tt}$ which can be done by projecting the 4-metric $\boldsymbol{g}$ onto $\tilde{H}$ as,

$$^{(4)}\tilde{h}^{\mu\nu} = g^{\mu\nu} - \tilde{N}^\mu \tilde{N}^\nu, \tag{.2.14}$$

$$^{(4)}\tilde{h}^{tt} = g^{tt} - \tilde{N}^t \tilde{N}^t, \tag{.2.15}$$

$$= -\alpha^{-2}, \tag{.2.16}$$

where $^{(4)}\tilde{\boldsymbol{h}}$ is a 4-tensor belonging to $\mathcal{M}$ and $\tilde{N}^t = 0$. Using the pushforward of $\tilde{\boldsymbol{h}}$ on $\tilde{H}$ to $^{(4)}\tilde{\boldsymbol{h}}$ on $\mathcal{M}|_{p \in \tilde{H}}$, similarly to Sec. 4.3, it can be shown that $^{(4)}h^{tt} = h^{tt}$. Equations (.2.13) and (.2.16) combine to give,

$$\sqrt{-\tilde{h}} = \alpha \sqrt{\sigma}, \tag{.2.17}$$

again noting $\tilde{h} < 0$. Now we can re-write the flux (.2.8) term as,

$$\mathcal{F} = \alpha J_\mu \tilde{N}^\mu + \frac{1}{\sqrt{\gamma^{rr}}} \beta^i s_i \, \mathcal{Q}, \tag{.2.18}$$

$$\mathcal{F} = \alpha \gamma^{r\nu} J_\nu \tilde{N}_r + \frac{1}{\sqrt{\gamma^{rr}}} \beta^r \, \mathcal{Q}, \tag{.2.19}$$

$$= \frac{1}{\sqrt{\gamma^{rr}}} (\alpha \gamma^{r\nu} J_\nu + \beta^r \, \mathcal{Q}), \tag{.2.20}$$
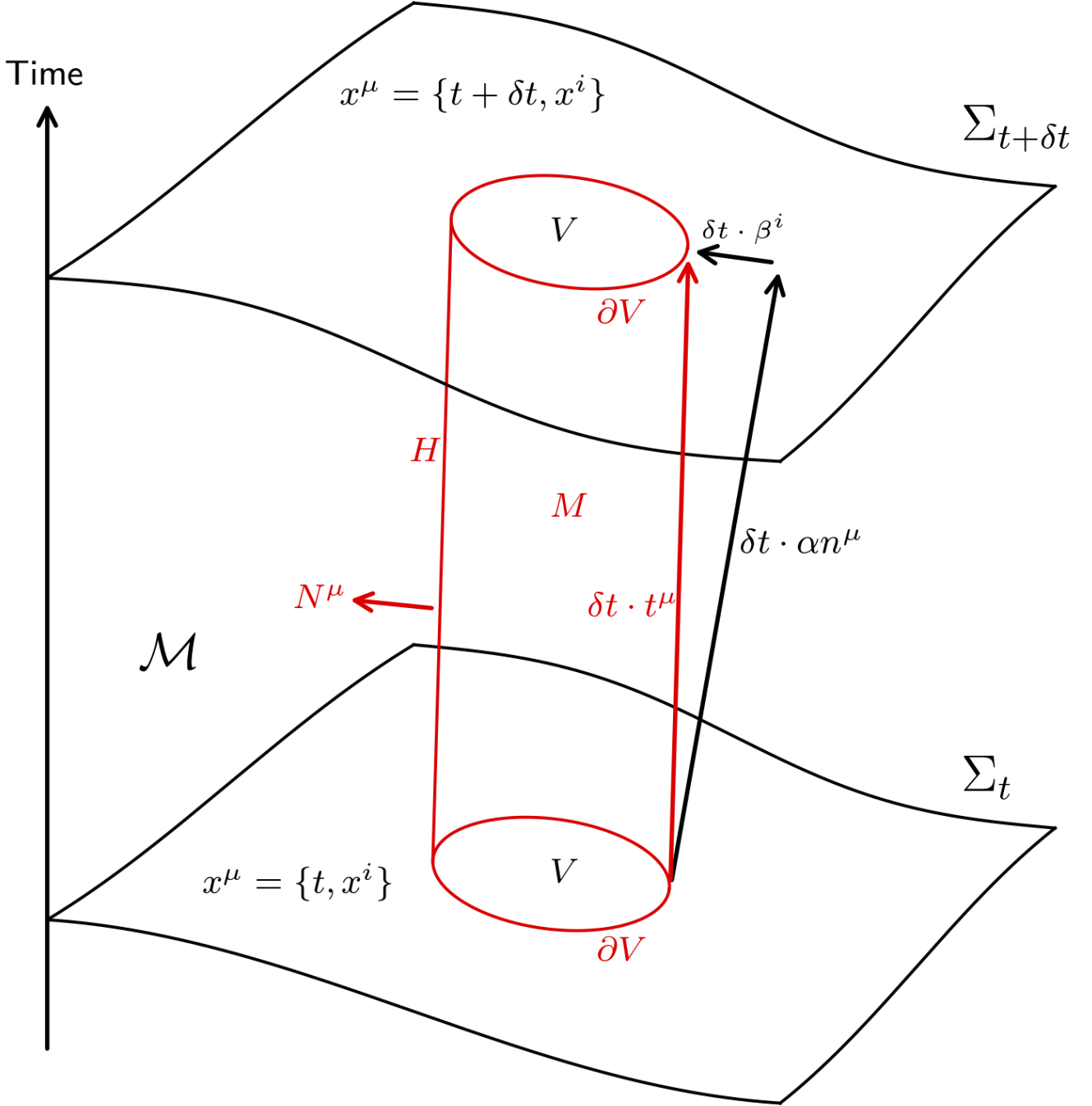
and this is identical to Eq. (4.3.17) found earlier.

Figure 4.1: Diagram of relevant geometry for derivation of QFS system in section 4.2 on manifold $\mathcal{M}$. Σ_t is the spatial hypersurface at time t and $\Sigma_{t+\delta t}$ is the the spatial hypersurface at a later time $t + \delta t$. V is the coordinate volume, with surface ∂V, that we wish to use as an extraction volume on Σ_t. The sides of the red cylinder are H, defined by ∂V evolved along integral curves of $\boldsymbol{t} = \boldsymbol{\partial_t}$. The interior of H between times t and $t + \delta t$ is M. Evolving ∂V forward in time with $\boldsymbol{n}$, as demonstrated with the long black arrow, gives a different coordinate volume on $\Sigma_{t+\delta t}$ than on Σ_t.
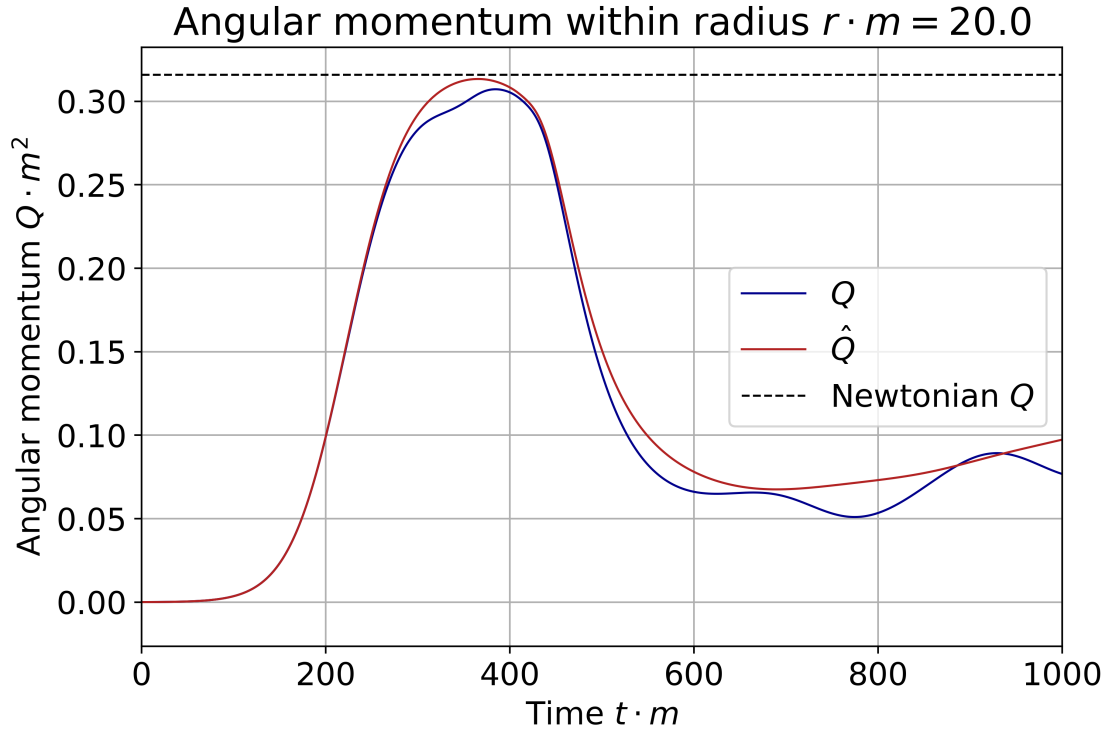
Figure 4.2: Integrated angular momentum within radius $r < 20\ m^{-1}$. Q is the angular momentum integral in Eq. (4.6.2) and $\hat{Q}$ includes the source term as in Eq. (4.6.7). The black dashed line indicates the Newtonian calculation for the angular momentum given in Eq. (4.6.11). The boson stars initially start outside the extraction radius.
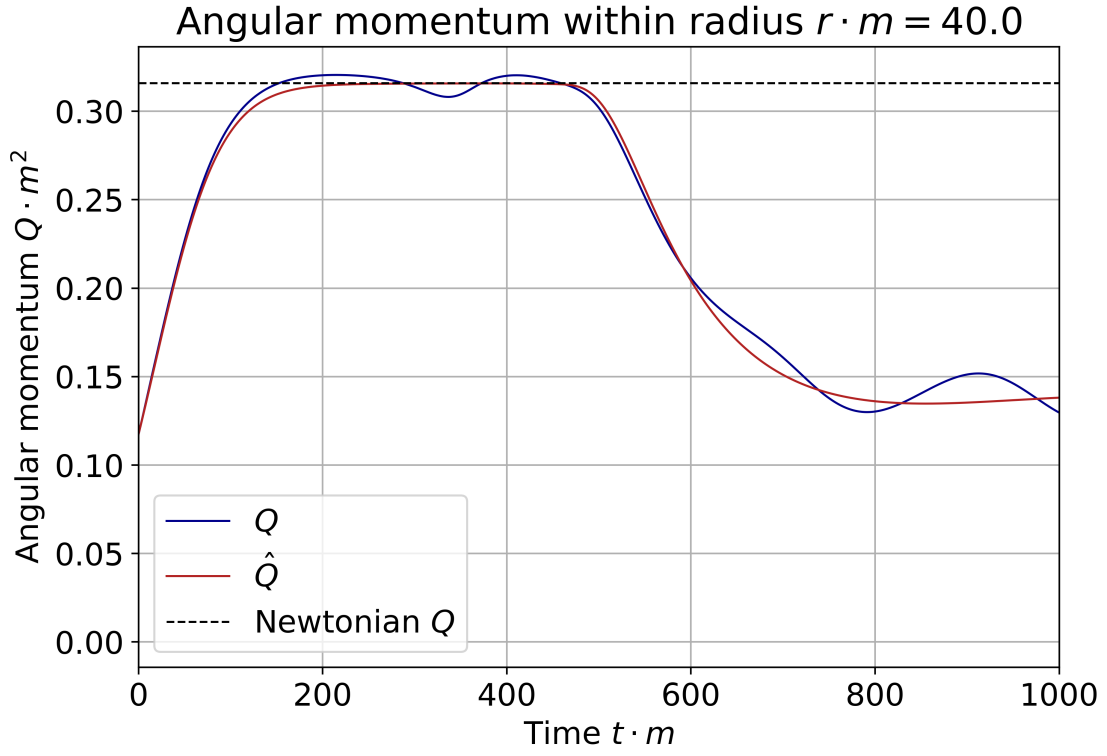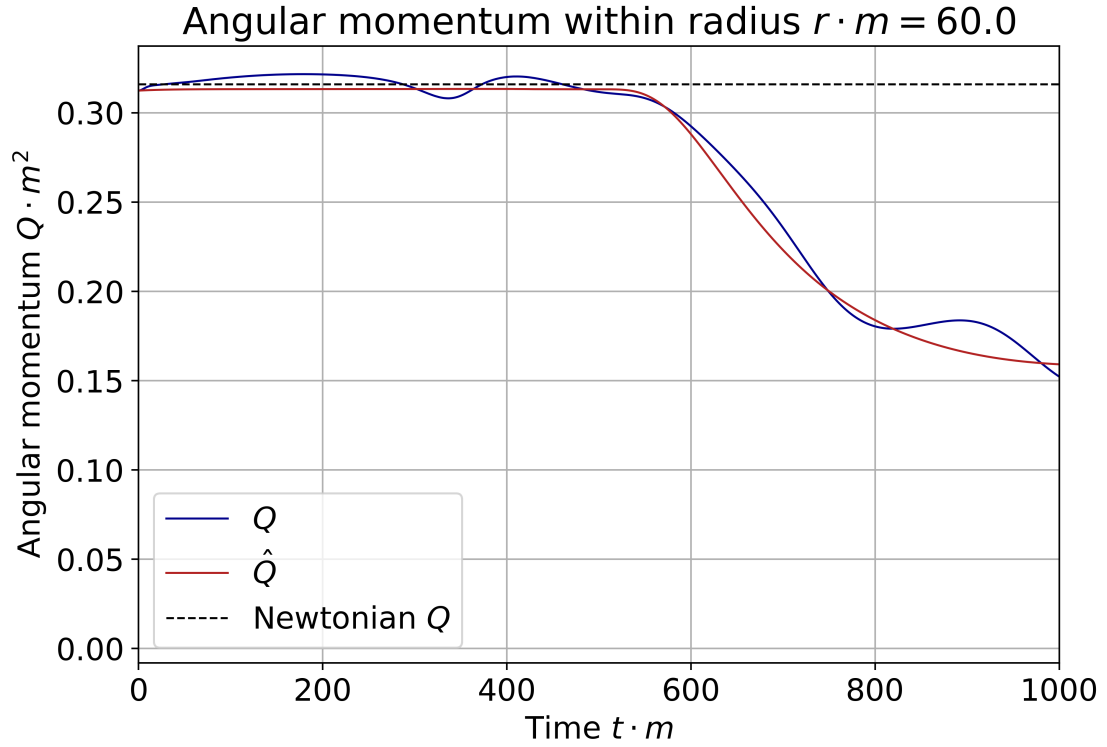
Figure 4.3: Integrated angular momentum within radius $r < 40\ m^{-1}$. Quantities plotted are identical to Fig. 4.2. The boson stars initially start intersecting the extraction radius.

Figure 4.4: Integrated angular momentum within radius $r < 60\ m^{-1}$. Quantities plotted are identical to Figs. 4.2 and 4.3. The boson stars initially start inside the extraction radius.
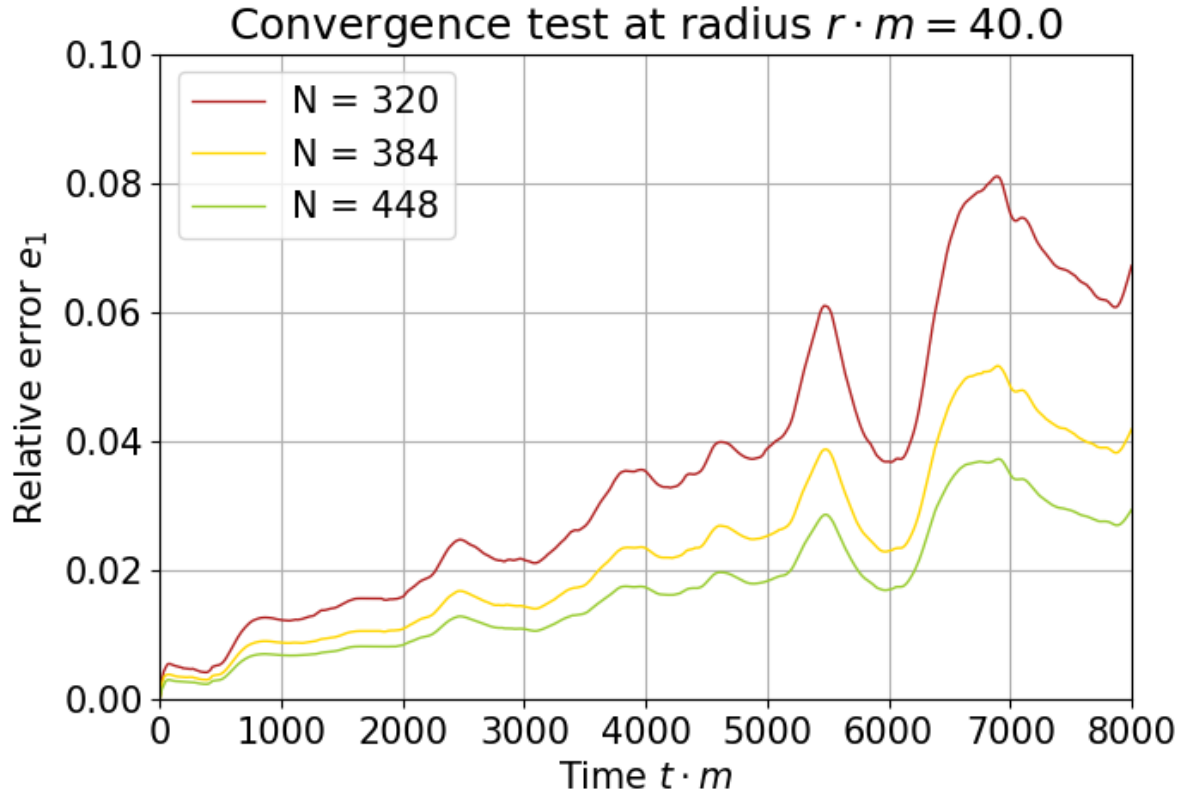
Figure 4.5: Relative error e_1, from Eq. (4.6.9), for the modified total angular momentum at extraction radius $r = 40 \ m^{-1}$; the modified total angular momentum $\hat{Q}$ includes the source term. Figure includes four convergence simulations with $N \in \{320, 384, 448\}$ gridpoints along the coarse grid.
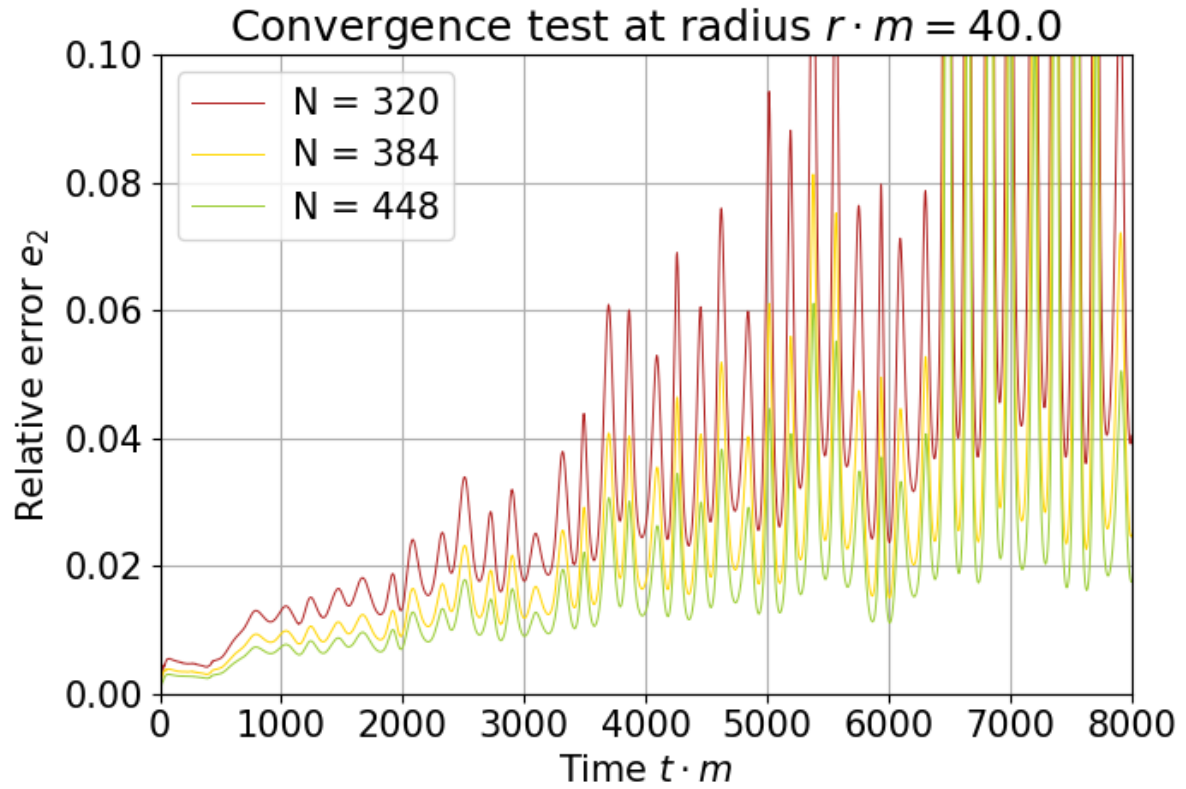
Figure 4.6: Relative error e_2, from Eq. (4.6.10), for the total angular momentum at extraction radius $r = 40\ m^{-1}$; the total angular momentum Q excludes the source term. Figure includes four convergence simulations with $N \in \{320, 384, 448\}$ gridpoints along the coarse grid.
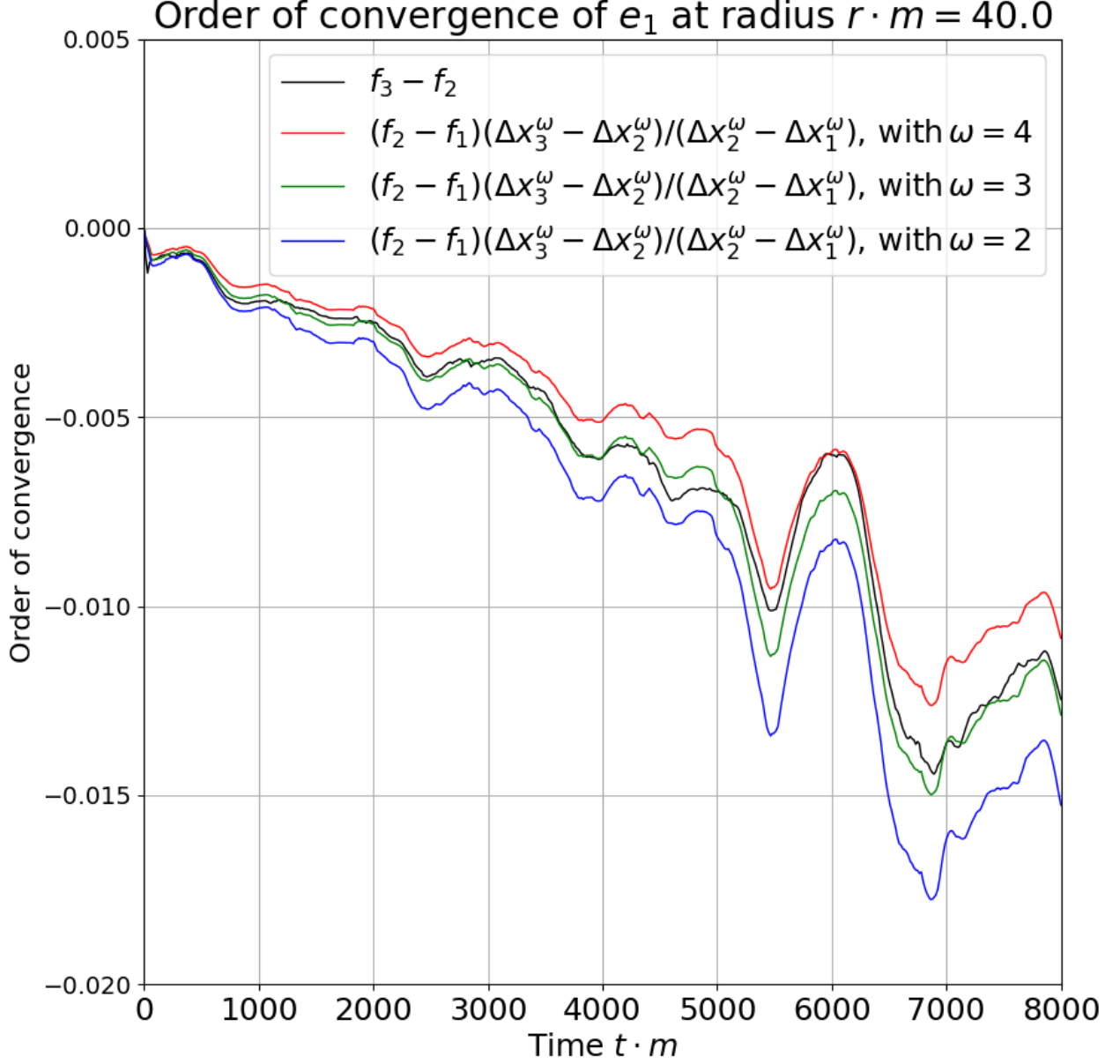
Figure 4.7: Estimating the order of convergence ω of the angular momentum error e_1 in Fig. 4.5 at extraction radius $r = 40 \, m^{-1}$. The black curve shows the difference between f_3 and f_2; the relative error e_1 of the two highest resolution simulations in Section 4.6. The three coloured curves show the difference between the two lowest resolution simulations f_2 and f_1, but modified by $(\Delta x_3^\omega - \Delta x_2^\omega)/(\Delta x_2^\omega - \Delta x_1^\omega)$ in accordance with Eq. (4.6.13), for three idealised orders of convergence $\omega = \{2, 3, 4\}$. The black curve is in best agreement with the green curve giving an estimate of $\omega = 3$ for the order of convergence.
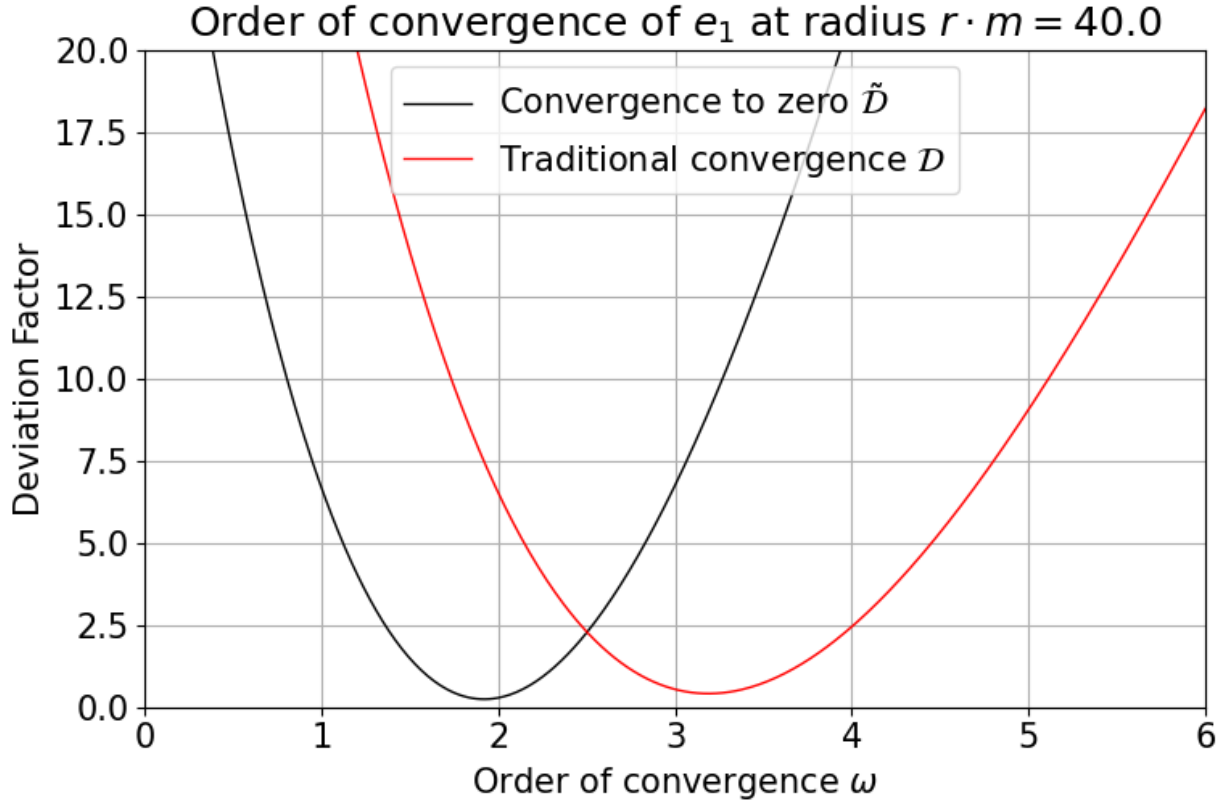
Figure 4.8: Estimating the order of convergence ω of the angular momentum error e_1 in Fig. 4.5 at extraction radius $r = 40\ m^{-1}$. The red curve gives the deviation from ideal traditional convergence $\mathcal{D}$, defined by Eq. (4.6.14), as a function of ω. The black curve shows the deviation from ideal convergence to zero $\tilde{\mathcal{D}}$, using the definition given in Eq. (4.6.16), as a function of ω. For both curves the estimated order of convergence is found by minimisation with respect to ω; this gives $\omega = 3.2$ for traditional convergence and $\omega = 1.9$ for convergence to zero.
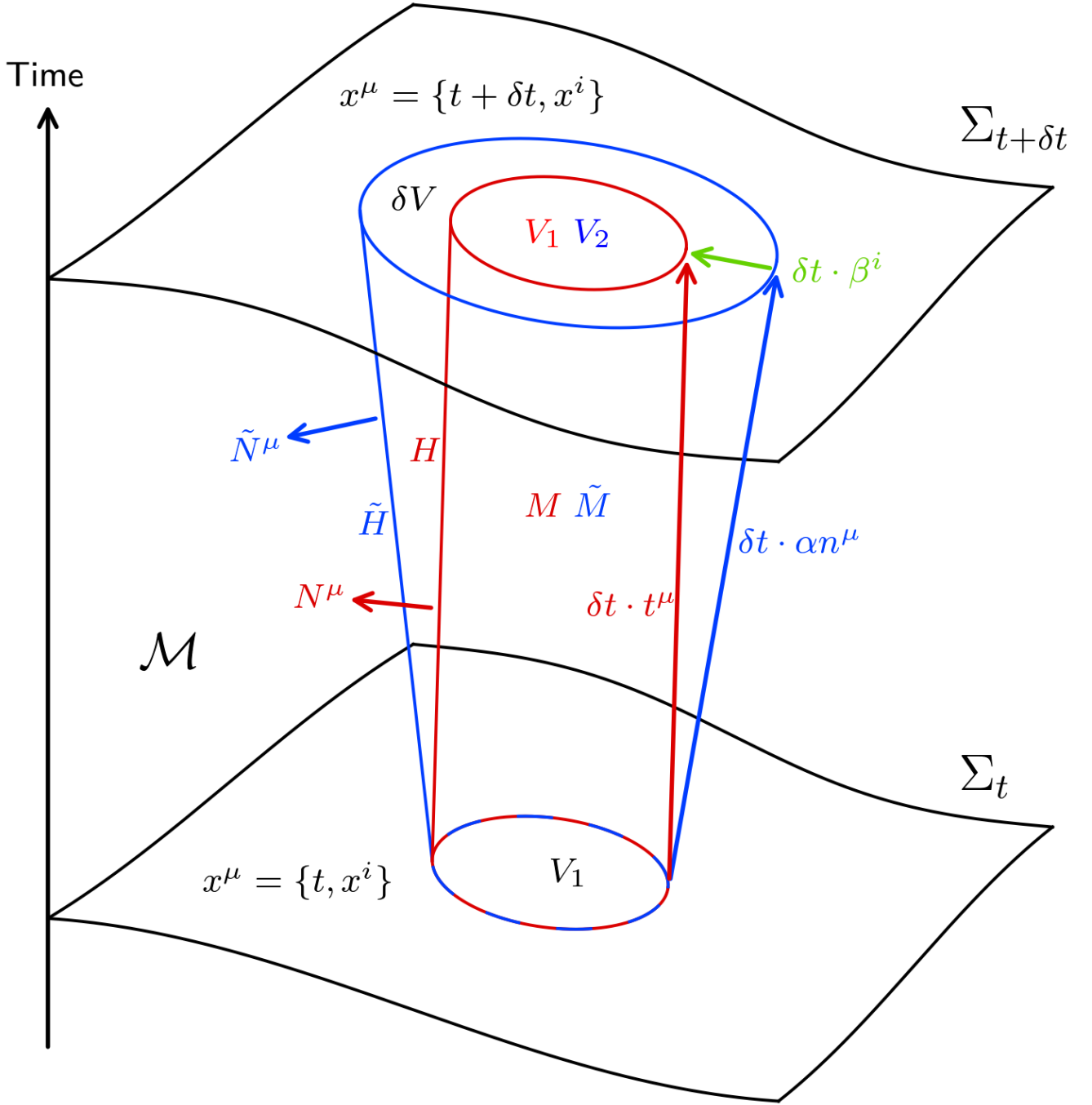
Figure 9: Comparison of two possible geometries for derivation of QFS system in section 4.2 on manifold $\mathcal{M}$. Σ_t is the spatial hypersurface at time t and $\Sigma_{t+\delta t}$ is the the spatial hypersurface at a later time $t + \delta t$. V_1 is the coordinate volume, with surface ∂V_1 (not labelled), that we wish to use as an extraction volume on Σ_t. The red cylinder, defined by ∂V_1 evolved along integral curves of $\boldsymbol{t} = \boldsymbol{\partial_t}$, is the same as in Fig. 4.1. Evolving ∂V_1 forward in time with $\boldsymbol{n}$, as demonstrated with the blue cylinder, gives a different coordinate volume ∂V_2 (not labelled) on $\Sigma_{t+\delta t}$. Similarly to the red cylinder, the blue cylinder has sides labelled by $\tilde{H}$ and an interior $\tilde{M}$. The difference in the volumes V_1 and V_2 on $\Sigma_{t+\delta t}$ is denoted by δV.

Bibliography

Bibliography

Bibliography

[1] blank